Mechanical Behavior and Damage Mechanisms

of Woven Graphite-Polyimide Composite Materials

by

Linda Wagnecz

Thesis submitted to the Faculty of the

Virginia Polytechnic Institute and State University

in partial fulfillment of the requirements for the degree of

Master of Science

in

Engineering Mechanics

APPROVED:

Wayne W. Stinchcomb

Wayne W. Stinchcomb, Chairman

Kenneth L. Reifsnider

Kenneth L. Reifsnider

John C. Duke, Jr.

John C. Duke, Jr.

Edmund G. Henneke, II

Edmund G. Henneke, II

June, 1987

Blacksburg, Virginia

Mechanical Behavior and Damage Mechanisms

of Woven Graphite-Polyimide Composite Materials

by

Linda Wagnecz

Wayne W. Stinchcomb, Chairman

Engineering Mechanics

(ABSTRACT)

The behavior of 8-harness satin woven Celion 3000/PMR-15 graphite-polyimide was experimentally investigated. Unnotched and center-notched specimens from $(0)_{15}$, $(0)_{22}$, and $(0,45,0,-45,0,0,-45,0,45,0)_2$ laminates were tested. Material properties were measured and damage development documented under monotonic tension, sustained incremental tension, and tension-tension fatigue loading. Damage evaluation techniques included stiffness monitoring, penetrant-enhanced X-ray radiography, laminate deply, and residual strength measurement. Material properties of the woven graphite-polyimide were comparable to those of woven graphite-epoxy. Damage development in woven graphite-polyimide was quite different than in non-woven graphite-epoxy. Matrix cracking was denser and delamination less extensive in the graphite-polyimide material system, and as a result, increases in notched residual tensile strength were much lower. A ply level failure theory was used to successfully predict the notched tensile strength of the $(0,45,0,-45,0,0,-45,0,45,0)_2$ laminate based on experimental data from the $(0)_{22}$ laminate. A simple method was used to simulate fatigue damage in a $(0)_{22}$ notched specimen to predict residual strength as a function of fatigue life. The advantages and disadvantages of the ply level failure theory used in this study are discussed.

ACKNOWLEDGEMENTS

The author would like to express thanks and appreciation to the following people for both directly and indirectly supporting this work:

- Dr. Stinchcomb, for all of the time and effort he spent as committee chairman, offering guidance and encouragement with the experimental program and thesis writing and editing processes.

- Dr. Reifsnider, for his advice with the analytical work and for his bright outlook on research.

- Joe Vittosser, for helping with the materials testing and for being a good friend while visiting as a research associate.

- Dr. Duke and Dr. Henneke, for serving as committee members and for helping to edit this document.

- Chuck Bakis and Bob Simonds, for their assistance in the laboratory, and Ahmad Razvan, for performing all of the deplying and scanning electron microscopic work.

- Members of the technical and secretarial staff of the Engineering Science and Mechanics Department, for their assistance with laboratory equipment, photography, machine shop work, and secretarial services.

- Fellow members of the LBRG, a subsidiary of the CLBR, for making the past two years enjoyable by promoting a *"Laid Back"* attitude.

- Laura and Tiger, for continually reminding the author that life as a graduate student is *"real tough."*

- Mr. and Mrs. Alexander Wagnecz, the authors parents, for many years of encouragement and support.

- Brian (MH), the author's fiance, for buying the author textbooks instead of flowers on Valentine's Day.

- General Electric Aircraft Engine Group of Evendale, Ohio, for funding this work, and Matt Buczek, for serving as project monitor.

Table of Contents

List of Illustrations

List of Tables

I. INTRODUCTION

Advanced fiber reinforced composite materials are becoming more widely used in high performance applications as design engineers begin to accept their reliability. Now, composites are being used in primary structures of both military and commercial aircraft [1-3]. Composite materials, exhibiting high specific strengths and stiffnesses, allow considerable weight and fuel savings when used in place of conventional engineering materials. Additional savings in cost result from the ease in which composite structures can be manufactured; complex structures can be made with fewer parts and without the extensive machining often required by metals. However, for the full value of advanced composite materials to be utilized, extensive testing must be carried out to eliminate the over-conservative design criteria commonly set on new material systems.

A recent advance in composite materials technology is the use of cloths woven from high strength fibers to replace the typical unidirectional fiber reinforcement. Woven cloths were designed in order to improve impact tolerance, damage resistance, and ease of material handling while retaining the general properties of fiber reinforced laminates. Two of the weave patterns used in composites are plain and satin weaves. In a plain weave fabric, a bundle of fibers is woven over one transverse bundle then under the next and so on. In an n-harness satin weave, the fiber bundle passes over n-1 transverse bundles before looping under one in a repeating pattern. Satin weaves with either 5-harness or 8-harness structures are one of the more popular types of weaves, as they contain less fiber bending and as a result, have greater strengths than plain weave fabrics.

During the last ten years, much effort has been spent in the development of a lightweight, fiber reinforced composite capable of withstanding extreme temperatures. In the hope of developing such a material for use on the space shuttle, the National Aeronautics and Space Administration (NASA) at Langley Research Center established the Composites for Advanced Space Transportation Systems (CASTS) program. Various types of graphite-reinforced polyimides have been shown to retain their strength and stiffness fairly well in temperatures as low as -250°F (-157°C) and as high as 600°F (316°C) [4-9]. However, their properties may degrade if exposure to high temperatures is longer than 1000 hours [9]. Besides applications on space structures, this material may be very useful in jet engines and supersonic cruise aircraft. The present study is motivated by the desire to use woven Celion 3000/PMR-15 graphite-polyimide, a material combining the advantages of woven reinforcement and a high temperature matrix, for fan blades in gas turbine engines.

Literature Review

One of the goals of this study is to determine the damage mechanisms of 8-harness satin woven Celion 3000/PMR-15, a graphite-polyimide composite, and to determine their effects on material behavior. Ideally, to separate the effects of the fiber architecture and the matrix, one would compare a woven and a non-woven version of the same material system. However, documentation of both woven and non-woven graphite-polyimide is very incomplete. It is hoped that knowledge learned from other material systems will be helpful in understanding the behavior of this particular material. In this section, relevant literature concerning woven material, graphite-polyimide composites, and damage development will be summarized.

Woven Materials

Some of the advantages of woven fiber reinforced composites are easier handling [10], improved energy absorption [11] due to interaction of fiber yarns [12], and as a result, improved impact tolerance [13,14]. Statistical scatter in experimental results was reported to be small for satin weaves under monotonic loading and bending fatigue compared to those found with non-woven composites [13,15,16], possibly due to more uniform processing.

The disadvantages of woven reinforcement include fiber crimping, or bending, and resin rich pockets due to the weave [17]. A woven architecture has been shown to decrease monotonic tensile strength in various layups approximately 15-25% for a 5-harness satin weave compared to similar non-woven laminates [13], which is typical of the decrease in strength of non-woven composites with misaligned fibers due to improper layup [18]. A study comparing various types of weaves [15] shows that satin weaves are significantly stronger than plain weaves, which have more fiber crimping. One might expect that the less crimp present, the stronger the composite. If this is true, then an 8-harness satin weave would be stronger in both tension and compression than a 5-harness satin weave and would be very comparable in strength to a non-woven composite with similar fiber orientations.

Another disadvantage cited against woven material is less flexibility in design. Fibers must be placed in two perpendicular directions in order to form a ply. Also, ply thicknesses are severely limited. Researchers have developed various weave configurations to achieve more freedom in design. The configurations include braided, knitted, and uniaxial, triaxial, and 3-dimensional weaves [17,19].

Halpin, Jerine, and Whitney [18] performed some of the earliest analytical research on woven composites in 1970. They modelled a plain weave fabric as a balanced symmetric non-woven laminate and reduced ply thicknesses to account for fiber crimping. Upper and lower bounds on elastic moduli and thermal expansion coefficients were found. It was concluded that fabric properties would always be less than those of a cross-ply laminate (0,90) and greater than those of a quasi-isotropic laminate. Furthermore, they suggested that a fabric with equal numbers of fibers in both directions could be treated as a (0,90) unidirectional tape laminate with minimal error. Ten years later, Ishikawa and Chou developed models to predict the behavior of fabric composites with various types of weaves [20-24]. Included are studies on elastic stress-strain response [20], thermal effects [21], nonlinearity [22], the 'knee point phenomenon' [23], and triaxial weaves [24].

In the early 1970's several researchers investigated the fracture behavior of fabrics [12,25,26]. Fracture was modelled with a linear discrete fracture theory using an effective crack length, found experimentally, to characterize a given material layup [12]. Once this constant was measured, the stress concentration factor could be found for all crack sizes in that given layup. Other researchers studying flexible woven fabrics suggested ways of increasing notched strength [25,26]. One solution was to increase the area of fabric involved in deformation by applying a lubricant to decrease shear resistance; the other was to incorporate several larger yarns spaced throughout the fabric to act as crack barriers.

Much experimental monotonic loading data have been published for woven composites. Tensile, compressive, and flexural moduli are reported for E-glass, S-glass, and graphite reinforced polyimide [27]. Tensile behavior of a glass-epoxy taffeta composite [28], graphite, aramid, and hybrid graphite/aramid reinforced epoxy [29], and glass, Kevlar, and graphite reinforced polyester [30] has also been documented. Notched and unnotched tensile strengths of plain, satin, and tridirectional graphite-epoxy woven composites are presented in Ref. [15]. Additional tension and compression data on notched and unnotched 5-harness satin graphite-epoxy were reported in [31]. Other sources containing both notched and unnotched quasi-static data on woven material include Refs.[6,13,32,33].

Two investigators have tried to model the notched strength of woven materials [32-34]. Lagace [32] found that notched tensile strength could be predicted for 5-harness satin woven graphite-epoxy using the Mar and Lin method [35,36] previously applied to non-woven laminates. Once a composite fracture parameter was experimentally measured for a given layup, notched strength could be calculated as a function of hole size. Lagace also noted that notch sensitivity is dependent on the size, but not the shape, of a flaw, which is consistent with the behavior of non-woven composite materials.

Bailie [33,35] attempted to use the Whitney-Nuismer average stress criterion [37,38] to model notched strength. This theory states that when the average stress a distance, a_0, away from the hole reaches the unnotched strength of the material, failure will occur. Bailie applied this criterion to the tensile [33] and compressive [34] failure of 8-harness satin woven graphite-epoxy laminates. He found that in tension, the characteristic distance, a_0 , was dependent on both layup and hole size [33]. Only one hole size was tested under compression, but a_0, was found to be dependent on layup and also on temperature [34]. Bailie noted that the tensile values he calculated for a_0, ranging from 0.24 in. to 0.31 in., were higher than those typically reported for non-woven graphite-epoxy, between 0.09 in. and 0.15 in., suggesting a lower stress gradient, and possibly more 'ductile' behavior, due to the less-anisotropic nature of a woven ply [33]. One interesting observation is that the compressive values for a_0 were larger than those in tension, ranging from 0.27 in. to 0.55 in. [34].

Much less extensive experimental research has been focused on fatigue and residual strength of woven fabric composites. Four-point bending fatigue of a sharply notched 8-harness satin woven graphite-epoxy laminate was discussed in Ref.[16]. Unnotched, low cycle tensile fatigue and subsequent residual strength tests were performed on both unidirectional and bidirectional fiberglass fabric composites [39]. Comparisons of the fatigue behavior of 8-harness satin graphite-PEEK and graphite-epoxy were made in Ref.[40]. Tensile fatigue tests were also carried out on a glass-epoxy taffeta weave [28].

An excellent study, published in 1985, was done by Curtis and Moore [31] on the fatigue behavior of 5-harness satin woven and non-woven graphite-epoxy (T300/BSL914C). Both notched and unnotched specimens of five different stacking sequences were subjected to both 0-tension ($R=0$) and tension-compression ($R=-1$) fatigue cycling, while damage was monitored. Fatigue performance of woven material was not as good as that of non-woven material and was found to be influenced by stacking sequence. Additional tension-tension ($R=0.1$) fatigue research to be published on 5-harness satin graphite-epoxy was done by Schulte, Reese, and Chou [29]. Also tested were aramid-epoxy and hybrid graphite/aramid-epoxy.

Curtis and Bishop [13] introduced the concept of a mixed woven laminate containing non-woven 0 degree plies and woven $\pm$ 45 degree layers. The 0-tension [41] and tension-compression [42] fatigue and residual strength responses of these materials have been studied. Their impact [13] and post-impact fatigue [14] behavior have also been documented. Mixed woven laminates have higher residual tensile and compressive strengths during fatigue than all-woven laminates [41-43] and are more tolerant to impact damage than non-woven laminates [13,14].

Graphite-Polyimide Composites

Because polyimide matrix systems are relatively new, a large amount of literature on graphite-polyimides involves materials development, processing, and screening. Ref.[44] presents a thorough literature review of such topics. Two NASA conference proceedings provide detailed Information on graphite-polyimide composites [45] and on high temperature composites [46], published in 1979 and 1985, respectively. From this literature, one would conclude that it is possible to produce high quality graphite-polyimide composites with monotonic properties and fatigue behavior comparable to those of graphite-epoxy at room temperature, but far superior in high temperature environments. Because polyimide composites release a large amount of volatile gases during curing, they are very susceptible to the formation of voids if proper curing cycles are not followed. High void contents tend to decrease material strength and stiffness. Some concern has been expressed over the ability to maintain consistent material quality from batch to batch.

Many investigations have been concerned primarily with finding basic material properties for a variety of graphite-polyimide systems. Quasi-static unnotched tensile, compressive, and shear properties have been reported for Celion 3000/PMR-15 [47], Celion 6000/PMR-15 [4,47,48], T300/V-378A [27], HTS/710 [7,9], Celion 6000/LARC-160 [49], and graphite/PMR-15 [8]. One researcher [47] concluded that Celion 3000 fibers were slightly stronger than Celion 6000 fibers in a PMR-15 polyimide matrix. The majority of studies on notched properties involved high (600°F) and sometimes low (-250°F) temperature testing. Works on notched materials include Celion 6000/PMR-15 [4,47,48], HTS/710 [7,9], and HTS/PMR-15 [5]. Tensile strength and stiffness of unnotched graphite-polyimide were slightly lower than those of graphite-epoxy at room temperature. Notch sensitivity was dependent on notch size, but not shape, as observed with graphite-epoxy [5]. However, graphite-polyimides were much less notch sensitive than graphite-epoxies, having a lower reduction in strength due to stress concentrations such as holes and sharp notches [48].

The effect of extreme temperatures (-250°F to 600°F) on the tensile strength and stiffness of Celion 6000/PMR-15 was studied by Garber, Morris, and Everett [4]. For unnotched coupons, temperature had no effect on fiber-dominated laminates. However, for matrix-dominated laminates, such as $(\pm 45)_{ns}$, higher properties corresponded to lower temperatures. For notched fiber-dominated specimens, higher strengths were obtained at 600°F than at room temperature (75°), while the opposite was true for matrix-dominated coupons. At cryogenic temperatures (-250°F), specimens were either stronger or about the same strength as at room temperature, although numerous grip-related failures were observed. The Whitney-Nuismer average stress characteristic distance, a_0, was found to be between 0.1 in. and 0.3 in. for various stacking sequences, exhibiting a slight dependence on temperature.[4] Results show that similar trends occur for unnotched and notched fiber-dominated Celion 6000/PMR-15 specimens [7]. Large scatter was present in similar data on a HTS/710 laminate, and the effect of temperature on tensile strength was not as obvious [7].

A limited amount of fatigue testing has been done on graphite-polyimide composites. Maier, et al, [50] tested unnotched, non-woven Celion 6000/H795E $(0_2, +/-45, 0_2, +/-45, 90)_s$ specimens under tension-tension (R=0.1) and tension-compression (R=-1.0) loading. The fatigue strength of this material was found to be only slightly less than that of non-woven graphite-epoxy, showing a relatively weak influence of matrix brittleness on fatigue performance.

Others investigated the effect of temperature on the fatigue life of non-woven composites. Rummler and Clark [9] subjected HTS/710 to flight-simulated fatigue loads at a temperature of 450°F (232°C). They concluded that the maximum service temperature of this material is significantly reduced when long-term, high temperature exposure is combined with fatigue loading.[9] Illg and Everett [5] performed tension-compression (R=-1.0) fatigue tests on notched $(0, +/-45)_s$ HTS/PMR-15. Fatigue performance was best at cryogenic temperatures (-250°F) and worst at elevated temperatures (600°F). At room temperature, a notched specimen, subjected to maximum loads of 60% of its notched tensile strength, had a life of about one million cycles.[9]

Damage Development

A relatively small amount of literature has been published describing damage development in woven and in woven or non-woven graphite-polyimide composites. Sources discussing woven materials, all published within the last 5 years, included quasi-static [29,31-33] and fatigue [29,31] loading. Damage development in mixed-woven composites containing non-woven 0 degree layers and woven ± 45 degree layers has been well-documented [13,14,41,42]. Damage studies have been conducted on unnotched graphite-polyimide specimens subjected to fatigue loading [50], but none have been discovered on notched graphite-polyimide. Below, a brief summary of these works will be given.

Under quasi-static loading, woven materials fail differently than those that are non-woven. Bailie [33] noted that the failure surfaces of 8-harness satin graphite-epoxy specimens were very localized, containing none of the large delaminations often found in laminates made from unidirectional tape. Curtis and Moore [31] found that the same was true for 5-harness satin graphite-epoxy. Bailie attributed this to the nature of an individual ply. Woven plies are less anisotropic than unidirectional ones, resulting in lower interlaminar stresses, the driving forces behind delamination. Bailie [33] tested specimens with circular center holes and measured strains near the notch. He found significant nonlinear response both through-the-thickness and tangent to the hole at high loads, suggesting that some forms of damage do occur under quasi-static tensile loading prior to the catastrophic failure.

Lagace [32] and Curtis and Moore [31] observed that little 0 degree matrix splitting occurred in 5-harness satin graphite-epoxy specimens. Splitting, or matrix cracking, is another damage mechanism commonly found in non-woven composites. Lagace claimed that the woven architecture increases quasi-static notched strength by providing a barrier to crack propagation, as woven (0,90) laminates were stronger under monotonic tension than non-woven ones.[32] Curtis and Bishop [13] and Curtis and Moore [31] found that the opposite was true under monotonic tension; they claimed that because stress-relieving mechanisms such as delamination and splitting are inhibited by the weave, notch sensitivity is increased in woven materials [13].

One other difference was noted between the quasi-static failure of 5-harness satin woven and of non-woven unnotched specimens. Schulte, Reese, and Chou [29] noted that transverse matrix cracks in graphite-epoxy, aramid-epoxy, and hybrid graphite/aramid-epoxy woven $(0)_8$ laminates were irregularly spaced and had not reached the Characteristic Damage State [51] commonly found in non-woven composite materials.

Fatigue studies on a total of six unnotched 5-harness satin graphite-epoxy laminates [29,31] showed that woven materials do not perform as well as their non-woven counterparts under 0-tension [29,31] and tension-compression [31] fatigue loading. Curtis and Moore [31] claimed that this was due to the local stress concentration effect at the fiber bundle cross-overs. From ultrasonic C-scans, it was observed that damage developed at these crossovers throughout fatigue life. This damage is believed to initiate the 0 degree fiber fracture that results in ultimate specimen failure.

Schulte, Reese, and Chou [29] also predicted the fiber crossovers as being problem areas based on local stress fields near the undulations. They, too, observed 0 degree fiber fracture just prior to specimen failure. Fiber damage occurred in $(0)_8$ woven graphite-epoxy specimens after local delaminations developed at the intersection of transverse and longitudinal matrix cracks. These investigators measured stiffness throughout fatigue life and found that a large decrease in stiffness took place over the last 50% of life. This large drop in stiffness occurs more abruptly in non-woven composites; for the non-woven cross-ply laminate, this period lasted for only the final 5% of life. Fatigue failure of the $(0)_8$ woven material occurred when the initial stiffness had dropped a total of 25%, as compared to 20% for the non-woven cross-ply laminate.

In general, less 0 degree splitting and delamination were seen in woven than in non-woven unnotched graphite-epoxy. Failure surfaces were also more localized as was the case with monotonic loading [29,31]. One additional type of damage was observed in woven materials, but not in non-woven materials. Curtis and Moore [31] saw that in woven graphite-epoxy laminates with poor fiber distribution, resin rich areas are present around fiber tows. Translaminar cracks that develop around the fiber tows can link together during fatigue loading and cause material failure; this type of failure mechanism was observed in $(+45,-45,-45,+45)_s$ specimens.

Fatigue studies on notched graphite-epoxy specimens again showed woven materials to be inferior to non-woven materials under 0-tension (R=0) and tension-compression (R=-1.0) loading. Besides the strength degradation associated with damage at fiber bundle crossovers, inhibition of longitudinal splitting and delamination at the notch cause woven and mixed-woven laminates to have lower residual strengths than similar non-woven laminates [29-32]. It should be noted that moisture had a significant effect on damage development in mixed-woven materials [30,32].

The only literature found on damage development in graphite-polyimide composites was published by Maier [50]. He tested non-woven, unnotched, tapered $(0_2,+/-45,0_2,+/-45,90)_s$ specimens under tension-tension (R=0.1) and compression-compression (R=-10) fatigue. Axial stiffness and acoustic emission were monitored throughout life. X-ray radiography and light microscopy were also used to determine the extent of damage.

Maier [50] described damage as occuring in three distinct stages, similar to those found in graphite-epoxy: the formation of cracks in ±45 degree and 90 degree plies, delamination at the free edges, and specimen failure. In Stage I, stiffness dropped 7-10% in a small number of cycles. This stage occurs faster in polyimide composites due to matrix brittleness; matrix cracking starts earlier and grows faster than in more ductile graphite-epoxy systems. Stage II was characterized by a slow, but steady, decrease in stiffness as matrix damage continued to grow. Final failure during Stage III occured shortly after the stiffness had fallen a total of 10-15%. Acoustic emission data supported the separation of damage development into these three stages. It should be kept in mind that the tapered geometry of the specimens probably had some effect on the damage mechanisms, especially on delamination that originated where the tapering ended.

Summary

Based on the literature reviewed, woven composite materials have a promising future. Their advantages include easier handling, better impact resistance, and the possibility of more uniform processing than non-woven composites. Slight reductions in strength and fatigue behavior are among the disadvantages of woven composites. An 8-harness satin woven ply is expected to have properties very similar to those of a (0,90) tape laminate.

Various analytical studies have modelled the behavior of woven materials, the earliest having been done in 1970. Experimental studies have concentrated mainly on measuring material properties, although some effort has gone into predicting notched quasi-static strength. Limited work has been done to characterize damage development in these materials.

Likewise, most of the research on graphite-polyimide composites has been aimed at determining material properties, but not damage mechanisms. It has been found that properties of graphite-polyimides are comparable to those of graphite-epoxies at room temperature. Graphite-polyimides are also able to retain their strength and stiffness well during short term exposure to both low (-250°F) and high (600°F) temperatures. One of the most popular types of graphite-polyimide, based on the extensive amount of the testing performed on it, was Celion 6000/PMR-15. Celion 3000/PMR-15 has recently been found to be slightly stronger than Celion 6000/PMR-15.

From the damage development studies on woven materials, it was discovered that a woven architecture, such as a 5-harness satin weave, limits delamination and 0 degree matrix splitting in graphite-epoxy. As a result, failure surfaces are more localized, although significant nonlinear strain response occurs near notches prior to ultimate material failure. The effect of inhibiting delamination and 0 degree splitting was debated; some felt it would increase notched strength while others felt it would decrease notched strength. Fatigue studies showed that woven and mixed-woven laminates had less global delamination and splitting than non-woven laminates, but also had lower increases in residual strength. It was claimed that local delaminations at fiber bundle crossovers resulted in 0 degree fiber damage and strength degradation. Thus, it appears that the weave constrains global damage development, but may at the same time cause local damage. It was concluded that the architecture had an adverse effect on stress redistribution in notched specimens.

The limited damage development research on non-woven graphite-polyimide showed that unnotched specimens subjected to fatigue loading behave similarly to graphite-epoxy specimens. Damage development was separated into three stages based on stiffness change and acoustic emission. The main difference between graphite-polyimide and graphite-epoxy was that the first stage of damage, consisting of matrix cracking in off-axis plies, occurs faster in graphite-polyimide due to matrix brittleness. However, matrix brittleness had little effect on fatigue behavior, with graphite-polyimide performing almost as well as graphite-epoxy. Much more work must be done to understand the damage process and its effect on long term performance of woven and non-woven graphite-polyimide composites.

Problem Statement

The primary objectives of the present study were to determine the damage mechanisms of an 8-harness satin, woven Celion 3000/PMR-15 graphite-polyimide and to understand the effects these damage mechanisms have on the strength, stiffness, and life of this material system. To examine material behavior, both notched and unnotched specimens were tested under quasi-static, sustained incremental, and cyclic tensile loading conditions. Various destructive and non-destructive techniques were used to evaluate the effect of mechanical loading on the state of damage in the material. Mechanical properties were measured and damage development documented. Special attention was given to the effects of the fiber architecture and the matrix system on material response. A ply level failure theory was used to predict the notched strength of one laminate based on experimental data from another laminate under monotonic loading. A simple method was used to simulate fatigue damage in a $(0)_{22}$ notched specimen to predict residual strength as a function of fatigue life. The advantages and disadvantages of the ply level failure theory used in this study are discussed.

II. EXPERIMENTAL PROCEDURES

Material and Specimens

The specimens tested in this study were made from Celion 3000/PMR-15 graphite-polyimide woven into two-dimensional, 8-harness satin pre-preg tapes. As shown in Figure 1, a bundle of fibers passes over seven bundles, then under one, in a repeating pattern. Figure 2 shows a scanning electron microscope (SEM) micrograph of an actual ply. For convenience, reference to a theta-degree ply will mean that the primary material direction, or warp, is at an angle of theta from the laminate axis, while the fill is perpendicular to that direction. In this pre-preg system, 24 fibers are located in the warp for every 23 fibers in the fill, although the fill direction was found to be slightly stronger. Also, small yarns of Kevlar fibers were woven into the plies every 2 in.. These tracer fibers are used to check ply orientations during and after layup.

Three different laminates were tested:

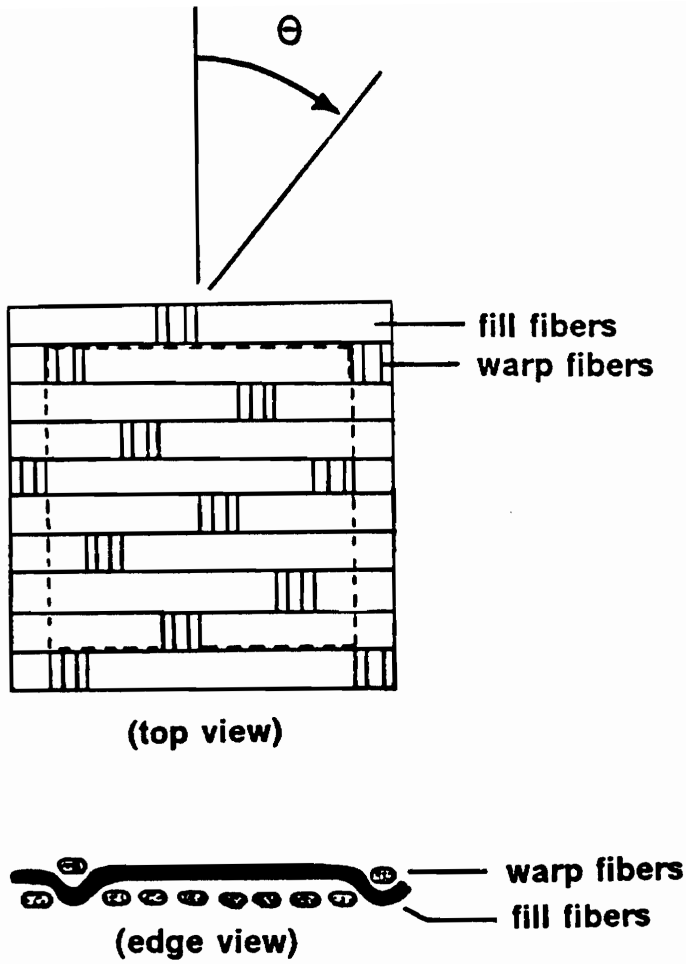

Figure 1. Fabric pattern of an 8-harness satin weave.

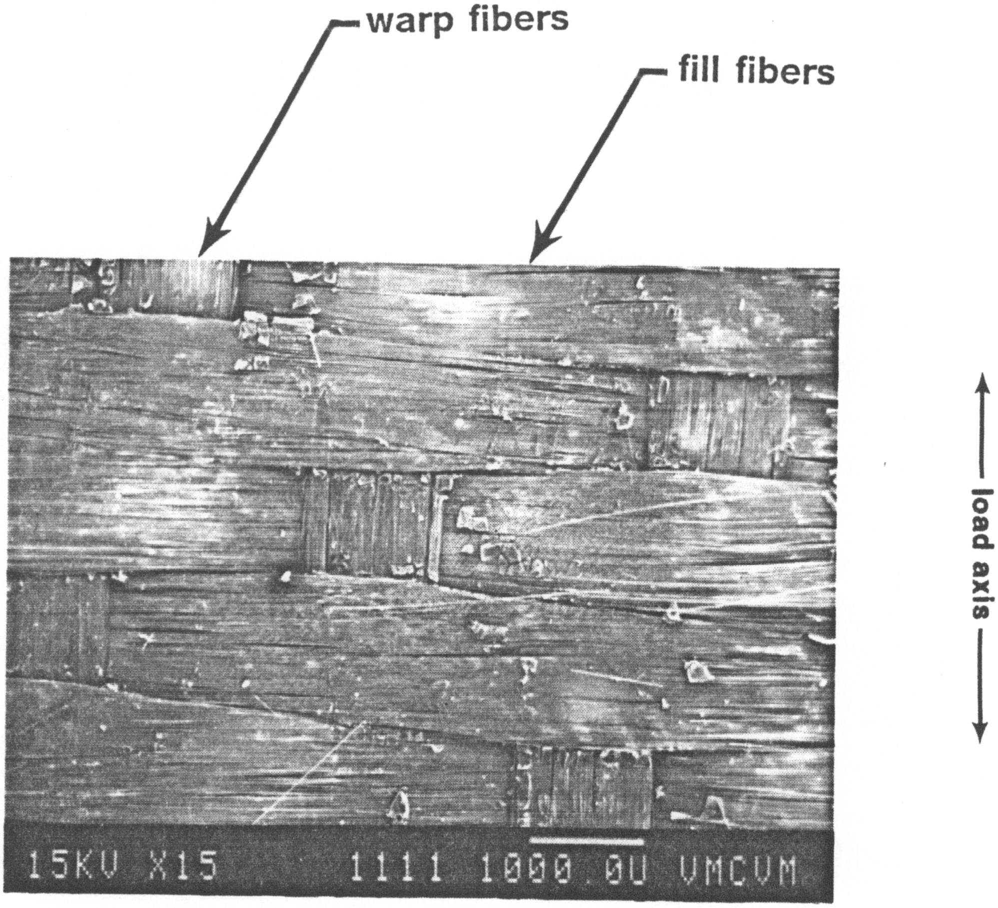

Figure 2. SEM micrograph of a 8-harness satin woven ply.

- $(0)_{22}$ -- (also referred to as a 22-ply 0 deg. laminate)

- $(0)_{15}$ -- (also referred to as a 15-ply 0 deg. laminate)

- $(0,+45,0,-45,0,0,-45,0,+45,0)_2$ -- (also referred to as a 20-ply 0/45 deg. laminate)

These materials, layed up and cured by General Electric Aircraft Engine Group of Evendale, Ohio, are all slightly unsymmetric. As shown in Figure 1, sevens eighths of the area of one side of a ply is covered by warp fibers, while the other eighth is covered by fill fibers. The opposite is true on the back side. A ply of woven material can be approximated as a (0,90) laminate made from unidirectional tape, so the $(0)_{15}$ material is similar to a $(0,90)_{15}$ tape laminate. In order to have a fully symmetric laminate, for each ply that faces upward, the corresponding ply on the opposite side of the midplane must face downward. An example of a symmetric and an unsymmetric two-ply 0 degree layup is given in Figure 3. It should be noted that the thicker the laminate, the less effect this lack of perfect symmetry has on material behavior.

Panels received from General Electric were about 13½ in. by 13½ in. square. Prior to machining, all were examined for major defects by performing an ultrasonic C-scan. Although the panels were slightly warped due to a combination of residual thermal stresses and the small degree of asymmetry noted above, their quality assessed by the ultrasonic technique appeared good. Panel thicknesses were approximately 13.5 ± 0.5 mils per ply.

Specimens, stored at ambient temperature and humidity, were machined by shop personnel in the ESM Department at Virginia Tech. A water cooled circular diamond wheel was used for cutting straight edges, while a diamond-tipped core drill was used for creating notches. Unnotched coupons were nominally 1 in. wide, while notched ones were 1½ in. wide with a 3/8 in. diameter center circular hole. From preliminary tensile tests, it was learned that gripping of short (4.75 in.) specimens would require large grip pressures to prevent slipping.

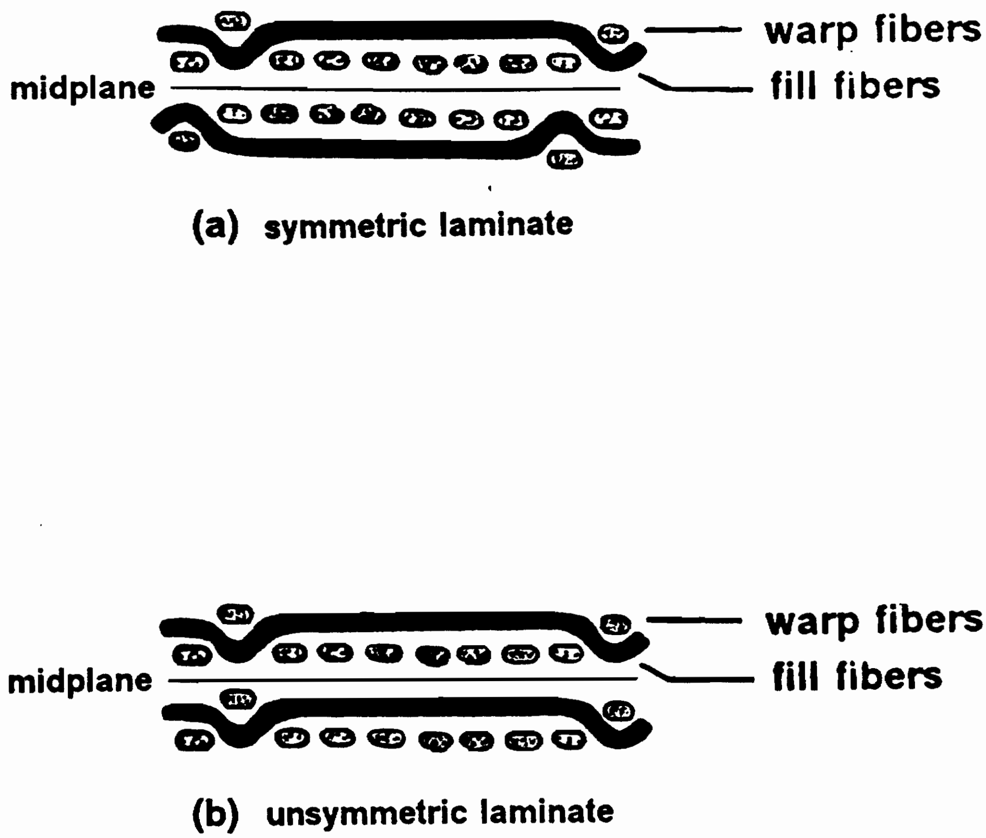

Figure 3. A 2-ply (a) symmetric and (b) unsymmetric 0 degree laminate.

Later specimens were cut longer, up to 6.75 in. long, but an ungripped length between 2.5 in. and 2.75 in. was used for all specimens, with the exception of a few compression specimens used to study the effect of unsupported length on notched compressive strength. This ungripped length allowed the largest specimen area to be gripped, while still leaving enough room between the grips for a one inch MTS extensometer.

Mechanical Tests

Mechanical tests were performed on a 50 kip servo-hydraulic, closed loop MTS testing machine, shown in Figure 4. Strains were measured with a one inch gage length MTS extensometer held in place by small rubber bands. As shown in Figure 5, the knife edges of the extensometer were located in v-notched aluminum tabs that were glued to the specimen with rubber cement.

Strain gages were not used after a few gages broke at relatively low strains, although these 5/16 in. gages supposedly had a strain limit of 5%. It was assumed that these failures were due to matrix cracking or non-uniform strain fields underneath the gages. Because the laminates were made from woven material, local strains varied significantly from place to place. The average strains measured by an extensometer over a one inch gage length were, therefore, closer to the global laminate strains than the those measured by the smaller strain gages.

Two layers of sandpaper were placed between the specimen and the hydraulic grips, with the rough sides facing the specimen, to reduce grip-induced damage and to provide extra friction to hold the specimen in place. Some specimens were especially hard to grip. The

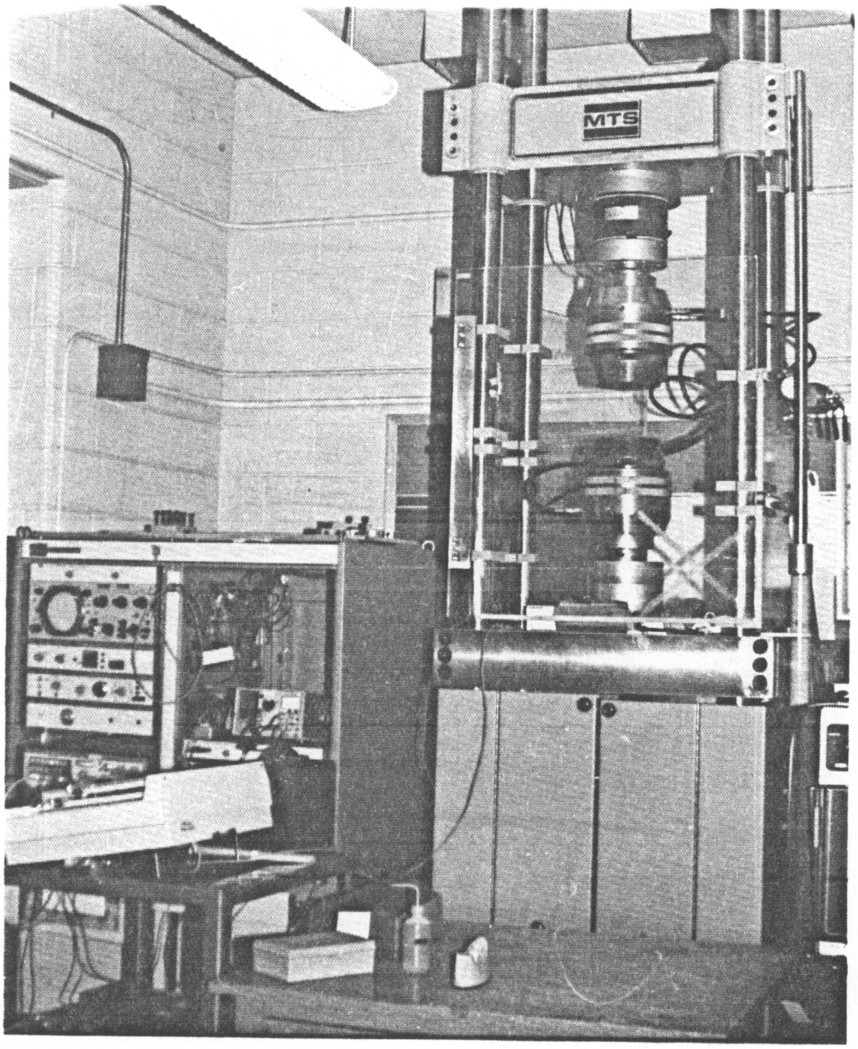

Figure 4. MTS testing machine.

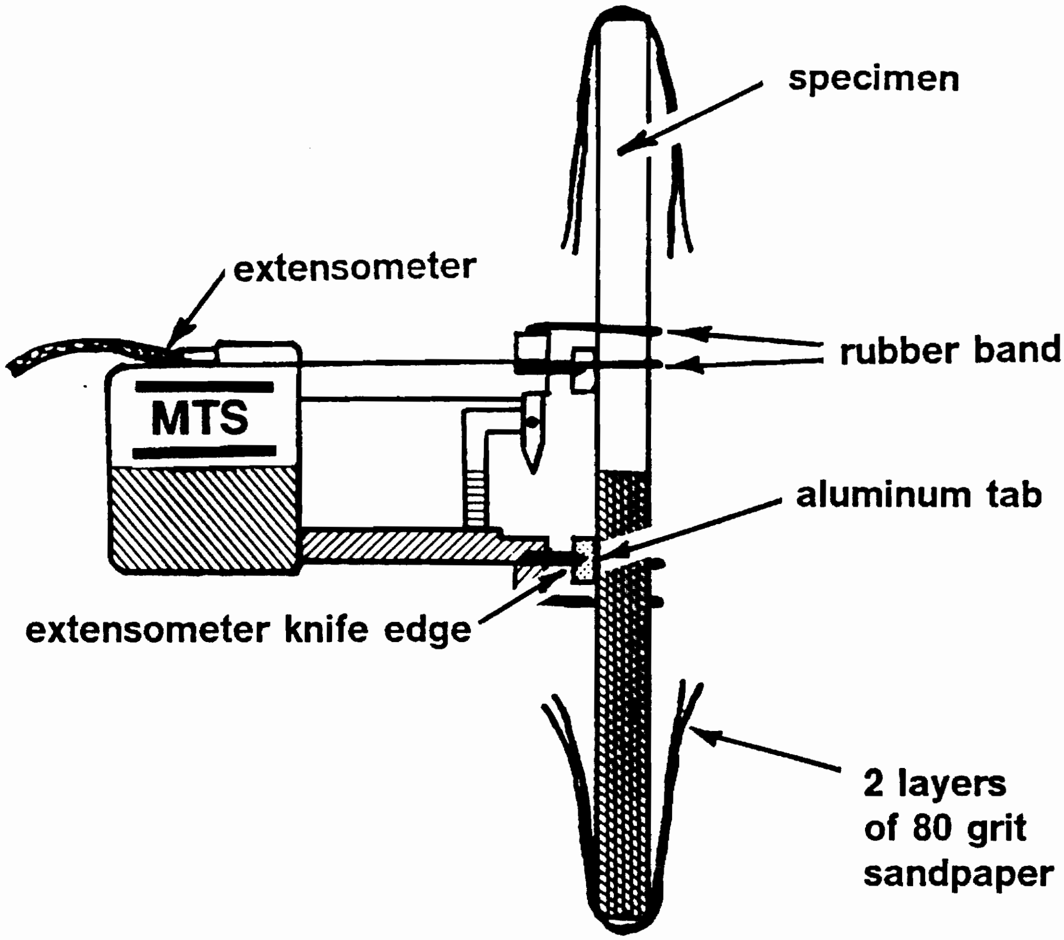

Figure 5. An extensometer attatched to a specimen with aluminum tabs and rubber bands.

worst case was gripping of unnotched $(0)_{22}$ specimens during monotonic tensile tests. These coupons, failing at loads just above 30 kips, were only 6.75 in. long (half of a panel width). By trial and error, it was found that these specimens could be held securely in the testing machine using a maximum grip pressure of 1300 psi, if at least 2.15 in. was gripped at each end. This could only be accomplished if 80 grit sandpaper was used between the specimen and the gripping surfaces. Finer sandpapers, such as 180 and 320 grit, slipped at the specimen/grit interface. Failure at the grip edges occured in all unnotched specimens. Attempts were made to use end tabs, but aluminum and glass-epoxy tabs glued to several specimens with various high strength epoxies sheared off at high loads. Possible solutions to this gripping dilemma include testing only long, thin unnotched specimens with end tabs and replacing the worn down knurly surfaces of the grips with newer ones.

Monotonic Loading Tests

Monotonic tensile and compressive tests were done on both notched and unnotched specimens to determine initial material properties. In most cases, testing was performed under load control. Several tests were run in stroke control to avoid extensive post-failure damage. Specimens for stroke-controlled tests were first gripped when the machine was set in load control. This was necessary to avoid large loads induced in the specimen by the hydraulic gripping action. As the grips are closed, they pull the specimen in tension, but the machine registers no change in stroke. Under load control, internal feedback in the machine prevents the load from straying from the set point. However, in stroke control, since no change in stroke is registered during gripping, the machine will not adjust itself, and specimens could be easily damaged or broken in the process. After specimens were gripped in load control, the load, stroke, and strain were zeroed, the hydraulic power was turned off, and the machine was switched to stroke control. DC errors in the feedback were zeroed, load interlocks were set as a safety precaution, and the machine was turned back on. This procedure was very effective, as the axial loads induced by the grips remained well below 4 ksi (1 kip).

Sustained Incremental Loading Tests

A newly developed test method, referred to as the incremental loading test [52], was used to study damage development during sustained quasi-static loading. Early tests were done under load control, while more recent ones utilized strain control. Specimens for strain-controlled tests were gripped in the same manner described in the previous section for stroke-controlled testing. This method was used to insure that the proper load zero was maintained. During gripping, strain zeros are often shifted as much as 200 microstrain due to misalignment of the grips and accidental touching of the extensometer or rubber bands holding it in place.

In an incremental load-controlled test, a small load is applied on the specimen, and time is given for the material to 'creep.' As creep, or stress relaxation, occurs, the strain will increase as the load is held constant. These changes are very small and difficult to measure at low load levels. However, when a critical load (or strain) is reached, matrix cracking begins to occur throughout the specimen and material elongation is easier to observe. During a strain-controlled test, the load is allowed to decrease and material relaxation occurs while the strain is held constant. Figure 6 shows exaggerated stress-strain curves for a load and a strain control test. At this time, data collection and analysis has not yet been completely refined. Therefore, rather than concentrating on quantitative results, one must look at the basic trends observed during these incremental loading tests and seek to understand what these trends imply about material behavior.

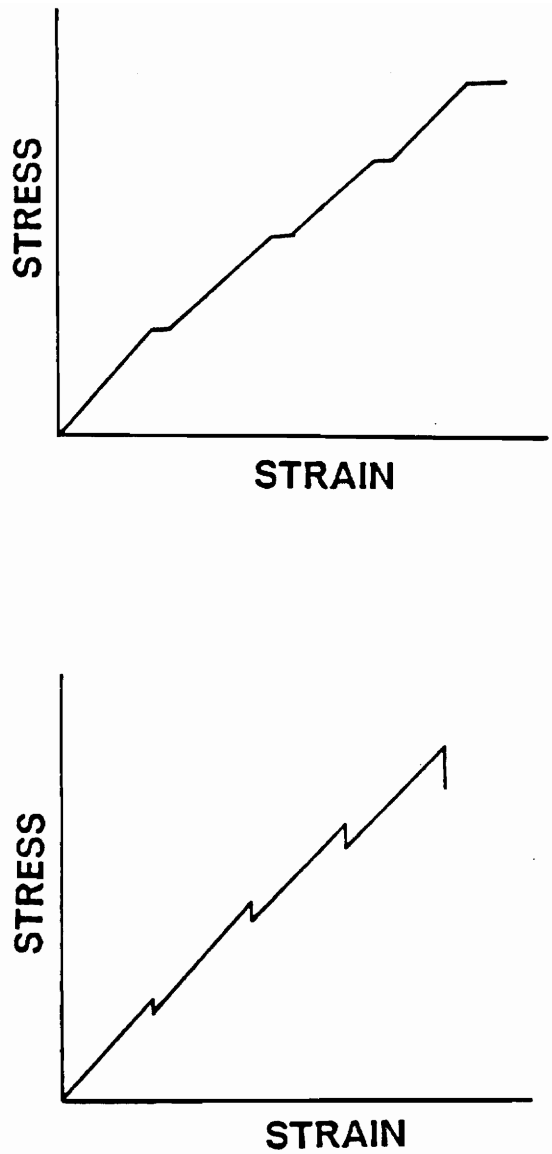

Figure 6. Stress-strain curves for (a) load controlled and (b) strain controlled incremental loading test.

Tension-Tension Fatigue Tests

Cyclic tension-tension fatigue tests were performed under load control on both notched and unnotched specimens. In all cases, the ratio of minimum to maximum load, or R, was 0.1. The first ten cycles were applied manually for stiffness monitoring purposes, while the remaining cycles were run at 10 Hz using a sine wave function generator. Stiffness monitoring, to be discussed in the Damage Evaluation section, was performed during the majority of the tests to determine the change in longitudinal stiffness with the number of loading cycles. Some fatigue tests were run to specimen failure to gather life data, while others were stopped for destructive evaluation of the specimen. Laminate deply and residual strength testing, also described in the Damage Evaluation section, were carried out after a prescribed number of cycles or change in stiffness.

Damage Evaluation

Various experimental methods were used to evaluate the state of damage in the material system before, during, and after mechanical loading was applied. These methods included both nondestructive and destructive techniques. On the following pages, a brief description of the damage evaluation techniques utilized in this study is presented. A more detailed description can be found in References [53,54].

Nondestructive Evaluation

Nondestructive evaluation refers to those methods used to examine damage in a material that do not affect the strength, stiffness, or life of that material. Nondestructive techniques are particularly useful in following damage initiation and growth in a single specimen throughout its life. The nondestructive evaluation methods used in this study include ultrasonic C-scan, stiffness monitoring, penetrant-enhanced X-ray radiography, and thermography.

Ultrasonic C-scan

As mentioned earlier, an ultrasonic C-scan was performed on all material before specimens were machined to check the quality of the panels. This nondestructive evaluation technique uses high frequency sound waves emitted by an ultrasonic transducer to give an estimate of damage. The degree of damage can be estimated, but individual types of damage cannot be identified. The material being examined is placed in a tank of water, a coupling medium which minimized losses in the ultrasonic signal. Sound waves are passed through the material and back, and the reflected signal is measured. Loss of amplitude of the sound waves, or attenuation, is associated with damage such as delaminations, voids, and inclusions.

Figure 7 shows a portion of a typical C-scan of a $(0)_{15}$ laminate done using a 5 MHz signal. The lightest areas correspond to the areas with the highest levels of attenuation. From this C-scan, it appears that the quality of the material is rather poor. Note the fine grid-like pattern and the larger white lines running vertically and horizontally. The fine markings are apparently due to the rough surface pattern found on all of the woven panels. The lines correspond to Kevlar tracer fibers used by the manufacturer to check ply orientations during layup. The white areas on this C-scan represent ultrasonic signals that are only 60% or less

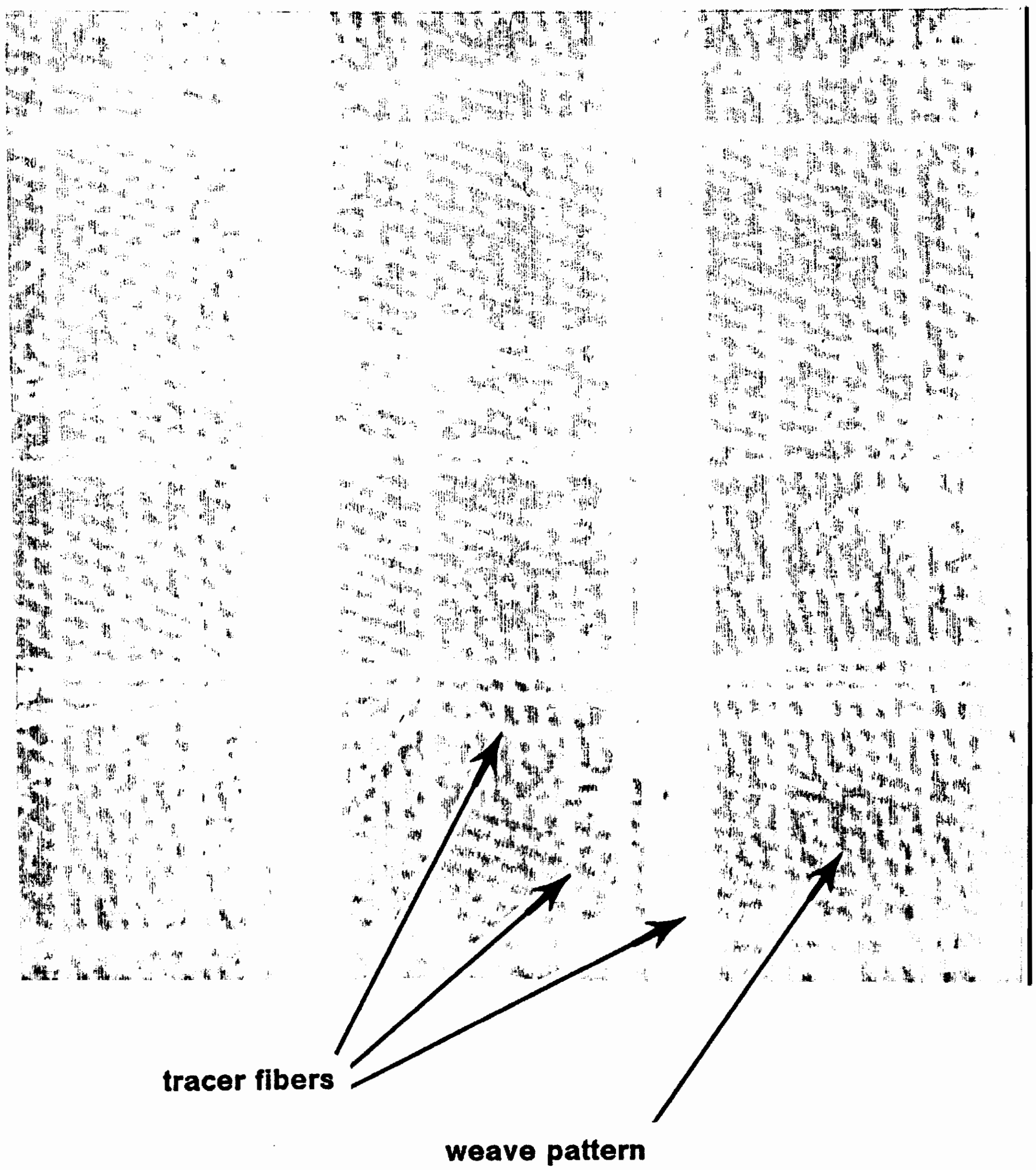

Figure 7. C-scan of a portion of a typical 15-ply 0 degree panel.

of the maximum reflected signals. The problem with using this evaluation method on woven material is that the damaged areas are difficult to distinguish from the non-damaged areas. Therefore, this technique was only used to screen panels for their relative initial quality. Several panels of material were rejected due to extremely high signal attenuation. In these rejected panels, maximum signal amplitudes were less than 10% of the amplitudes found in similar panels, probably due to a high void content.

Stiffness Monitoring

It has been shown that changes in stiffness can be used as a damage indicator in non-woven composites [55-59]. It was assumed that the same would hold true for woven composite materials. Therefore, longitudinal stiffnesses were recorded using a one inch MTS extensometer during all fatigue tests. For notched specimens, the extensometer was centered across the hole. It should be noted that for notched, non-woven composites, changes in stiffness have been found to depend on the gage length of the extensometer [60]. Because damage is more concentrated around the hole, the longer the gage length, the smaller the measured change in stiffness.

Secant stiffnesses were measured by interrupting the fatigue test and setting the load level to zero. If the strain zero had changed, it was reset to zero. The load was manually ramped up to the maximum cyclic stress, and the strain was recorded. The load was manually returned to zero and the strain checked. If the strain zero had shifted by 20 microstrain or less, this value was subtracted from the strain reading; if it was greater than 20 microstrain, a new measurement was made until the strain zero had stabilized. Shifts in the reference strain usually occured during the first few fatigue cycles and after the specimen had been replaced in the machine following X-ray radiography. This was attributed to the extensometer 'settling' into the v-notched tabs.

X-Ray Radiography

Penetrant enhanced X-ray radiography was used extensively in this study to examine the internal damage state of test specimens. When a zinc iodide penetrant solution was applied to specimen edges (and notch, if present), matrix cracks and delaminations which intersect these surfaces in any way would soak up the low surface tension fluid and become opaque to X-rays. Such areas prevent an X-ray beam from reaching the X-ray sensitive film and appear as dark areas on the radiograph.

Radiographs were taken with a cabinet X-ray system. Both double emulsion (Kodak M-5) and single emulsion (Kodak SR-5) X-ray films were used. A tube voltage of 30 kV was used for front views, while 90 kV was needed for edge views. The tube current ranged from 2 to 3 milliamps. Exposure times varied between 0.5 and 3 minutes, depending on the specimen width or thickness and the type of view and film used. Exposures were about 2 to 3 times longer for the single emulsion film than for the double emulsion film.

The penetrant solution consisted of the following:

- 60 grams zinc iodide (ZnI_2)
- 10 milliliters water
- 10 milliliters isopropyl alcohol
- 10 milliliters Kodak Photo-Flo 200

It was found that the solution penetrated damage in the hole area of notched fatigue specimens well if applied to the specimen during cyclic loading. Due to the highly corrosive nature of the penetrant, the specimen edges were not easy to wet without risking harm to the grips. Therefore, when details of the edge damage were important, as with unnotched specimens, sufficient time was needed to allow the solution to seep into matrix cracks. It was found that if specimen edges were kept moist with the zinc iodide for 24 hours, virtually all of the cracks could be seen on the radiographs.

Figure 8 shows a damaged fatigue specimen X-rayed after 5500 load cycles. The two dark areas above and below the hole are the aluminum tabs and rubber cement which hold the extensometer in place, while the thick dark lines are the Kevlar tracer fibers. In the first radiograph, the penetrant was applied at the notch prior to cycling and at the edges for several minutes after the specimen was removed from the testing machine. The second radiograph shows the same specimen after its edges and notch were kept moist with the penetrant for 24 hours with no additional loading. Note the extensive matrix cracking at the free edges that is now visible. The notch area remained about the same as it was in the previous picture. This time dependence was not discovered until late in the test program. Therefore, it should be kept in mind that in some of the radiographs, edge damage may be more extensive than it appears to be.

Thermography

When a material is elastically deformed, it generates heat, resulting in small but measurable change in temperature. Because this temperature change is related to the sum of the principle strains [61], thermographic techniques can be used to monitor the redistributions of strain fields in a specimen subjected to fatigue loading. Analytical predictions and experimental measurements of the thermoelastic response of graphite-epoxy laminates have been done successfully [62].

The Ometron SPATE (Stress Pattern Analysis by the measurement of Thermal Emission) 8000 system used in this study relied on an infrared camera to measure the local surface temperatures of a specimen. A thin coating of flat black paint insured a uniformly high thermal emissivity over the entire area scanned. Thermographic scans were taken while the speci-

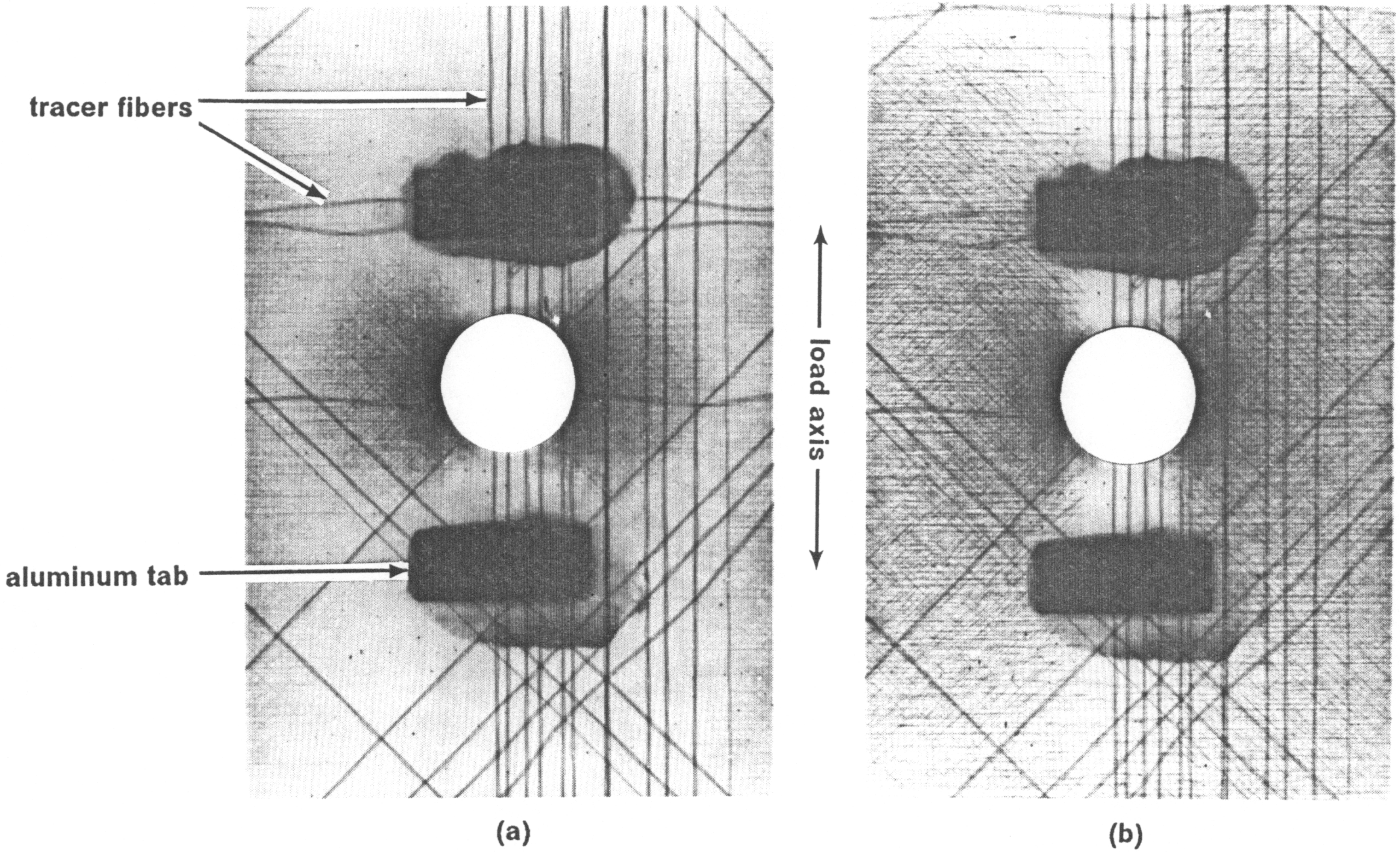

Figure 8. An X-ray radiograph taken (a) before and (b) after zinc iodide was applied for 24 hours.

men was fatigued at a reduced stress level low enough to prevent further damage growth in the material during the scan. Thermal signals detected at the loading frequency of 10 Hz were displayed on a color monitor and were stored for later use. It should be noted that because the thermal conductivity of graphite-polyimide is relatively low, the surface temperatures of the composite laminate primarily reflect the behavior of the surface ply.

Destructive Evaluation

Two destructive evaluation techniques, residual strength testing and laminate deply, were used to obtain additional information about damage. These techniques result in the destruction of the specimen and can, therefore, only be used once during the life of a specimen. Nondestructive methods such as stiffness monitoring and X-ray radiography can be used to estimate the percentage of fatigue life that has been reached prior to destructive testing. This allows material behavior to be evaluated as a function of life when several specimens are tested.

Residual Strength Tests

After a predetermined change in stiffness or number of fatigue cycles, several specimens were tested for residual tensile strength. This quasi-static strength measurement was used to determine the effect of damage on the strength of a specimen. Initial strength was assumed to be equal to the mean strength of similar 'virgin' specimens tested under similar monotonic loading conditions. As with other monotonic tests, the load was manually ramped up until the ultimate failure of the specimen. The strain was recorded during all tests with a one inch MTS extensometer.

Laminate Deply

Laminate deply was used to determine the extent of fiber fracture in a specimen. In this technique, the majority of the matrix material is burned off of a laminate so that individual plies may be separated and examined. Because polyimide is a high temperature matrix, deplying was difficult to perform. Specimens were heated to 1112°F (600°C) in a tube furnace and held at that temperature for at least 5 hours. In some cases, additional heating was required to separate the inner plies after the first few surface plies had been removed. Following deply, the individual woven plies were examined for fiber fracture in a scanning electron microscope.

III. EXPERIMENTAL RESULTS AND DISCUSSION

Basic Material Properties

Monotonic Tests

The results of monotonic tensile tests performed on unnotched $(0)_{15}$, $(0)_{22}$, and $(0,45,0,-45,0,0,-45,0,45,0)_{2}$ specimens are presented in Table 1. Several coupons from each stacking sequence were loaded to failure as longitudinal strains were measured with a one inch extensometer. All unnotched specimens failed at the grips.

The $(0)_{15}$ and $(0)_{22}$ specimens had very similar mean tensile strengths of 105.6 and 105.0 ksi, respectively, showing that the thickness did not significantly affect the strength of these two laminates. The thinner specimens, having an average modulus of 9.7 msi, broke at an average strain of 10,900 microstrain. The thicker specimens had an axial modulus of 10.9 msi and strain to failure of 10,900 microstrain. Stress-strain curves were linear to failure and did

Table 1. Unnotched Tensile Properties

Layup	Specimen	Strength (ksi)	Failure Strain[1] (microstrain)	Axial Modulus (msi)
$(0)_{15}$	A1-1	109.1	10900	10.0
	A2-11	102.9	10700	9.66
	A2-12	104.7	11200	9.35
	Ave.	105.6	10900	9.67
$(0)_{22}$	1C-1	109.7	--	11.2
	1C-2	100.1	--	--
	V1-1	105.2	9800	10.7
	Ave.	105.0	9800	10.9
20-ply[2] Balanced	2A-9	83.3	10900	7.64
	2-6	84.9	12400	6.85
	Ave.	84.1	11650	7.25

[1] Measured with a 1 in. extensometer.
[2] Laminate stacking sequence was $(0,45,0,-45,0,0,-45,0,45,0)_2$

not show any discontinuities prior to failure as observed by Lagace [32] in woven and non-woven graphite-epoxy cross-ply laminates (0,90 deg. plies), possibly because the specimens did not fail in the gage length section. Longitudinal strains on both the front and back of a thick and a thin unnotched 0 deg. specimen were measured simultaneously during monotonic tension tests. It was found that the measured strain to failure was independent of which side the extensometer was mounted on.

Table 2 gives a comparison of tensile strengths for woven and non-woven cross-ply laminates having fibers in the 0 deg. and 90 deg. directions. It should be kept in mind that the coupons tested in this study are much thicker than those in any of the references, and thickness has been shown to affect fracture behavior in non-woven graphite-epoxy. Thicker laminates may be weaker or stronger than their thinner counterparts, depending on the interlaminar stresses associated with the stacking sequence.[62]

From the data presented in Table 2, it can be seen that a woven cross-ply laminate is generally weaker than the equivalent non-woven version when loaded in monotonic tension. Differences in unnotched tensile strength of 15-25% were noted between tape and cloth material; however, in most of the comparisons, the fiber and resin systems were not identical. When comparing the woven Celion 3000/PMR-15 from this study and the non-woven Celion 6000/PMR-15 tested by Garber and Morris [4], it appears that the woven material (105 ksi), having 50% of its fibers in the 0 deg. direction and 50% in the 90 deg. direction, is approximately half as strong as the non-woven material (210 ksi) having all of its fibers in the 0 deg. direction. This suggests that the cloth material is as strong as the tape material, however, since graphite-polyimide was in the early stages of development when tested by Garber and Morris [4] in 1982, it is quite possible that the properties of the non-woven graphite-polyimide composites are actually much higher.

Table 2. **Comparison of Tensile Strengths of Woven and Non-woven Cross-ply Laminates**

Material[1] [Ref.]	Layup[2]	Architecture	Unnotched Strength ksi (MPa)	Ratio of Notched to Unnotched Strength
T300/BSL914C [31]	$((0)_S)_S$	5-hs. satin cloth	86.6(597)	0.53[3]
		tape	104(714)	0.66[3]
T300/934 [29]	$(0)_8$	8-hs. satin cloth	93.5(645)	--
HTA/MY720 [29]		tape	123(850)	--
graphite/MY720 [13]	$(0)_S$	5-hs. satin cloth	81.9(565)	0.40[4]
		tape	102(701)	0.48[4]
HMF330C/34 [33]	$(0)_{4S}$	8-hs. satin cloth	103(709)	0.46[5]
T300/5208 [33]		tape	92.4(637)	0.57[6]
C3000/PMR-15[7] [this study]	$(0)_{15}$	8-hs. satin cloth	106(737)	0.60[8]
	$(0)_{22}$	8-hs. satin cloth	105(723)	0.59[8]
C6000/PMR-15[7] [4]	$(0)_8$[9]	tape	210(1450)	--
	$(90)_8$[9]	tape	4.02(27.7)	--

[1] Materials are graphite-epoxies unless otherwise specified.

[2] Refers to cloth layup unless otherwise specified; equivalent tape layups are found by replacing each cloth ply with a (0,90) tape ply.

[3] Notched specimens were 0.787 in. (20mm) wide with a 0.157 in. (4mm) diameter center hole.

[4] Notched specimens were 1.97 in. (50mm) wide with a 0.393 in. (10mm) long sharp center notch.

[5] Notched specimens were 5.0 in. (127mm) wide with a 1.0 in. (25.4mm) diameter center hole.

[6] Notched specimens were 1.0 in. (25.4mm) wide with a 0.25 in. (6.35mm) long sharp center notch.

[7] A graphite-polyimide composite.

[8] Notched specimens were 1.5 in. (38.1mm) wide with a 0.375 in. (9.53mm) diameter center hole.

[9] Refers to the tape layup.

The 8-harness satin specimens from this study (105 ksi) were very similar in tensile strength to 8-harness $(0)_{4s}$ graphite-epoxy (103 ksi) tested by Bailie et al [33]. Both were stronger than another 8-harness graphite-epoxy $(0)_8$ laminate (94 ksi) [29] and two 5-harness satin materials, a $(0)_{ss}$ laminate (86.6 ksi) [31] and a (0,90) laminate (81.9 ksi) [13].

The $(0,45,0,-45,0,0,-45,0,45,0)_2$ specimens had an average unnotched tensile strength of 84.1 ksi. This laminate was not as stiff as the 0 deg. laminates, having a mean axial modulus and strain to failure of 7.3 msi and 11,650 microstrain, respectively. Stress-strain curves were linear until the last 10-15% of life, when cracking could be heard, possibly a result of grip-induced damage in the 0 deg. surface plies.

A comparison of tensile strengths for woven and non-woven balanced laminates containing fibers in the 0, 90, and +/-45 deg. directions is presented in Table 3. Once again, the specimens tested in this study are much thicker than those used in other studies. No data on tensile strengths of laminates equivalent to the woven $(0,45,0,-45,0,0,-45,0,45,0)_2$ graphite-polyimide could be found, so the proportion of fibers in each direction must be kept in mind when comparing tensile strengths.

As with the cross-ply laminates, in general, the woven balanced composites were not quite as strong as similar non-woven ones. The woven Celion 3000/PMR-15, having 30% 0 deg., 30% 90 deg., 20% 45 deg., and 20% -45 deg. fibers, compared favorably with non-woven graphite-polyimide [4] and woven graphite-epoxy [13,31,33]. Having only 5% more 0 deg. fibers than various 5- and 8-harness satin graphite-epoxy laminates, the 8-harness graphite-polyimide was 15-25% stronger under monotonic tensile loading.

Table 4 lists monotonic tensile properties of notched $(0)_{15}$, $(0)_{22}$, and $(0,45,0,-45,0,0,-45,0,45,0)_2$ laminates. Two to three tests were run on each layup. Axial strains were measured with a one inch extensometer centered across the hole. Strengths

Table 3. Comparison of Tensile Strengths for Woven and Non-woven Balanced Laminates

Material[1] [Ref.]	Layup[2]	Architecture	Unnotched Strength ksi (MPa)	Ratio of Notched to Unnotched Strength
T300/BSL914C [31]	$(0,45)_S$	5-hs. satin cloth	62.6(432)	0.54[3]
		tape	81.9(565)	0.62[3]
	$(45,0)_S$	5-hs. satin cloth	62.6(432)	0.57[3]
		tape	66.5(459)	0.71[3]
graphite/MY720 [33]	$(0,45)_S$	5-hs. satin cloth	65.7(453)	0.45[4]
		tape	81.2(560)	0.50[4]
HMF330C/34 [33]	$(0,45)_{2S}$	8-hs. satin cloth	70.2(484)	0.49[5]
	$(0,45,0,0)_{2S}$	8-hs. satin cloth	86.1(594)	0.54[5]
T300/5208 [33]	$(0,\pm 45,90)_{2S}$[6]	tape	71.6(494)	0.45[7]
C3000/PMR-15[8] [this study]	$(0,45,0,-45,0,-0,-45,0,45,0)_2$	8-hs. satin cloth	84.1(580)	0.62[9]
C6000/PMR-15[8] [4]	$(0,45,90,-45)_{2S}$[6]	tape	46.2(319)	0.69[10]
	$(45,0,-45,0)_S$[6]	tape	61.4(423)	0.62[10]

[1] Materials are graphite-epoxies unless otherwise specified.

[2] Refers to cloth layup unless otherwise specified; equivalent tape layups are found by replacing each cloth ply with a (0,90) tape ply.

[3] Notched specimens were 0.787 in. (20mm) wide with a 0.157 in. (4mm) diameter center hole.

[4] Notched specimens were 1.97 in. (50mm) wide with a 0.393 in. (10mm) long sharp center notch.

[5] Notched specimens were 5.0 in. (127mm) wide with a 1.0 in. (25.4mm) diameter center hole.

[6] Refers to the tape layup.

[7] Notched specimens were 1.0 in. (25.4mm) wide with a 0.25 in. (6.35mm) long sharp center notch.

[8] A graphite-polyimide composite.

[9] Notched specimens were 1.5 in. (38.1mm) wide with a 0.375 in. (9.53mm) diameter center hole.

[10] Notched specimens were 1.0 in. (25.4mm) wide with a 0.188 in. (4.76mm) diameter center hole.

Table 4. Notched Tensile Properties

Layup	Specimen	Strength[1] (ksi)	Failure Strain[2] (microstrain)	Ratio of Notched to Unnotched Strength
$(0)_{15}$	A1-13	64.2	15600	0.61
	A2-2	63.3	14800	0.59
	Ave.	63.8	15200	0.60
$(0)_{22}$	1C-13	61.2	13560	0.59
	1C-15	62.4	13030	0.60
	1B-14	62.9	13500	0.60
	Ave.	62.4	13360	0.60
20-ply[3] Balanced	2A-18	52.7	10150	0.63
	2A-14[4]	49.9	10090	0.59
	2-9	52.9	--	0.63
	Ave.	51.8	10120	0.62

[1] Calculated using gross cross-sectional area.
[2] Measured with a 1 in. extensometer centered across hole.
[3] Laminate stacking sequence was $(0,45,0,-45;0,0,-45,0,45,0)_2$
[4] Test was run under stroke control.

were calculated using the gross cross-sectional area and an isotropic finite width correction factor [38] of 7.6%. All notched specimens failed through the center hole.

As was the case with the unnotched coupons, the notched $(0)_{15}$ and $(0)_{22}$ laminates had similar strengths but different strains to failure. Average tensile strengths of 63.8 and 62.4 ksi and average strains to failure of 15,200 and 13,400 microstrain were measured for the $(0)_{15}$ and $(0)_{22}$ specimens, respectively. Stress-strain curves were slightly nonlinear, with a decrease in slope occurring at approximately half of the ultimate strength. Figure 9 shows a typical stress-strain curve recorded during a tensile test performed on a $(0)_{22}$ coupon.

The $(0,45,0,-45,0,0,-45,0,45,0)_2$ laminate had an average notched tensile strength of 51.8 ksi and an average strain to failure of 10,100 microstrain. It is interesting to note that this material had a lower notched strain to failure than either 0 deg. laminate. Stress-strain curves for the $(0,45,0,-45,0,0,-45,0,45,0)_2$ layup were similar to those of the $(0)_{15}$ and $(0)_{22}$, as shown in Figure 9, with nonlinear response evident after about half of the ultimate strength was reached.

A series of notched compressive tests was performed on $(0)_{22}$ and $(0,45,0,-45,0,0,-45,0,45,0)_2$ coupons to find a suitable unsupported length for future tension-compression fatigue tests. This procedure, described by Bakis et al [63], involves measuring the compressive strength of specimens with various lengths. If the strength is independent of the unsupported length, it is highly probable that a crushing, rather than a buckling, failure has occurred as desired. For 32-ply quasi-isotropic tape laminates (0.165 in. thick, 1.5 in. wide, with a 3/8 in. diameter center hole), unsupported lengths of 2.4 in. to 2.5 in. allowed crushing failure in graphite-epoxy and graphite-PEEK [63].

Based on this data and on the fact that the woven 20- and 22-ply specimens (0.27 in. to 0.29 in. thick) were much thicker than the 32-ply tape specimen (0.165 in.), woven $(0)_{22}$ and $(0,45,0,-45,0,0,-45,0,45,0)_2$ coupons with unsupported lengths between 2.375 in. and 3.375

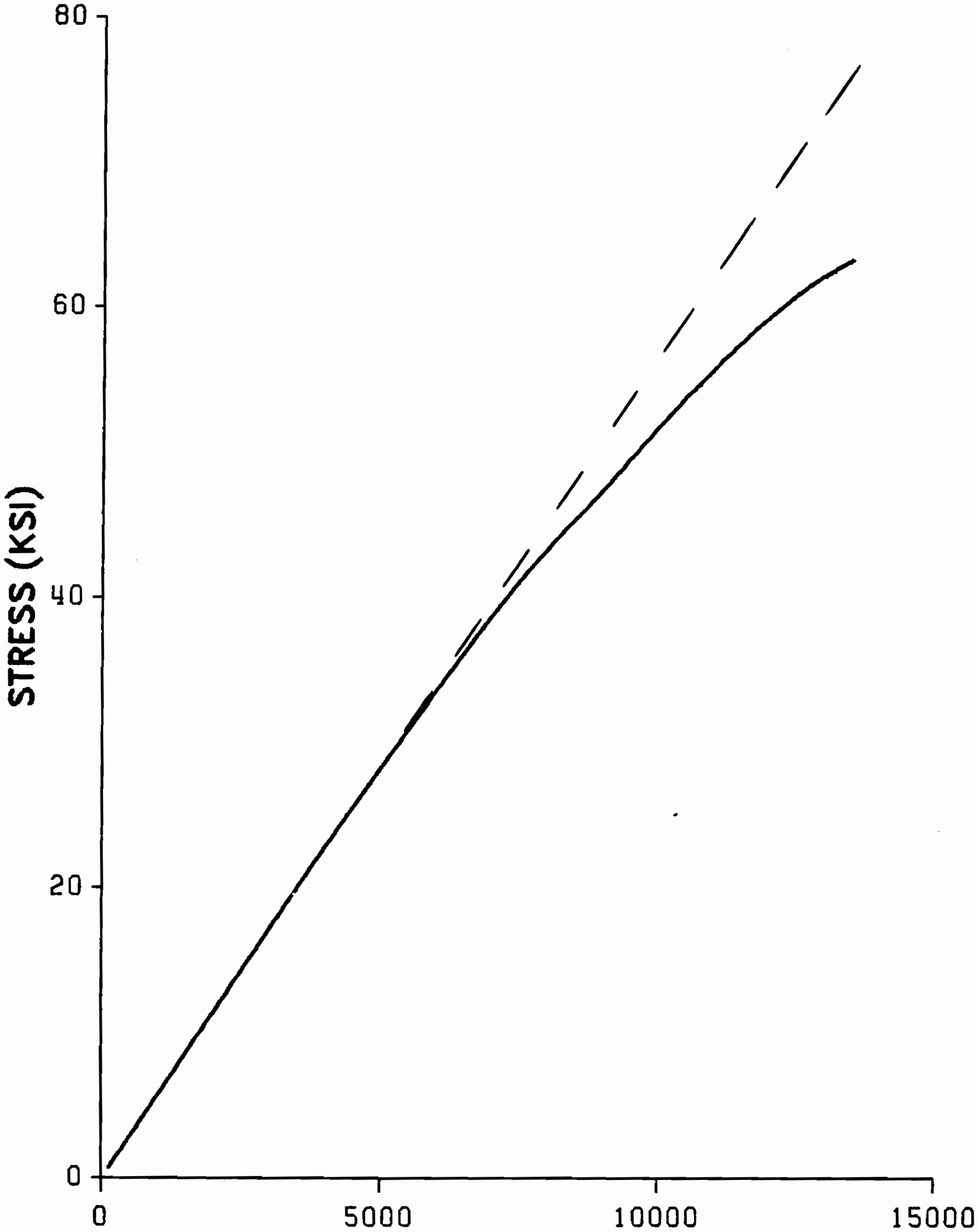

Figure 9. Stress-strain curve for a 22-ply 0 deg. notched coupon.

Table 5. Notched Compressive Properties

Layup	Specimen	Unsupported Length(in.)	Strength[1] (ksi)
$(0)_{22}$	1C-14	2.375	51.4
	1C-16	2.875	48.6
	1C-18	3.375	47.9
20-ply[2] Balanced	2A-13	2.375	43.7
	2A-16	3.125	48.6
	2A-17	3.188	42.5

[1] Calculated using gross cross-sectional area.
[2] Laminate stacking sequence was $(0,45,0,-45,0,0,-45,0,45,0)_2$

in. were tested. As is evident from the results in Table 5, no significant dependence of compressive strength on length was observed in either laminate. Strengths of about 50 and 45 ksi were measured for the $(0)_{22}$ and $(0,45,0,-45,0,0,-45,0,45,0)_2$ specimens, respectively. For non-woven $(0,45,90,-45)_{s4}$ T300/PEEK and T300/5208, notched compressive strengths of specimens having similar geometries to the specimens tested in this study were about 42 ksi and 41 ksi, respectively.

Sustained Incremental Loading Tests

A summary of sustained incremental loading tests performed on unnotched $(0)_{22}$ and $(0,45,0,-45,0,0,-45,0,45,0)_2$ coupons is presented in Table 6. Half of the tests were performed under load control, the other half under strain control. Each test lasted for approximately 40 to 50 hours. From Table 6, it is evident that the two layups behave quite differently during an incremental loading test. The $(0)_{22}$ specimens showed small decreases in stiffness of 3% or less late in life and failed at loads up to 10% lower than the original unnotched tensile strength measured on similar specimens. The $(0,45,0,-45,0,0,-45,0,45,0)_2$ coupons showed larger decreases in stiffness of up to 10% prior to failure, and at failure, exhibited increases in residual tensile strength of 7-14%. As will be discussed in a later section, the $(0,45,0,-45,0,0,-45,0,45,0)_2$ specimens develop quite a bit of damage under sustained loading which is similar to the damage observed during tension-tension fatigue. From the trends seen in incremental tensile strength, it appears that the damage developing in the unnotched $(0)_{22}$ material is primarily strength degrading, whereas the damage in the $(0,45,0,-45,0,0,-45,0,45,0)_2$ is acting in some manner as to increase strength.

A plot showing the behavior of an unnotched $(0,45,0,-45,0,0,-45,0,45,0)_2$ specimen subjected to strain-controlled sustained incremental loading is presented in Figure 10. Here, the change in stress at a given constant strain is plotted versus strain. The triangles are

Table 6. Sustained Incremental Loading Test Results

Layup	Specimen	Strength[1]	Final Modulus[2]	Type of Test
$(0)_{22}$	1C-9	89.4	97.	load control
	1C-12	93.7	99.	strain control
20-ply[3] Balanced	2-10	109.	89.	load control
	2-8	114.	96.	load control
	2-17	112.	96.	strain control
	2-18[4]	107.	--	strain control

[1] Percent of unnotched tensile strength of similar specimens.
[2] Percent of original axial modulus.
[3] Laminate stacking sequence was $(0,45,0,-45,0,0,-45,0,45,0)_2$
[4] Specimen was removed from machine and X-rayed several times and did not fail at the maximum load.

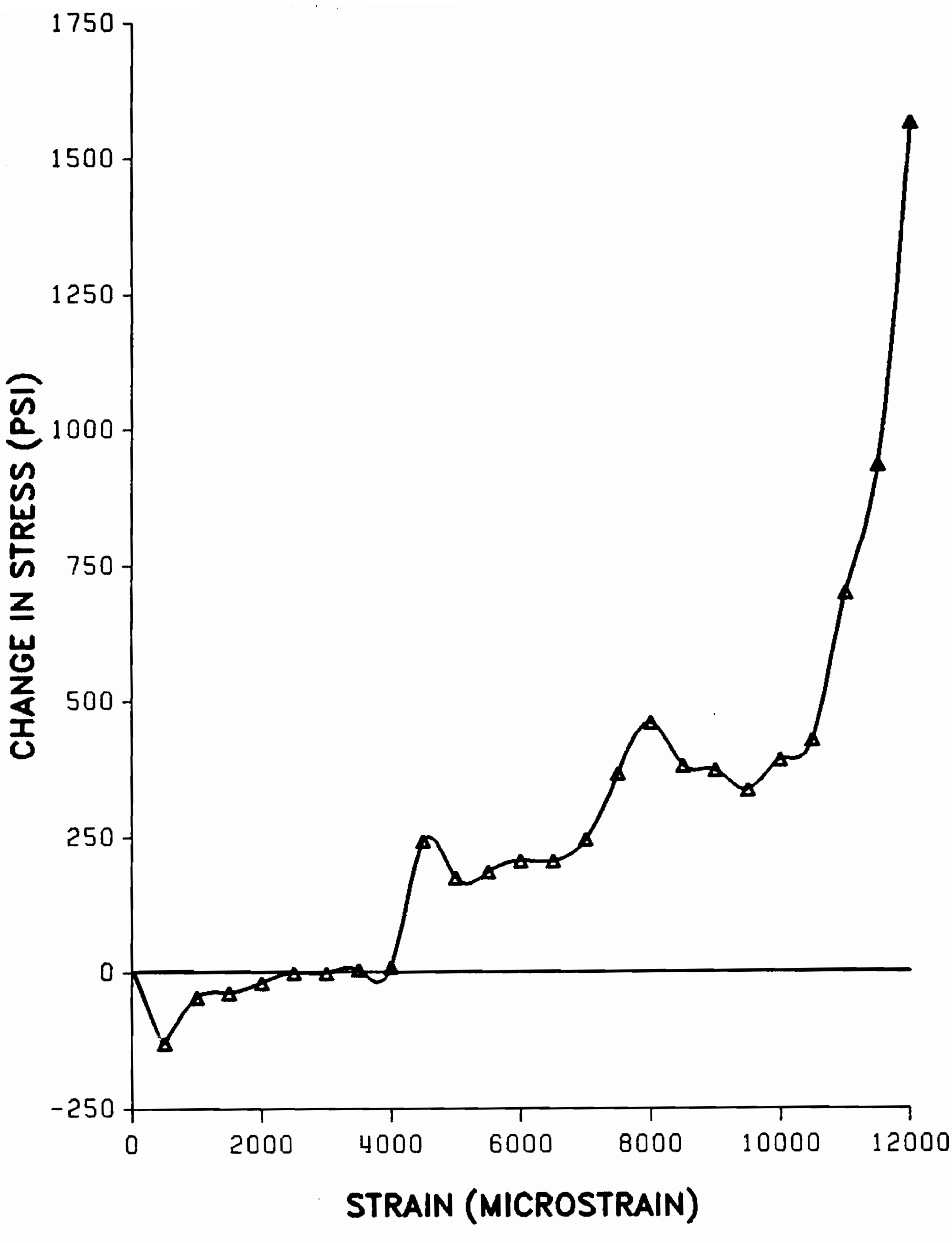

Figure 10. Incremental loading test response of an unnotched 20-ply 0/45 deg. laminate.

points at which relaxation data were taken. Several peaks appear on the curve which are believed to correspond to distinct stages in damage development, to be discussed in the Damage Mechanisms section. As mentioned earlier, problems in data collection are evident from the results. In the early region of the test, between 0 and 2,000 microstrain, the specimen appears to be getting stiffer, disobeying the basic laws of physics. It is believed that instabilities in the electronic equipment at such low strain settings were, in part, responsible for the abnormalities in the curves. From X-ray radiographs, it was concluded that no damage occurs in this early region, and the damage dependent change in stress should remain approximately zero until about 4,000 microstrain when the first matrix cracks are observed. However, non-damage related, but time dependent response could contribute to the stress changes recorded early in the life. Such changes would appear as positive stress changes in Figure 10.

Tension-Tension Fatigue Tests

Stress-life data for unnotched $(0)_{22}$ and $(0,45,0,-45,0,0,-45,0,45,0)_2$ material are summarized in Table 7. Because tabs could not be successfully bonded to specimen ends, all unnotched fatigue specimens failed due to grip-induced damage. Although every ply did not fail at the grips, 0 deg. fibers in both surface plies broke prior to failure in all specimens. Grip pressures between 1100 and 1200 psi were required to prevent coupons from slipping.

Figure 11 demonstrates the harmful effect of the grip. Note the large number of fiber fractures at the grip edge and 0.025 in. (10 mm) outside of the grips in two SEM micrographs. This $(0)_{22}$ specimen was deplied after 1.2 million fatigue cycles at 70% of the ultimate tensile strength, prior to any sign of impending fatigue failure. One would expect the fatigue lives of the unnotched specimens to be considerably higher if grip-induced damage could be avoided.

Table 7. Unnotched Tension-Tension Fatigue Results

Layup	Specimen	Maximum Stress[1]	Cycles to Failure
$(0)_{22}$	1C-4	80.	460
	1C-6	75.	2500
	1C-5	75.	12900
	1C-7	70.	720000
	1C-3	70.	1.2 M+
	1C-8	65.	1.4 M+
20-ply[2] Balanced	2-5	97.	410
	2-7	88.	3300
	2-4	88.	21500
	2-3	84.	150000
	2-2	79.	640000
	2-9	75.	940000
	2-1	71.	1.2 M+

[1] Percent of ultimate unnotched tensile strength.
[2] Layup was $(0,45,0,-45,0,0,45,0,-45,0)_2$.
+ Refers to runnouts.

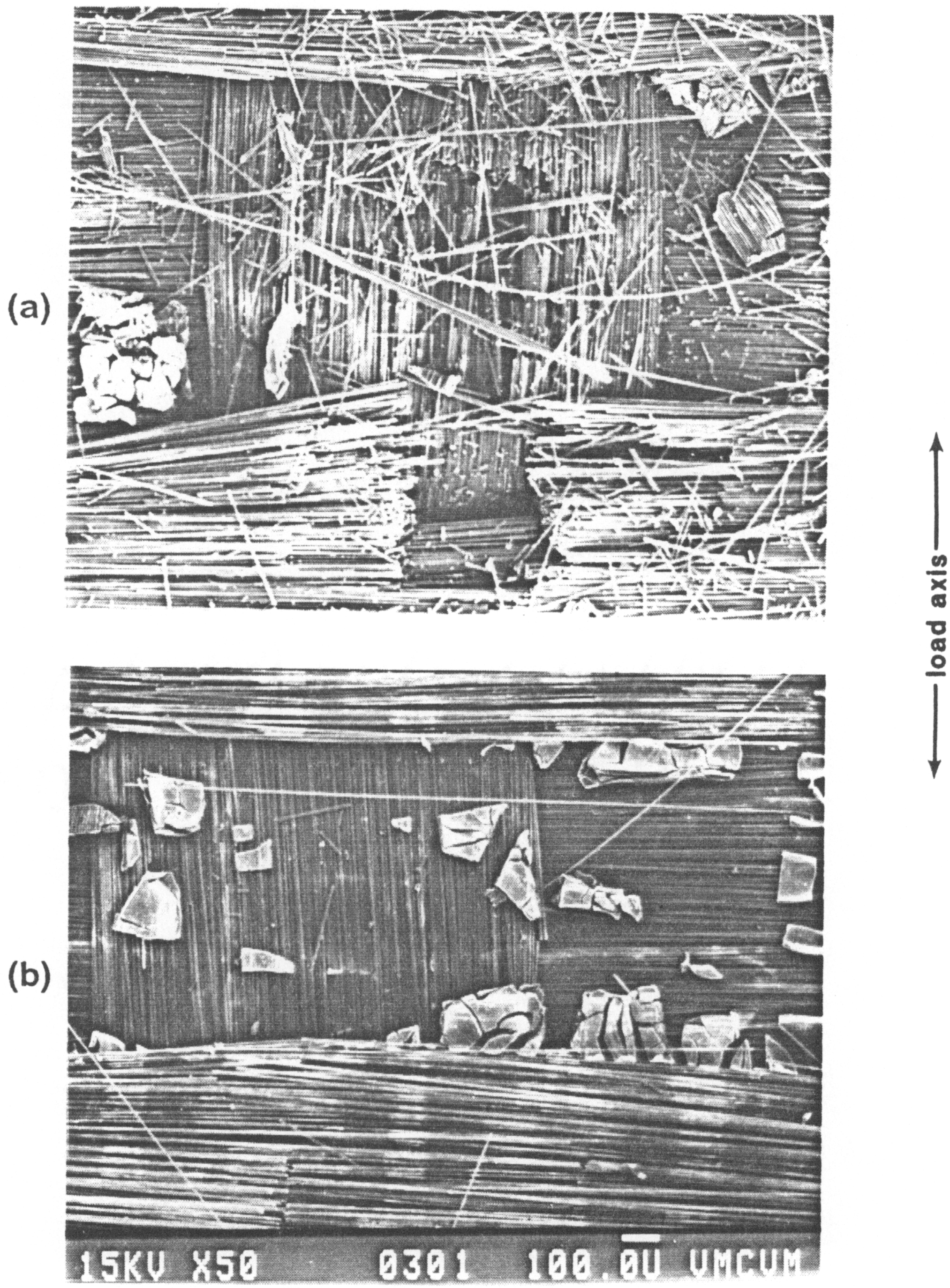

Figure 11. SEM micrographs of deplied surface plies of an unfailed 22-ply 0 deg. specimen (a) at the grip edge and (b) 0.025 in. away.

From Table 7, it can be seen that for the $(0)_{22}$ specimens, maximum stress levels of 90% and 70-75% of the unnotched tensile strength were required for lives on the order of 10^3 and 10^6 cycles, respectively. For the $(0,45,0,-45,0,0,-45,0,45,0)_2$ material, fatigue lives of 10^3 and 10^6 cycles corresponded to maximum stress levels of about 90% and 75% of the tensile strength. Fatigue failure occurred after a decrease in stiffness of about 10% to 25% for the $(0,45,0,-45,0,0,-45,0,45,0)_2$ and 5% to 10% for the $(0)_{22}$ laminates. When cycled at a given percentage of their strength, the $(0,45,0,-45,0,0,-45,0,45,0)_2$ specimens had longer fatigue lives than did the $(0)_{22}$ material. However, since the $(0)_{22}$ laminate was tested first and new gripping methods were being developed on this material, damage due to the slipping of specimens and unsuccessful tabbing attempts must have had a detrimental effect on fatigue performance.

Three stages of damage development based on stiffness change have previously been described for non-woven graphite-epoxy [54], and graphite-polyimide [50] and for 8-harness woven graphite-epoxy [29]. Stage I involves a significant drop in stiffness over a relatively short percentage of life, about 7-10% for non-woven graphite-polyimide [50] and 5-15% for non-woven graphite-epoxy. A levelling off of stiffness occurs in Stage II. The final stage, Stage III, involves another sharp decrease in stiffness over a short period of loading, lasting approximately 10-15% of life for both non-woven graphite-polyimide [50] and graphite-epoxy [54]. These stages were not quite as distinct for the 8-harness woven graphite-epoxy [29].

Two curves for $(0)_{22}$ unnotched coupons are shown in Figure 12. The normalized stiffness is the measured stiffness divided by the original stiffness, while the normalized life is the fraction of cycles to failure. One specimen (triangular data points), failing after 410 cycles and a decrease in stiffness of less than 10%, did not show much of a change in stiffness until the last 5% of life. The other specimen (square data points), which failed after 27,000 cycles, dropped only 2% in stiffness over its entire life, giving no warning of impending failure. The notched 0 deg. material had a much higher change in stiffness than did the unnotched material, with a total drop in modulus of about 15% to 25% at failure. A stiffness-life curve for

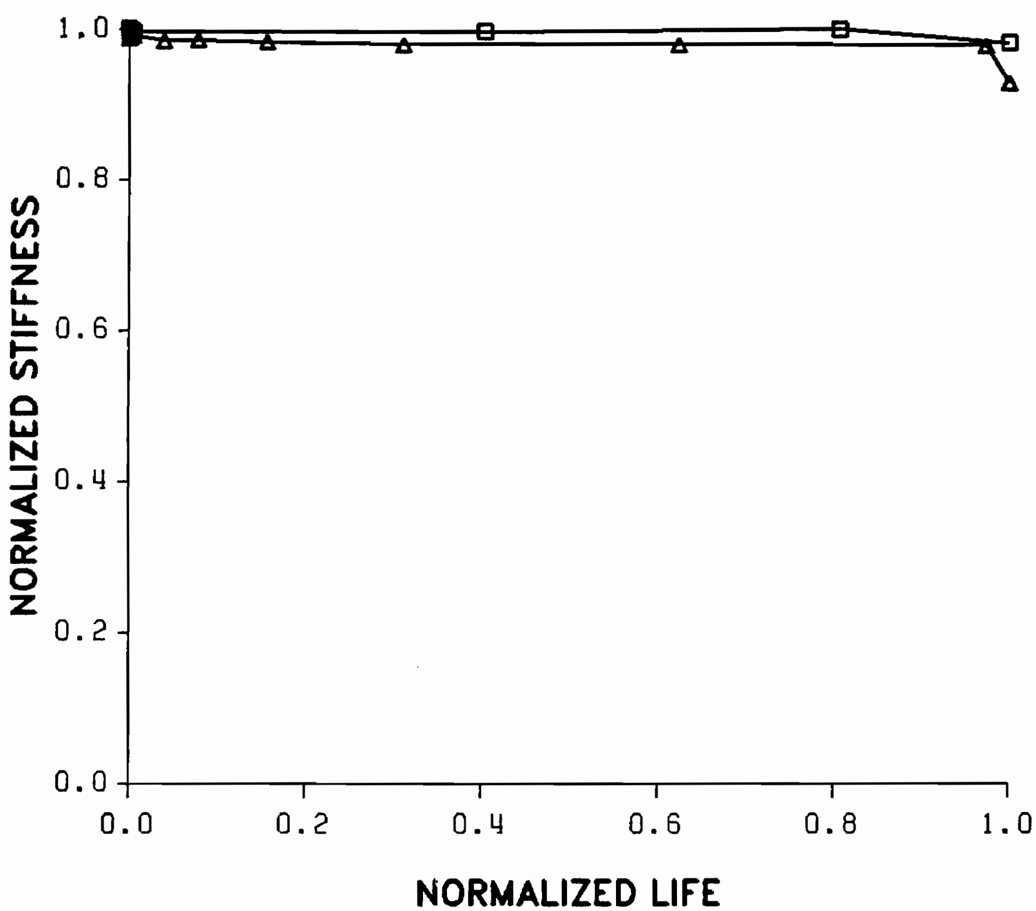

Figure 12. Stiffness-life curves of unnotched 22-ply 0 deg. specimens having lives of 460 (triangles) and 25000 (squares) cycles.

a notched $(0)_{22}$ is shown in Figure 13. The notched material shows more of the 3-stage behavior [50,54] than does the unnotched material. However, in this case, Stage III was not distinct, possibly because strain measurements were not taken close enough to failure to detect the final sharp decline in stiffness.

Figure 14 shows normalized stiffness-life curves for three unnotched $(0,45,0,-45,0,0,-45,0,45,0)_2$ specimens having lives on the order of 10^5 to 10^6 cycles. As can be seen from this figure, the stiffness-life curves for these coupons vary greatly. One specimen failed after a drop in stiffness of 25%, while the other two failed after a 10% drop in stiffness. The three curves also had different shapes. The plot for a specimen failing after 825,000 cycles, represented by triangular data points, showed a steady drop in stiffness throughout life, similar to that described for 8-harness woven graphite-epoxy [29]. Another specimen, whose stiffness-life curve has diamond shaped data points, exhibited the three distinct stages reported for non-woven graphite-epoxy [54] and graphite-polyimide [50] during its life of 638,000 cycles. The third specimen, which failed after 150k cycles, showed only a very slow decline in stiffness throughout its entire life. Clearly, the repeatability of this data is poor, probably due to the grip-related failure mechanisms which occurred in the unnotched coupons. If grip-related failures could be eliminated, normalized stiffness-life curves could possibly be independent of the applied stress and the number of cycles to failure. The stiffness-life behavior of the notched $(0,45,0,-45,0,0,-45,0,45,0)_2$ specimens, in which failure did not involve the gripped area, tended to exhibit the 3 stages described by Refs.[50,54]. An example of such a curve is shown in Figure 15. The specimen in this figure failed after 27,000 cycles.

Figure 16 shows a comparison of unnotched tension-tension fatigue stress-life data for the 8-harness satin $(0)_{22}$ coupons from this study and 5-harness satin (tabbed) graphite-epoxy [31], 8-harness graphite-epoxy (untabbed) [29], and 8-harness graphite-PEEK (tabbed) [40]. The plotted values of stress are the maximum applied stresses normalized by the unnotched tensile strength of the material. Data points with arrows denote runnouts. Because of the

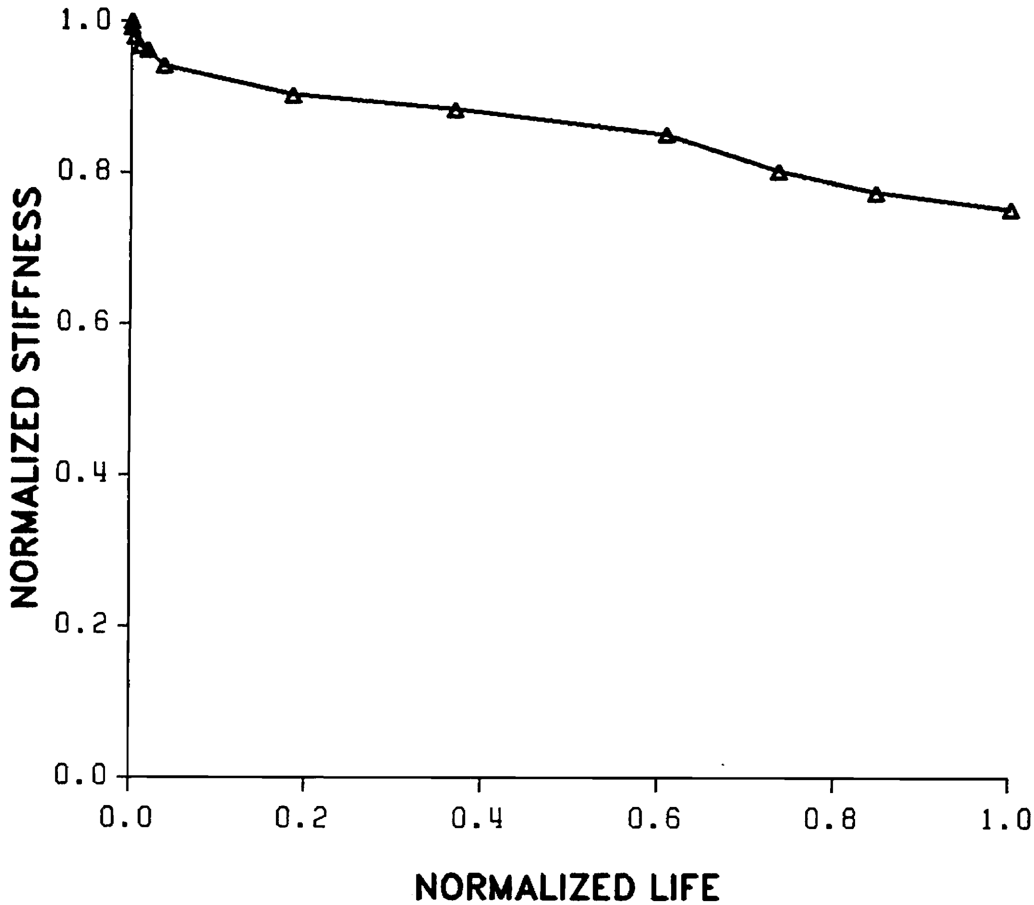

Figure 13. Stiffness-life curve of a notched 22-ply 0 deg. specimen having a life of 27000 cycles.

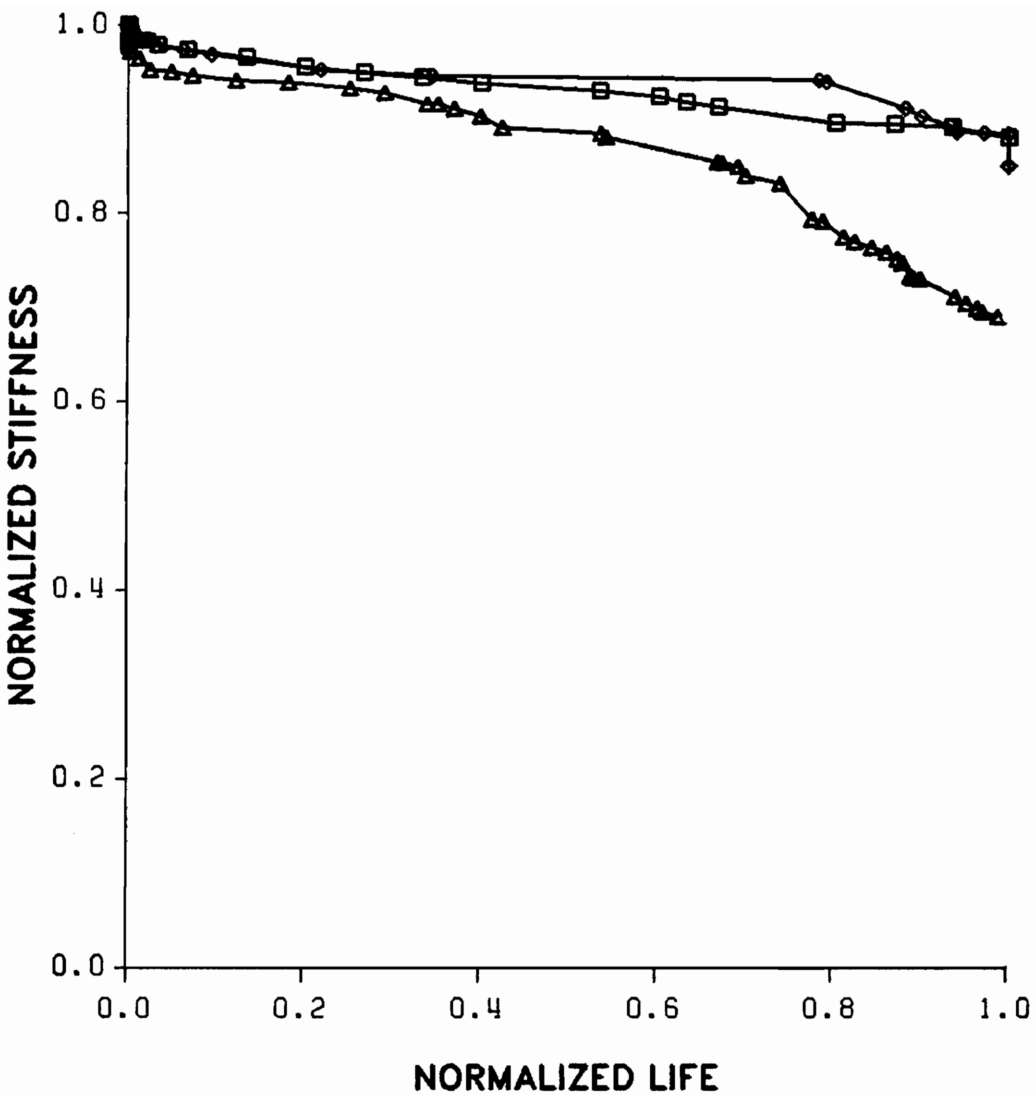

Figure 14. Stiffness-life curves of unnotched 20-ply 0/45 deg. specimens having lives of about 1 million cycles.

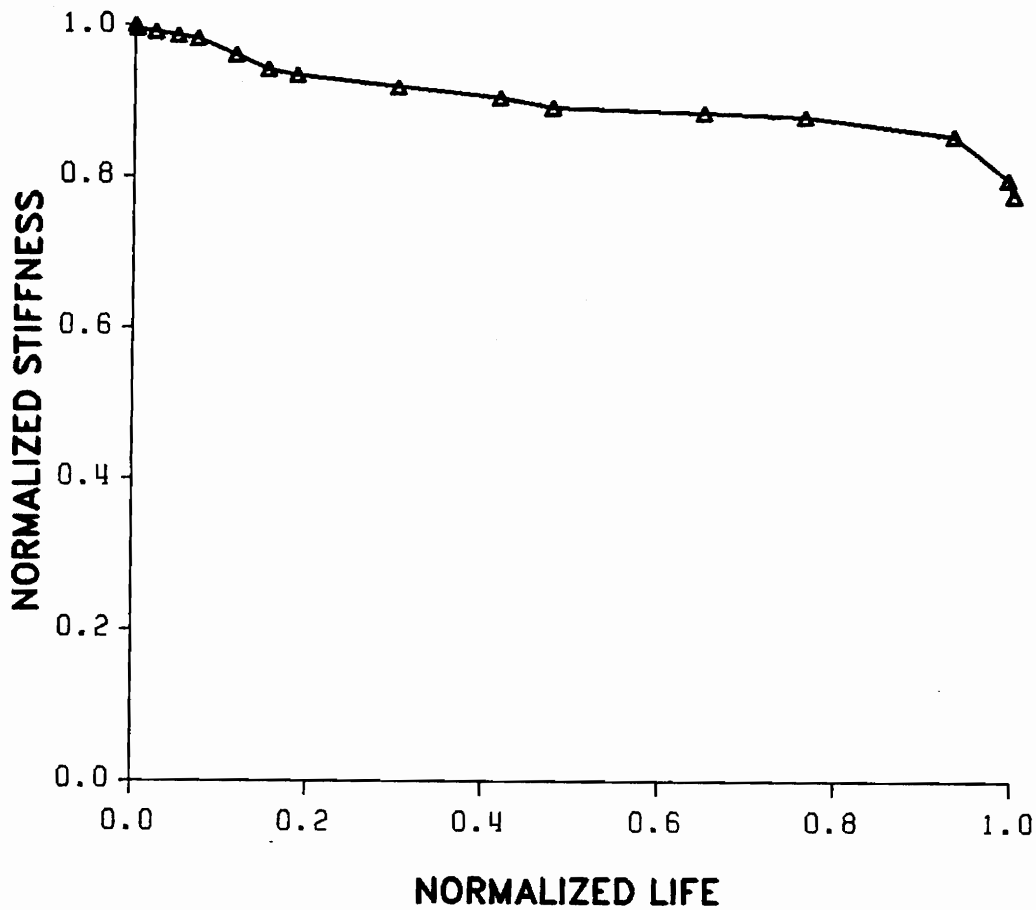

Figure 15. Stiffness-life curve of a notched 20-ply 0/45 deg. specimen having a life of 4030 cycles. (Test was run at 5 Hz)

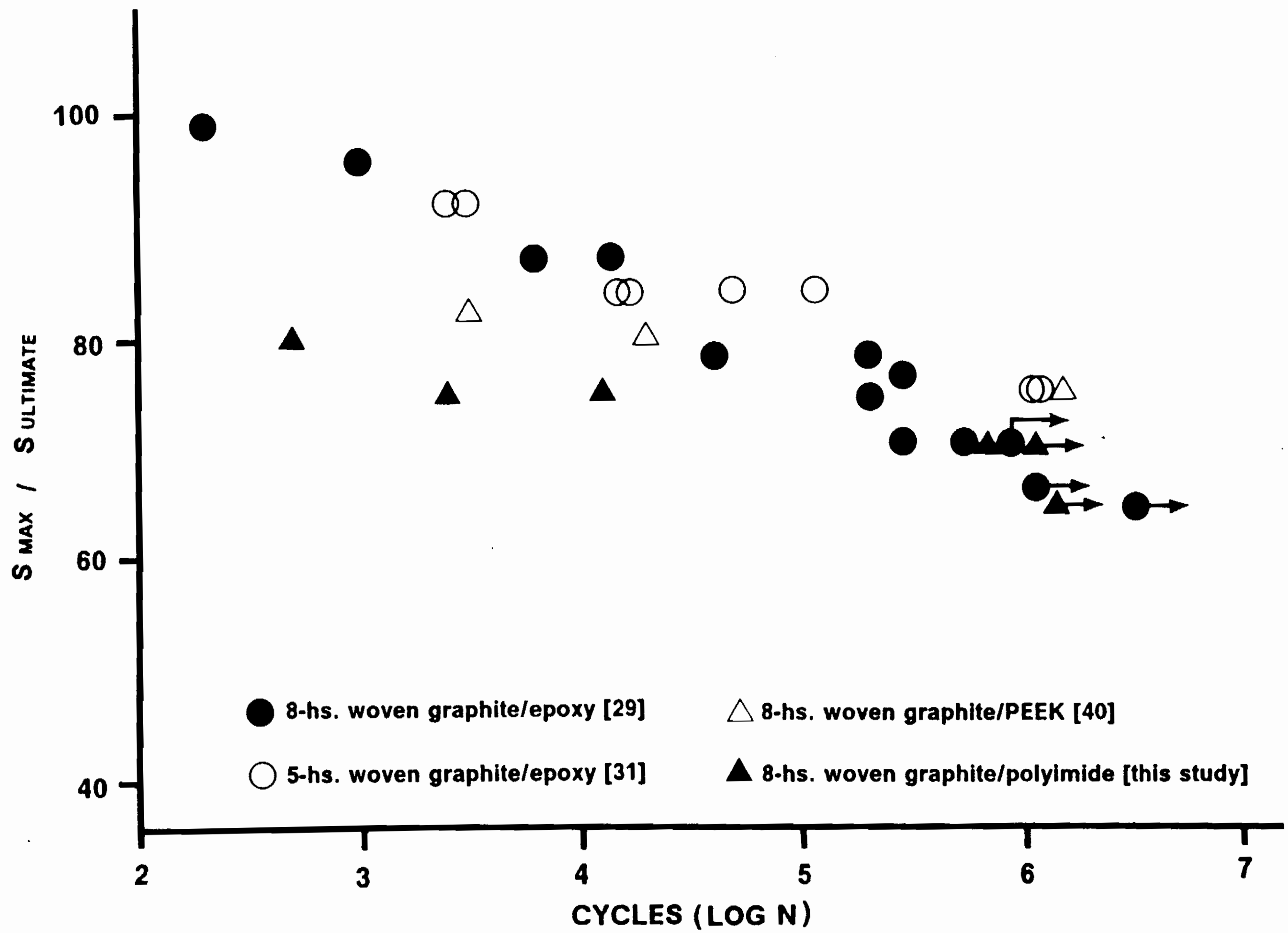

Figure 16. **Comparison of tension-tension fatigue data for woven cross-ply laminates. (Arrows denote runnouts)**

problems associated with grip damage in the unnotched specimens, the $(0)_{22}$ coupons from this study appear to have short fatigue lives compared to the other materials.

The plot in Figure 16 shows the basic difference in the fatigue response of thermosetting (epoxy) and thermoplastic (PEEK) material systems. The thermosetting composites tend to have better fatigue performance under high load, short life loading conditions than do the thermoplastics. Notched and unnotched thermosplastic specimens tend to have a "flatter" S-N curve, and at a life of about $10^4 - 10^5$ cycles or more, outperform the thermoset specimens.[64] The graphite-polyimide material tested in this study, which is considered to be a thermoset, appears to have the "flattness" in the S-N curves associated with thermoplastics.

Figure 17 gives a comparison of unnotched stress-life data for balanced woven laminates having fibers in the 0, 90, and +/-45 deg. directions. Once again, maximum applied stress values are normalized to unnotched tensile strengths. Here, it appears that the 8-harness $(0,45,0,-45,0,0,-45,0,45,0)_2$ graphite-polyimide is superior in fatigue to 5-harness graphite-epoxy (tabbed) [31] and 8-harness graphite-PEEK (tabbed) [40]. In this plot, the "flatness" of the S-N curves for the polyimide and PEEK material relative to the curve for the epoxy system is much more pronounced than in the previous figure.

A summary of notched fatigue tests run on $(0)_{22}$ and $(0,45,0,-45,0,0,-45,0,45,0)_2$ graphite-polyimide is presented in Table 8. Fatigue lives of 10^3 and 10^6 cycles corresponded to maximum stress levels of about 90% and 95% of the undamaged notched tensile strength for both laminates. Fatigue failure occurred after a drop in the original stiffness (measured over a 1.0 in. gage length centered across the hole) of about 15-25%.

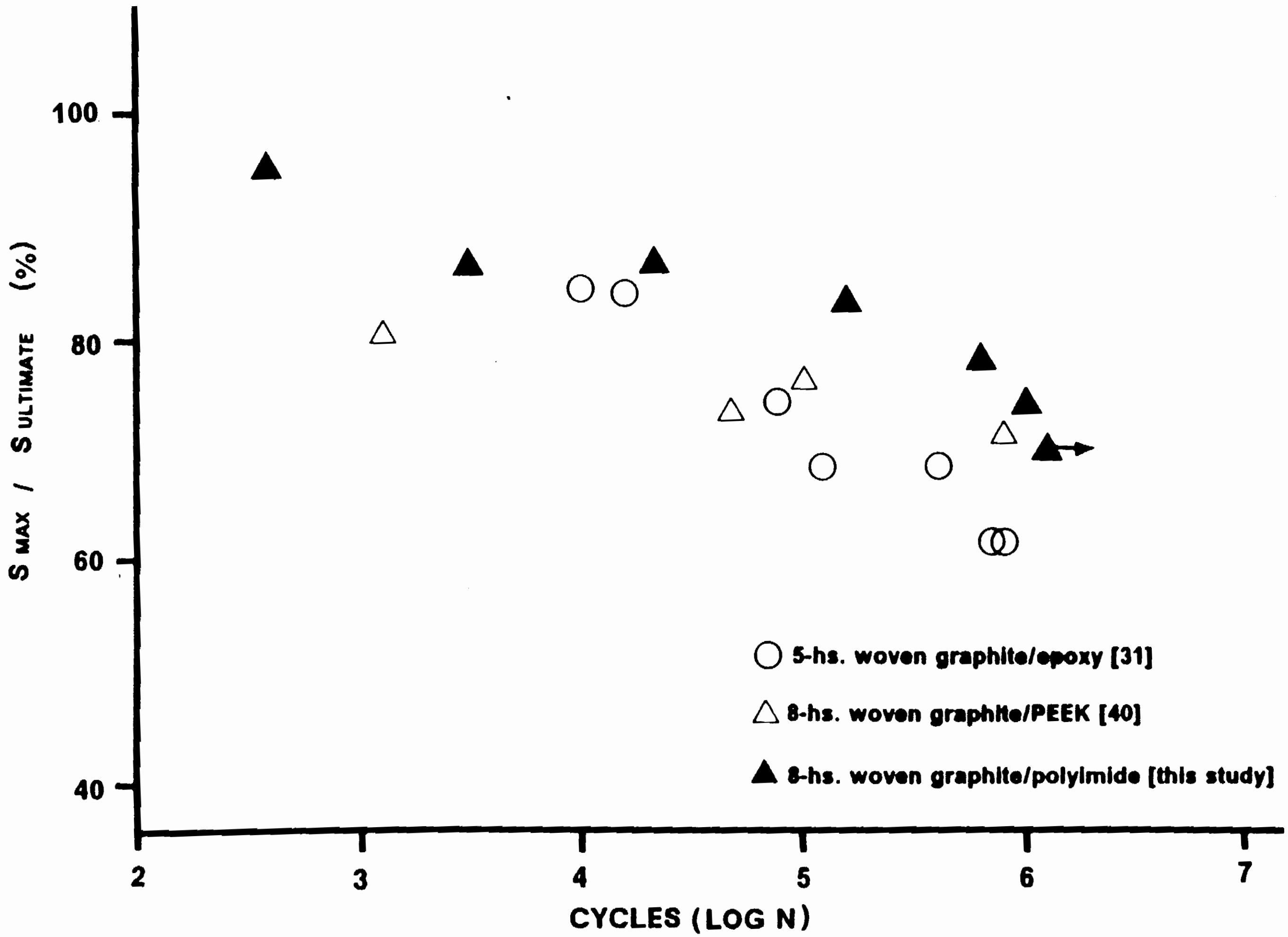

Figure 17. Comparison of tension-tension fatigue data for woven balanced laminates. (Arrows denote runnouts)

Table 8. Notched Tension-Tension Fatigue Results

Layup	Maximum Stress[1]	Cycles	Stiffness[2]	Notes
$(0)_{22}$	70.	3.4 M	--	residual strength = 107%
	89.	1.1 M	74.	fatigue failure
	90.	300 k	--	fatigue failure
	90.	1.1 M	75.	residual strength = 104%
	90.	66 k	85.	residual strength = 112%
	94.	150 k	--	fatigue failure
	96.	205 k	--	residual strength = 113%
20-ply[3] Balanced	91.	115 k	--	fatigue failure
	91.	580 k	85.	residual strength = 104%
	91.	1.8 M	87.	residual strength = 109%
	94.	1.3 k	--	fatigue failure
	94.	15 k	87.	residual strength = 106%
	94.	5.5 k	94.	residual strength = 104%
	96.	100	--	fatigue failure
	96.[4]	4 k	78.	fatigue failure

[1] Percent of ultimate unnotched tensile strength.
[2] Percent of original stiffness.
[3] Layup was $(0,45,0,-45,0,0,45,0,-45,0)_2$
[4] Test was run at 5 Hz instead of 10 Hz.

Residual Strength Tests

Residual strength tests were done on notched specimens fatigued at several stress levels. A "high" load test, run at a maximum stress of 94% to 96% of the monotonic tensile strength, lasted on the order of 10^4 cycles, while a "low" load test at 91% of the monotonic tensile strength lasted for about 10^6 cycles. Specimens were not expected to fail during a "very low" load test, run at 70% of the ultimate strength. Results are listed in Table 8. Information about the final stiffness and number of fatigue cycles is given in this table, while the stage of life for each specimen has been estimated and presented in Table 9. The estimated age of a specimen is based on stiffness measurements and damage as viewed in X-ray radiographs.

It can be seen that increases in residual strengths are slightly higher for the $(0)_{22}$ layup than for the balanced layup, with a maximum measured increase in strength of 13%. However, increases in residual tensile strength for mixed woven (containing woven 45 deg. plies and non-woven 0 deg. plies) and tape laminates of up to 25-30% during tension-tension fatigue have been reported [66-68]. Reason for this difference in residual strength behavior will be discussed in the Damage Mechanisms chapter of this report.

Damage Mechanisms

Monotonic Tests

Table 9. Notched Residual Tensile Strength Results

Layup	Type of Loading[1]	Portion of Life[2]	Residual Strength (%)
$(0)_{22}$	very low	early	107.
	low	middle	112.
	low	late	104.
	high	middle	113.
20-ply[3] Balanced	low	middle	104.
	low	late	109.
	high	middle	104.
	high	middle	106.

[1] Very low, low, and high loads corresponded to a maximum stress of approximately 70%, 90%, and 94% of the virgin notched tensile strength, respectively.
[2] The portion of life was estimated by stiffness monitoring techniques.
[3] Laminate stacking sequence was $(0,45,0,-45,0,0,-45,0,45,0)_2$.

Specimens loaded monotonically to failure showed the least amount of matrix damage of all those tested in this study. Figure 18a shows an X-ray radiograph of an unnotched $(0,45,0,-45,0,0,-45,0,45,0)_2$ coupon following monotonic tensile failure. As is evident from these and other radiographs, the extent of damage in tensile specimens prior to failure was limited to scattered matrix cracks, primarily in the 90 deg. direction in unnotched material and away from the hole when a notch was present. Figure 19 shows a series of radiographs taken at 50%, 80%, 94%, and 100% (after failure) of the ultimate strength of a notched $(0,45,0,-45,0,0,-45,0,45,0)_2$ specimen under quasi-static tensile loading. In the $(0,45,0,-45,0,0,-45,0,45,0)_2$ material, additional +45 and -45 deg. matrix cracking occurred at either side of the center hole in notched coupons. In the 0 deg. laminate, 0 deg. splitting tangent to the hole was also observed. Post failure damage included delaminations, 0 deg. matrix cracking, fiber fracture, and fiber bundle pullout in a very localized region surrounding the fracture site. Compressive damage in this material system is being studied by another graduate student in the Materials Response Group at Virginia Tech [68].

Sustained Incremental Loading Tests

Specimens subjected to sustained incremental tension loading contained considerably more damage than those loaded monotonically to failure. Figure 20 shows radiographs of an unnotched $(0)_{22}$ incremental tension specimen after 2 hours and 19 hours at 88% of its failure strength. This specimen was tested under load control. Initiation of 90 deg. matrix cracks was first observed at about 70% of the maximum load, however, very few of these cracks were present after 2 hours at 88% of the maximum load, as seen in Figure 20a. After 17 more hours of loading, a significant number of new 90 deg. matrix cracks appeared on the next radiograph, Figure 20b. The radiograph also shows several 0 deg. matrix cracks, which may not be visible in this figure. Figure 20b was the last radiograph to be taken prior to specimen

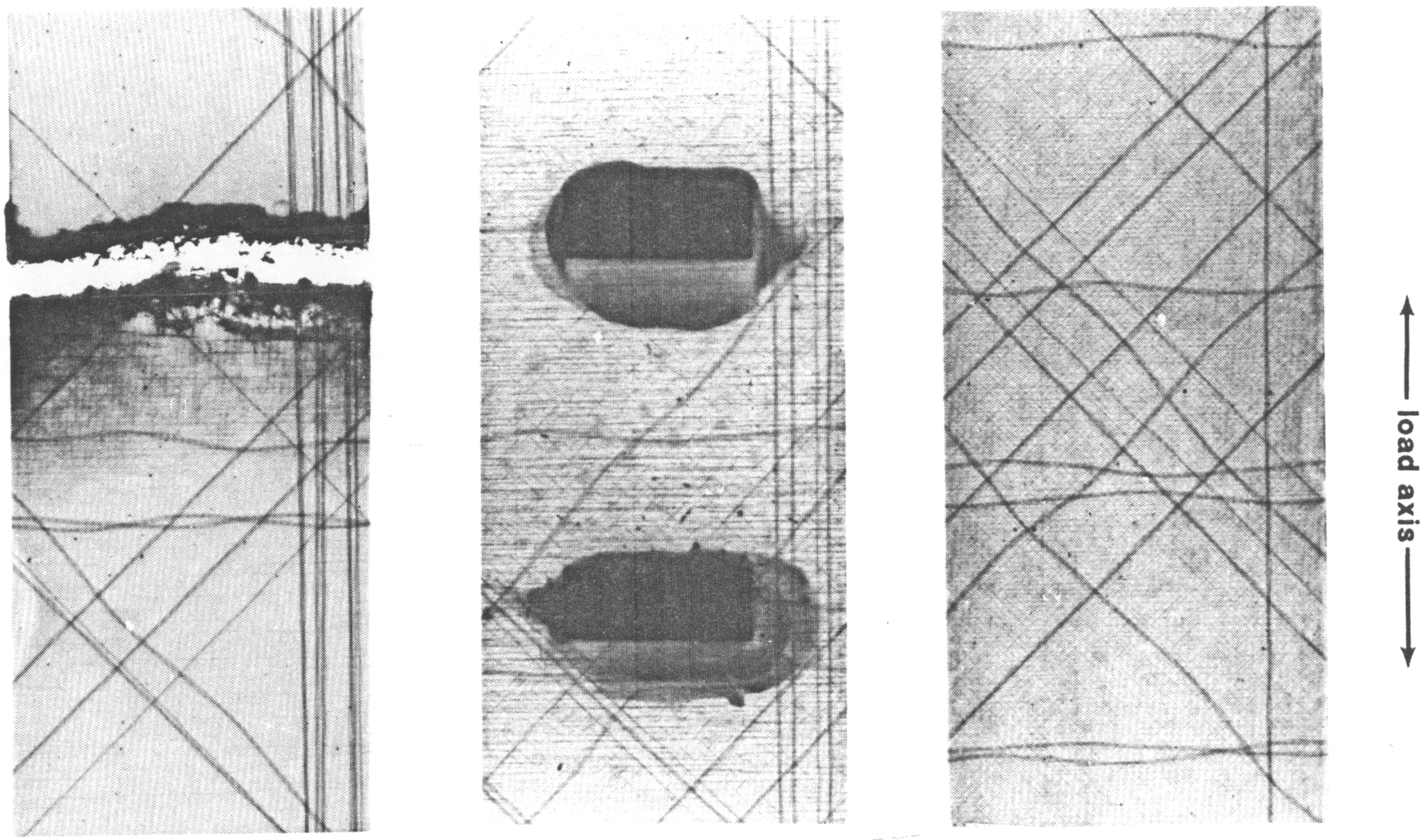

(a) (b) (c)

Figure 18. **Unnotched 20-ply 0/45 deg. specimens damaged under (a) monotonic tension (after failure), (b) incremental tension (late life), and (c) tension-tension fatigue (late life).**

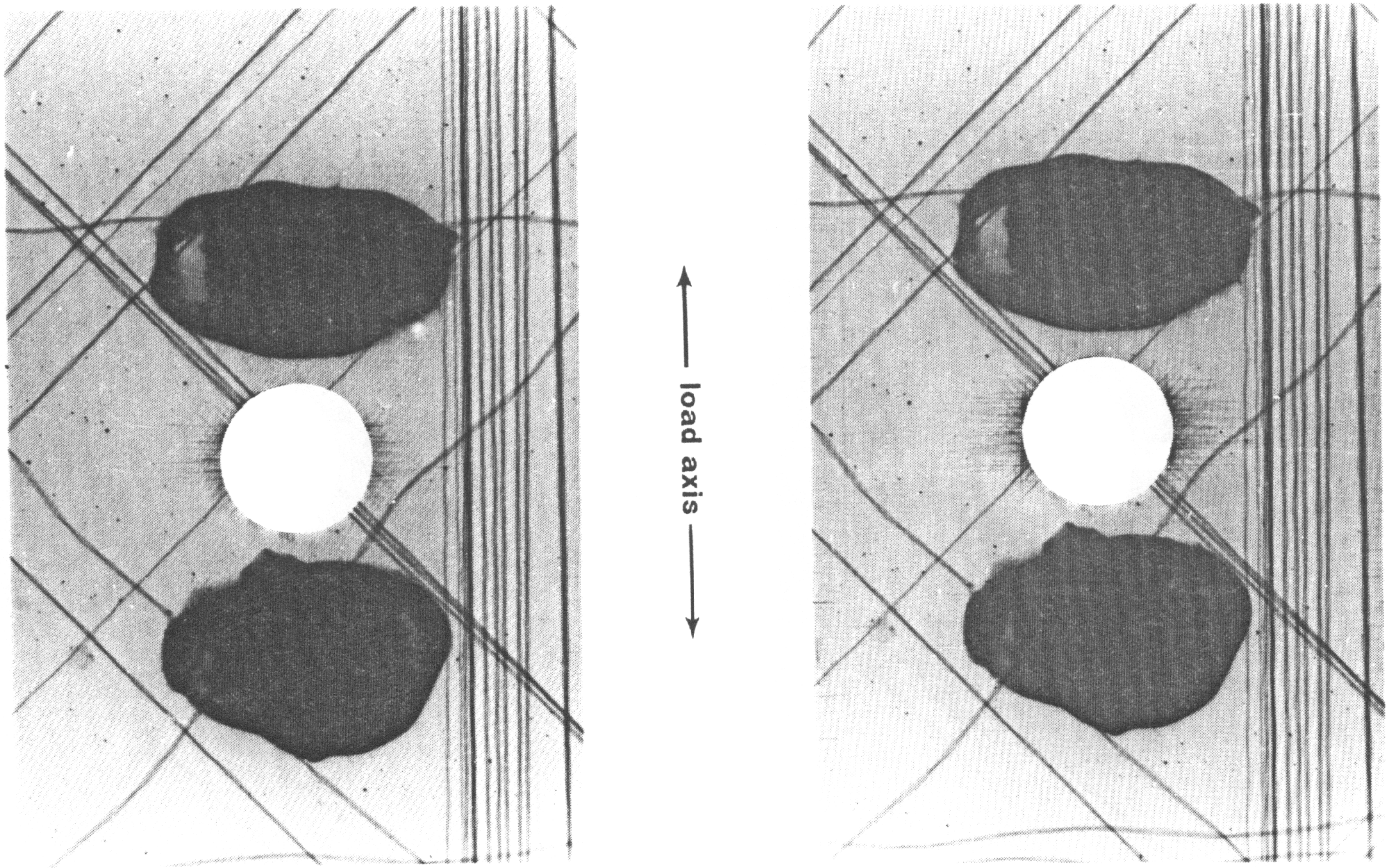

(a) (b)

Figure 19. Notched 20-ply 0/45 deg. monotonic specimen at (a) 50%, (b) 80%, (c) 94%, and (d) 100% (at failure) of its tensile strength. (continued on following page)

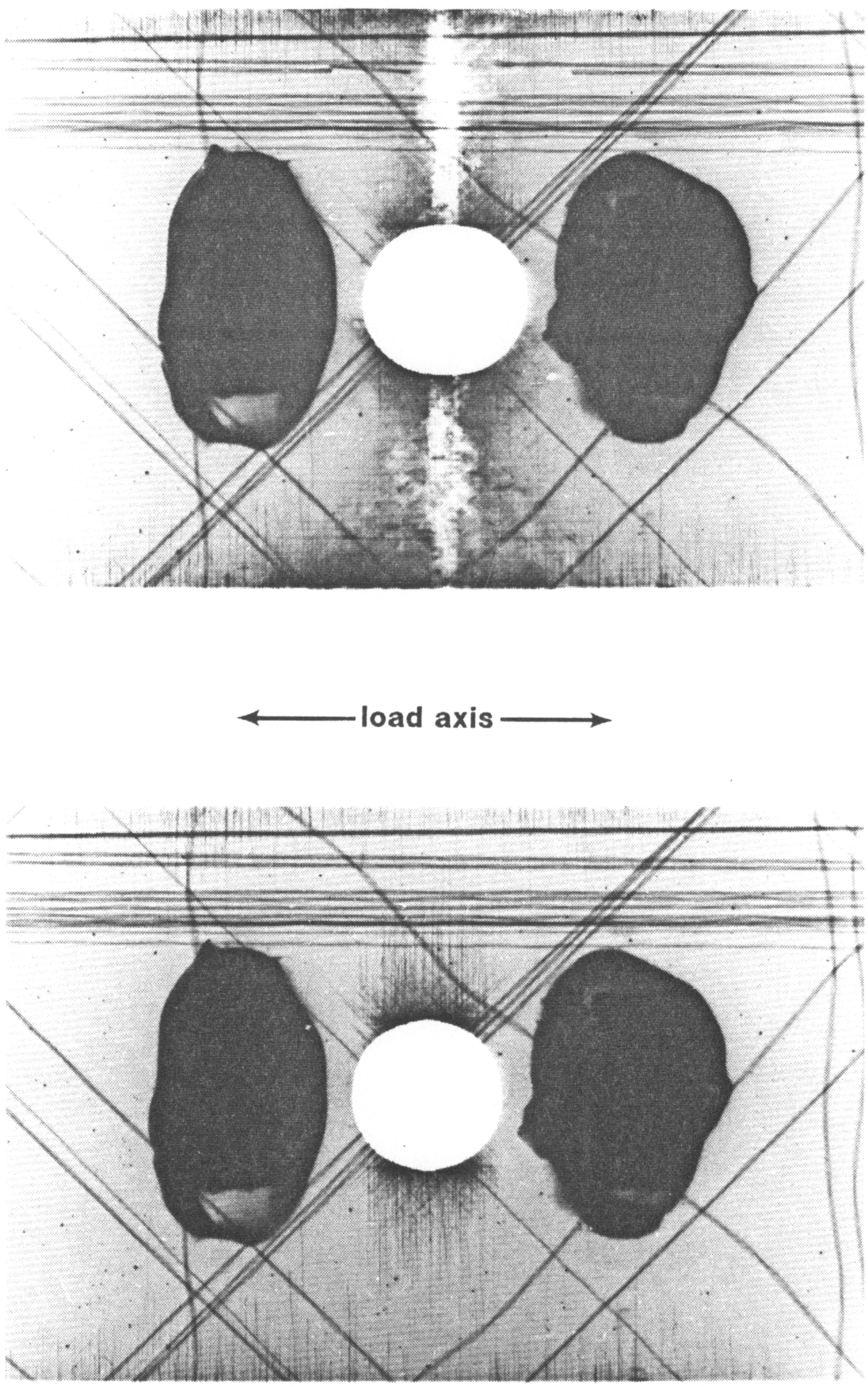

(d)

(c)

Figure 19. (continued from previous page)

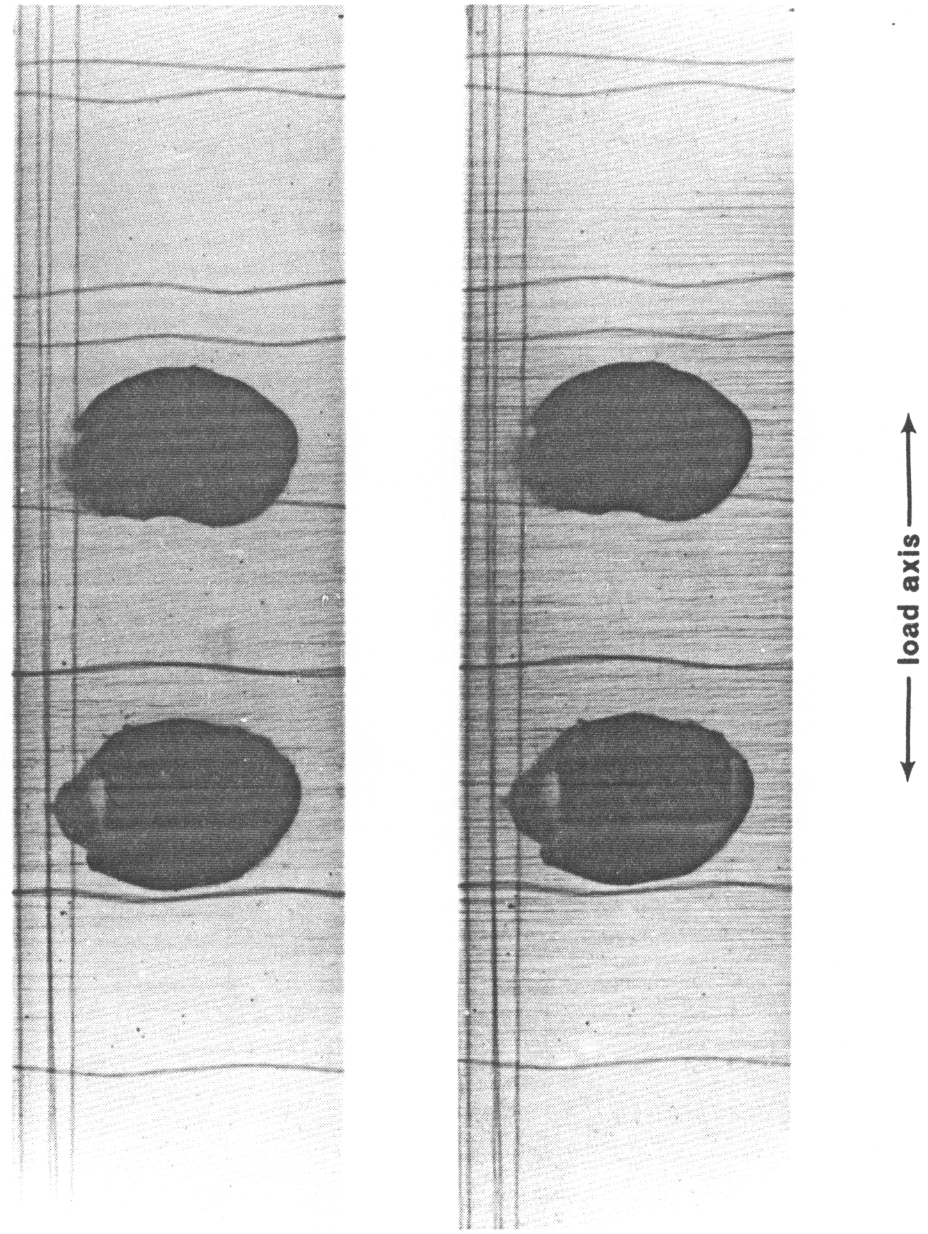

Figure 20. Radiographs of an unnotched 22-ply 0 deg. incremental tension specimen after (a) 2 and (b) 19 hrs at 88% of its strength.

failure. It is believed that more 0 deg. cracks, but none of the fiber bundle crossover damage observed in the $(0,45,0,-45,0,0,-45,0,45,0)_2$ material, were present before failure. These incremental tensile tests clearly demonstrate the time-dependence of damage in this woven graphite-polyimide material system.

Figure 21 shows the development of damage in the $(0,45,0,-45,0,0,-45,0,45,0)_2$ specimen described in the previous paragraph. This figure presents a series of front views of the coupon taken at strains of 7,000, 7,500, and 10,500 microstrain. Because the extensometer was taken off of the specimen and the specimen removed from the machine several times, these strain values may be slightly incorrect. Side views at these strain levels are shown in Figure 22. At 7,000 microstrain, Figure 21a and Figure 22a, initiation and growth of 90 degree matrix cracks were observed. These matrix cracks are present throughout the thickness, but are not quite as dense in the surface plies. The first 45 deg. cracks could be seen at a strain level of 7500 microstrain in Figure 21b and Figure 22b. At a strain of 10,500 microstrain, Figure 21c and Figure 22c, localized fiber bundle crossover damage and matrix cracks throughout the thickness in the 90, +45, and -45 degree directions throughout the thickness and the localized fiber bundle crossover damage were highly developed. The growth of 0 deg. matrix cracks, which develop just prior to fiber fracture and specimen failure, had just begun in these last figures. This specimen failed at a strain of about 11,500 microstrain and a residual strength of 107%. This type of damage resulted in increases in residual strength of up to 14% in the $(0,45,0,-45,0,0,-45,0,45,0)_2$ unnotched coupons.

A big contrast in damage states in $(0,45,0,-45,0,0,-45,0,45,0)_2$ unnotched coupons can be seen in Figure 18a and b. Figure 18a shows a radiograph of a specimen after monotonic tensile failure, while Figure 18b shows an incremental tension specimen loaded under strain control prior to failure, at strain of 10,500 microstrain. The incrementally loaded material contains very dense matrix cracks in the 90, +45, and -45 deg. directions. Also, a series of small dark spots following the weave pattern is present. These dark areas are either high

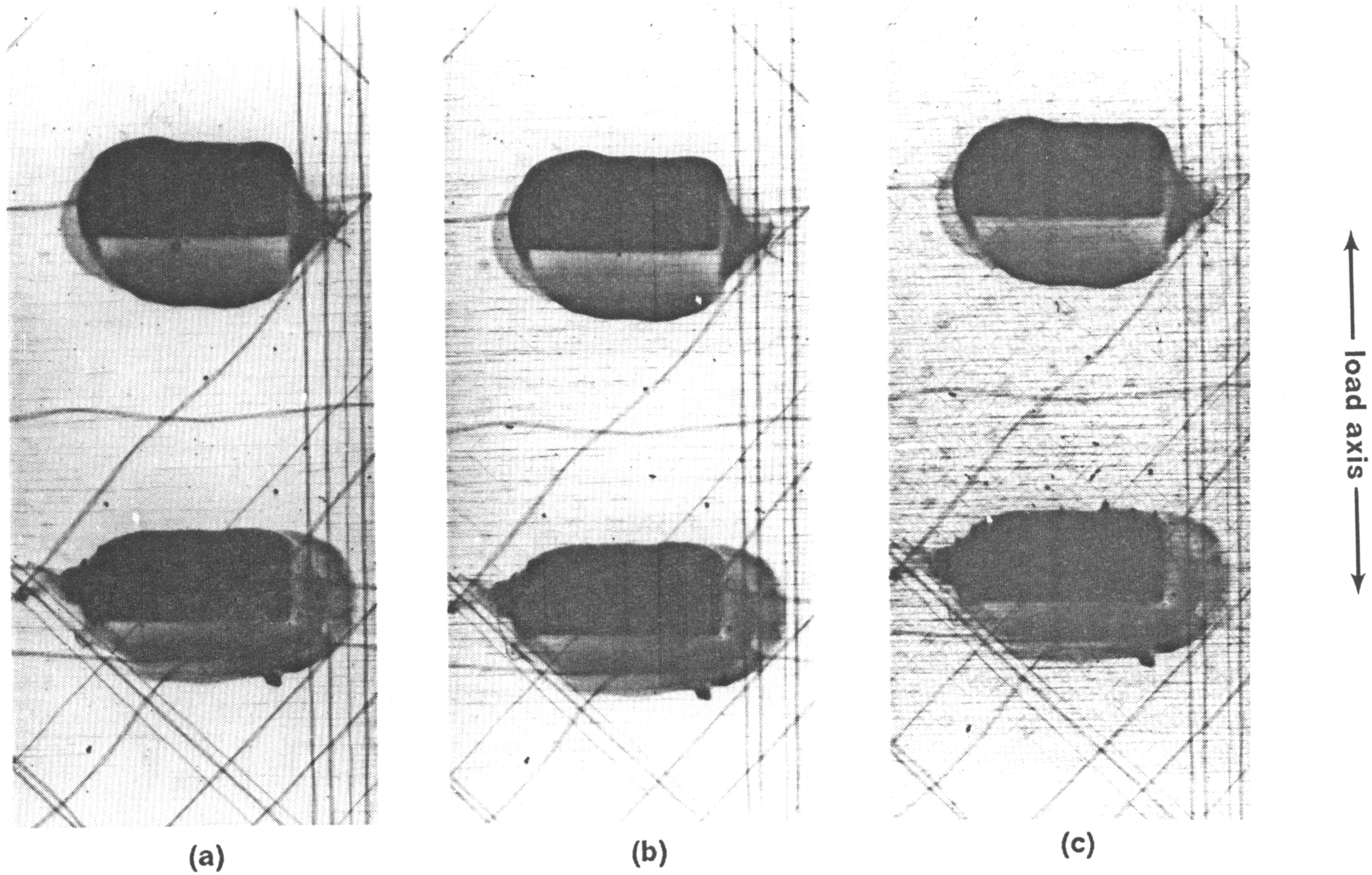

Figure 21. Radiographs showing front views of an unnotched 20-ply 0/45 deg. incremental tension specimen at (a) 7000, (b) 7500, and (c) 10500 microstrain.

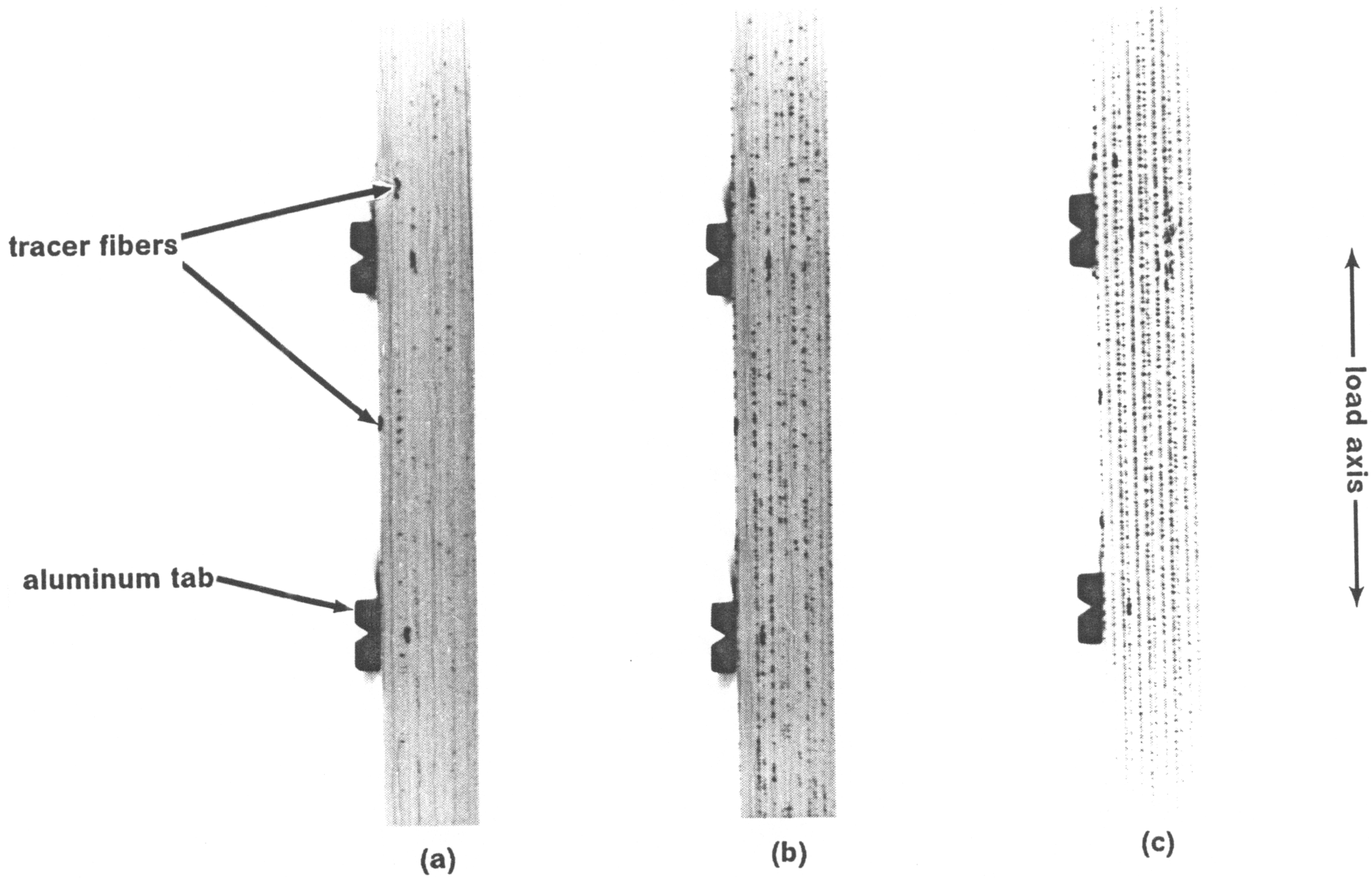

Figure 22. Radiographs showing edge views of an unnotched 20-ply 0/45 deg. incremental tension specimen at (a) 7000, (b) 7500, and (c) 10500 microstrain.

density intralaminar matrix cracks or local delaminations at the fiber bundle crossovers within a ply.

It is believed that if data acquisition could be properly controlled, repeatable "master curves" similar to the incremental loading curve in Figure 10 could be experimentally measured to characterize the damage development in a a given laminate. For example, if the information obtained from X-ray radiography about the unnotched $(0,45,0,-45,0,0,-45,0,45,0)_2$ laminate was included on the incremental loading curve shown in Figure 10, it would appear that the peaks and plateaus of the measured change in stress would correspond to distinct stages of damage development. This has been done in Figure 23. Up to about 4,000 microstrain, no damage was observed in the material. As discussed earlier, instabilities in the electronics created noise in this early region. The formation of 90 deg. matrix cracks was seen after 7,000 microstrain, but may have begun a little earlier. At about 7,500 microstrain, growth of the the 90 deg. cracks was nearly finished, and cracks in the +45 and -45 deg. directions started to appear. By 9,000 microstrain, +45 and -45 deg. crack growth had probably slowed down, at the same time the local damage areas (delamination or dense intralaminar matrix cracks at the fiber bundle crossovers) started to form. These local damage areas most likely became more intense with increasing strain, until the 0 deg. matrix cracking occurred from about 10,000 microstrain to failure. Final failure occurs when the load-bearing fibers begin to fracture. Such a curve for the 0 deg. laminates would be expected to end at about 8,000 microstrain on this diagram after the 90 deg. cracks became saturated and 0 deg. splitting and fiber fracture had begun.

Tension-Tension Fatigue Tests

The previous section showed that damage development under sustained tensile loading is time-dependent, while this section will present evidence that shows that damage develop-

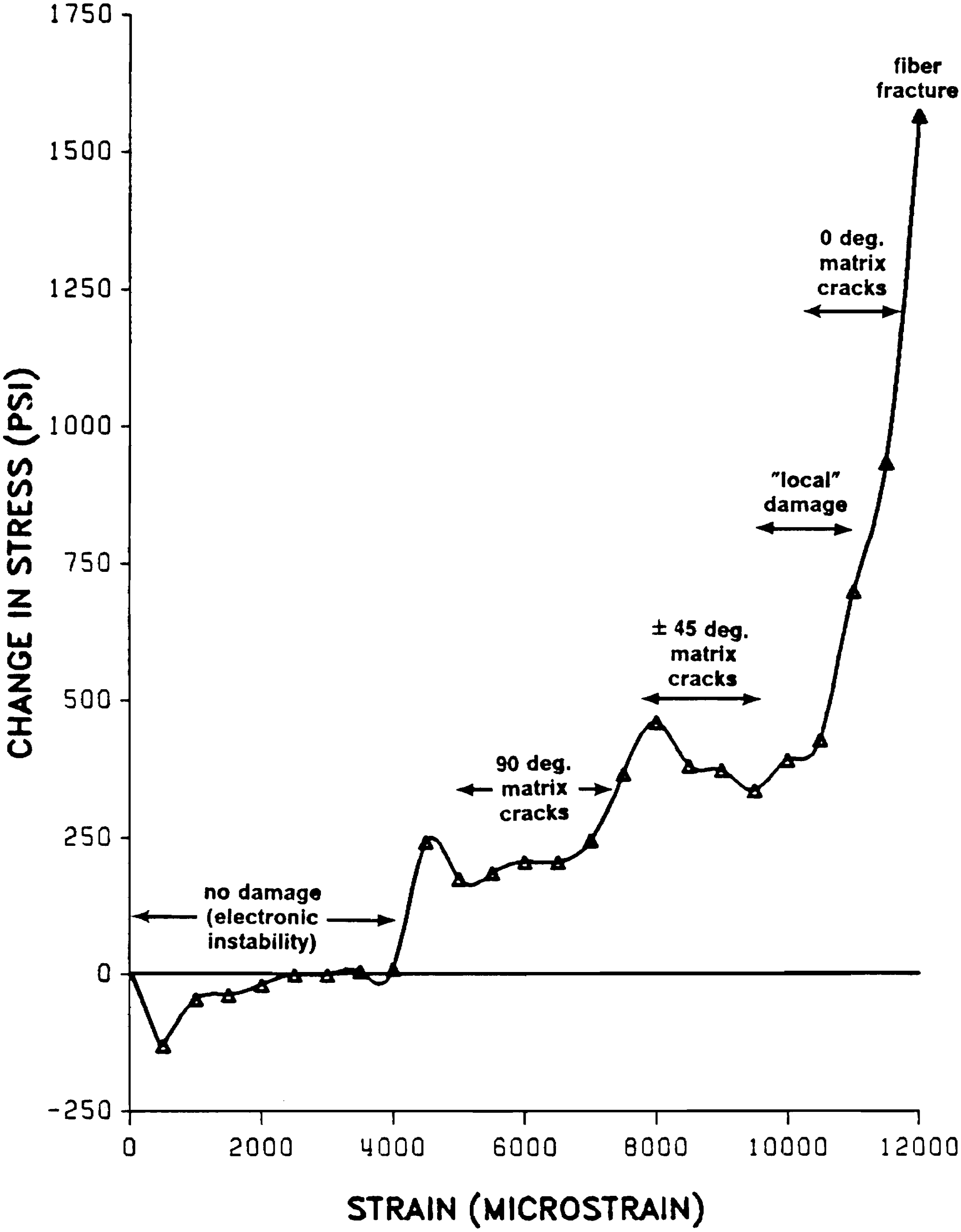

Figure 23. Incremental loading response of a 20-ply 0/45 deg. unnotched specimen with a description of damage observed in radiographs.

ment under cyclic tensile fatigue is dependent on the applied stress level, or on the life, of a specimen. Damage under low load, long life fatigue is more extensive than that under high load fatigue, monotonic tension, or incremental tension.

Figure 18 demonstrates these differences in damage under the three types of tensile loading. Figure 18a and b, previously discussed, show monotonic and incrementally loaded unnotched $(0,45,0,-45,0,0,-45,0,45,0)_2$ specimens. Figure 18c shows a radigraph of a $(0,45,0,-45,0,0,-45,0,45,0)_2$ coupon after 1.2 million cycles at a maximum stress of 71% of the tensile strength of similar specimens. Although the exposure of this radiograph is rather poor, it can be seen from the original that extensive 90, +45, and -45 deg. matrix cracking is present along with the dark spots assumed to be damage at fiber bundle crossovers. However, the damage in the +45 and -45 deg. direction is much more saturated than in the incrementally loaded specimen. It appears that the incrementally loaded specimen shown in Figure 18b has not quite reached the Characteristic Damage State [51] observed in the long term tension-tension fatigue specimen.

Differences also exist in the states of damage of specimens subjected to high and low cyclic loads. Figure 24 shows how the fracture surfaces of $(0)_{22}$ unnotched specimens vary according to loading conditions, while Figure 25 shows the same for $(0,45,0,-45,0,0,-45,0,45,0)_2$ unnotched coupons. Besides a range of short to long life tension-tension fatigue specimens, these figures also include failed monotonic and incremental tension specimens for comparison. In general, the longer the life, the more dispersed the fracture surface for cyclically loaded specimens. Monotonic tension coupons, having an equivalent life of 1 fatigue cycle, have the most localized failure site. Incrementally loaded specimens are similar in appearance to high load, short life fatigue specimens.

As the life is increased, more damage develops in the material prior to failure, and more delamination and fiber pullout are observed at failure. Figure 26 shows deplied 0 and +45 deg. layers from $(0,45,0,-45,0,0,-45,0,45,0)_2$ specimens failing from low load and high load

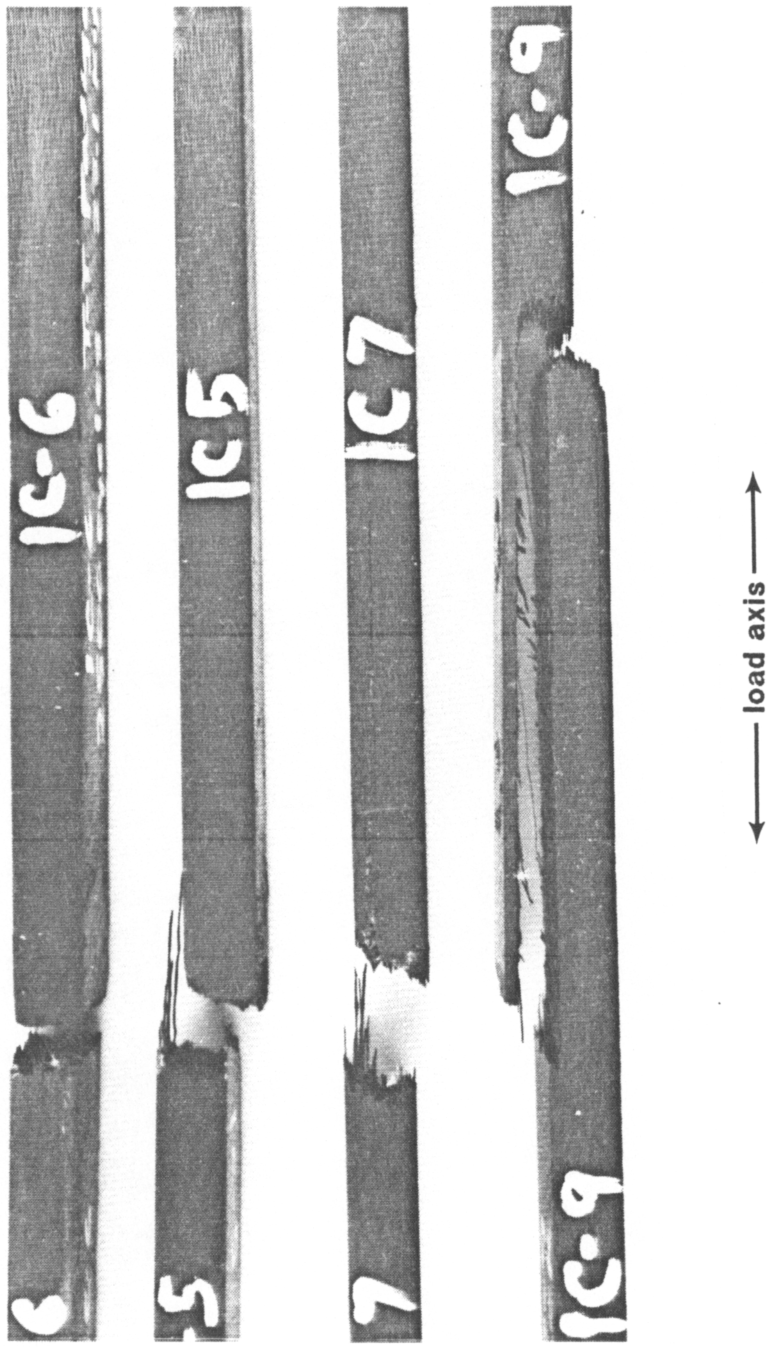

Figure 24. The variation of failure surface with loading conditions in 22-ply 0 deg. specimens. From left to right, specimens failing from: 2.5k cycles, 12.9k cycles, 720k cycles, and incremental tension.

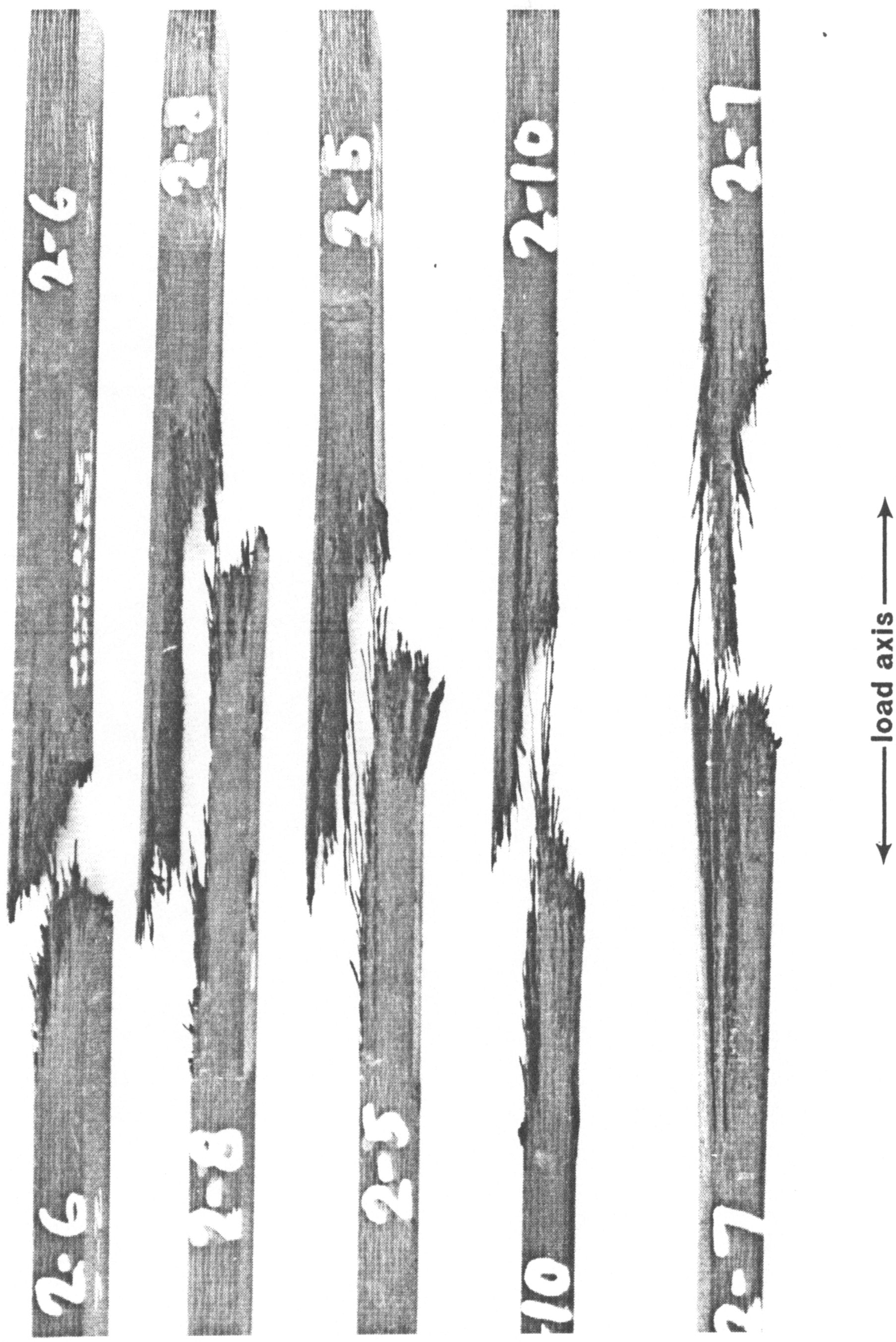

Figure 25. The variation of failure surface with loading conditions in 20-ply 0/45 deg. specimens. From left to right, specimens failing from: monotonic tension, incremental tension, 410 cycles, incremental tension, and 3300 cycles. (continued on following page)

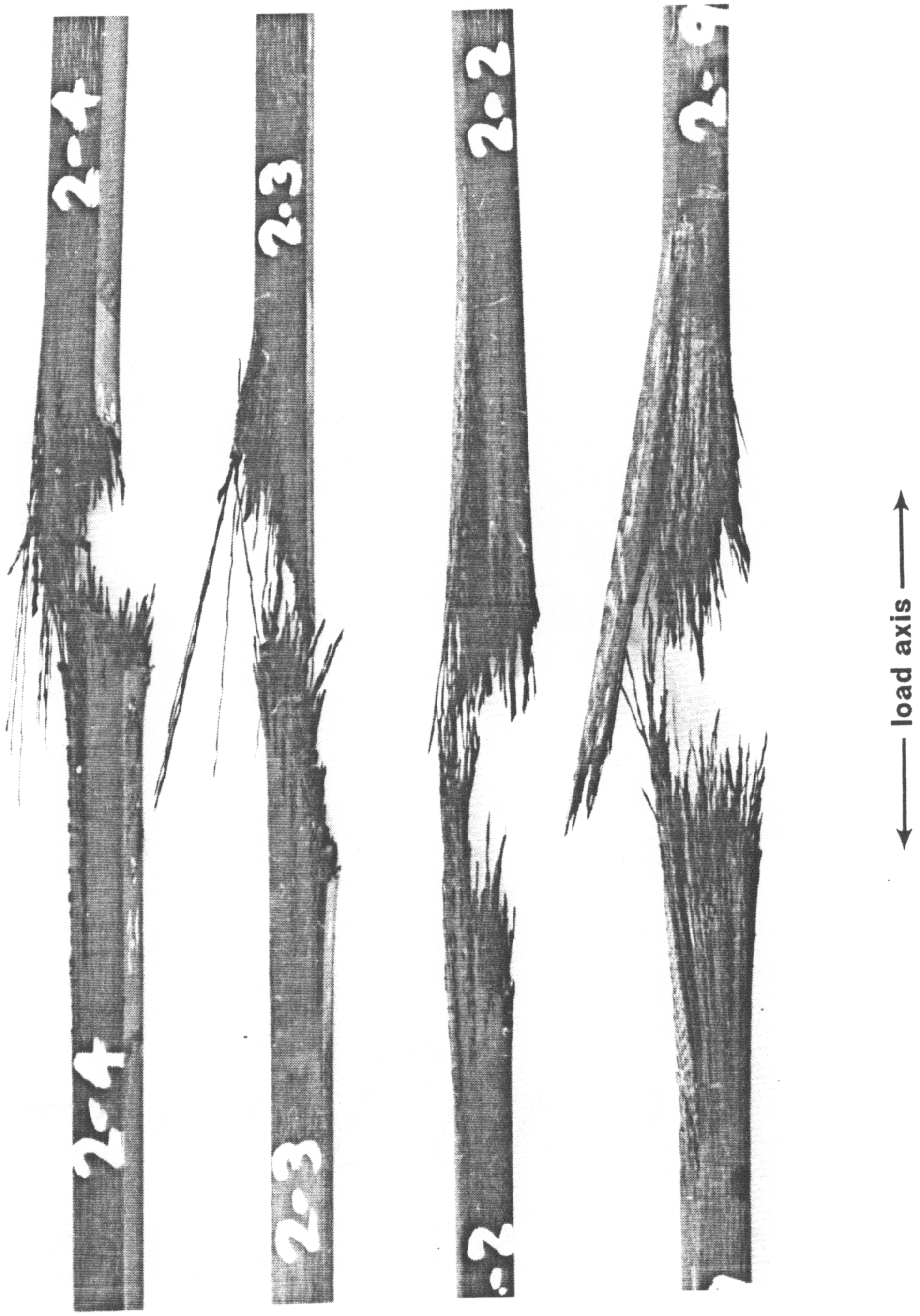

Figure 25. (continued from previous page) From left to right, specimens failing from: 21.5k cycles, 150k cycles, 640k cycles, and 940k cycles

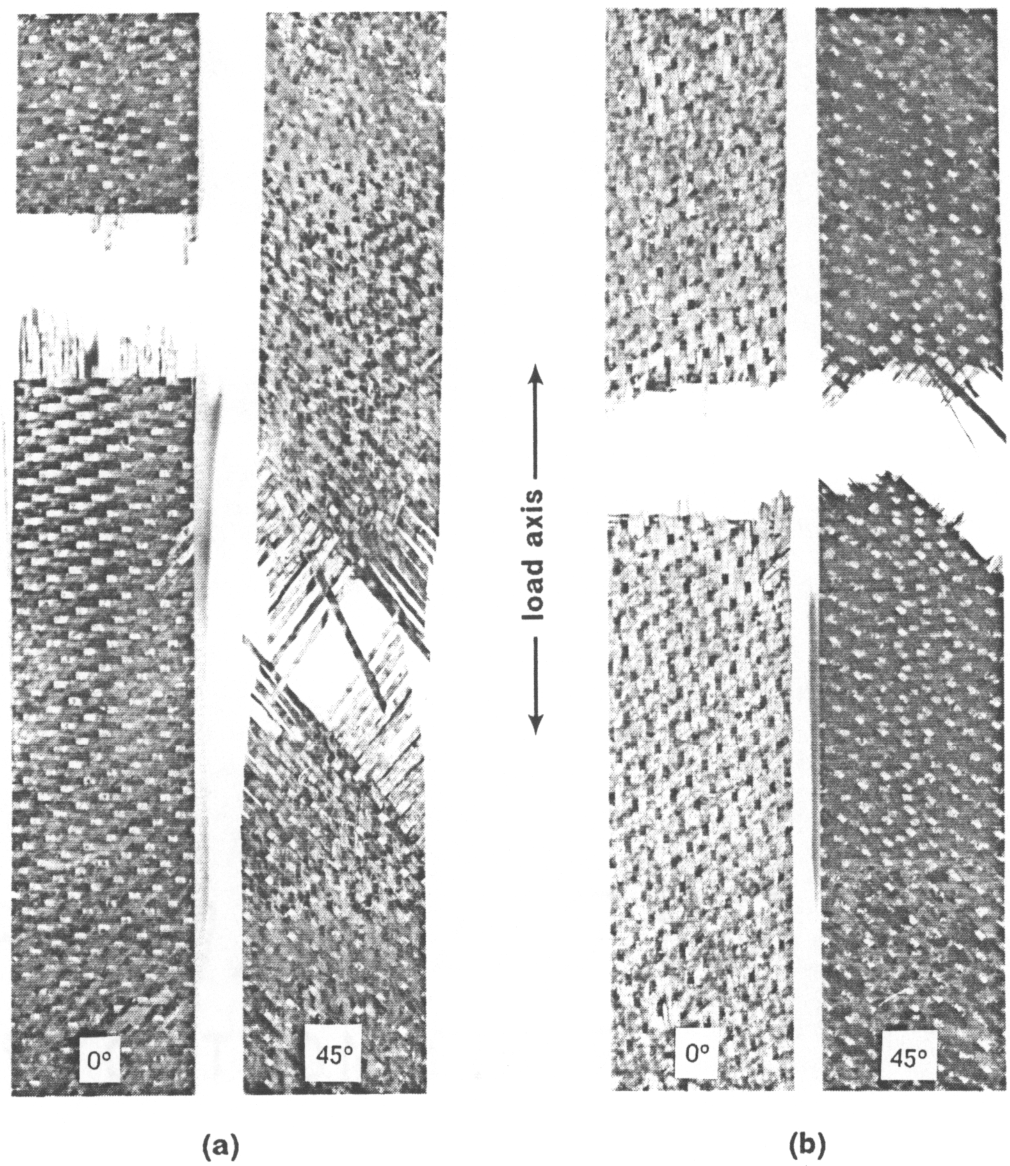

Figure 26. Deplied 0 and 45 deg. layers from unnotched 20-ply 0/45 deg. specimens failing from (a) low and (b) high cyclic loads.

fatigue. At low cyclic loads, the fracture surfaces of individual plies are irregular, indicating a dispersed damage field. At high loads, the fracture surfaces are more regular, suggesting more localized damage. Scanning electron microscopic examinations of deplied specimens support this idea; fiber fracture occurs in a much larger area surrounding the failure site under low load compared to high load fatigue. It has been suggested [69] that differences in fracture surfaces such as those seen in Figure 26 are a result of differences in failure modes. The high load specimen appears to have failed in tension, while the low load specimen had more of a shear failure.

It should be kept in mind that grip-induced damage was a problem in these unnotched coupons. It is believed that 0 deg. fiber fracture in the surface plies of fatigue specimens initiated delaminations in these plies, which were observed as early as half of the fatigue life. These delaminations, unlike the edge delaminations resulting from interlaminar stresses, occurred after the outermost 0 deg. plies had already broken due to the grips.

From the microscopic examination of deplied fatigue specimens, it appears that the failure mode of individual fibers may be influenced by the applied stress level. Figure 27a and b show SEM micrographs of broken 0 deg. fibers from $(0,45,0,-45,0,0,-45,0,45,0)_2$ unnotched specimens failing after 940,000 and after 410 fatigue cycles, respectively. The fibers from the long life coupon in Figure 27a at a magnification of 6,000X appear to have interacted with each other during failure. The fracture path is continuous from one fiber to the next, giving the appearance of "flow lines." No such interaction was seen in the fibers from the high load, short life specimen, shown at a magnification of 10,000X in Figure 27b. These fibers have a rougher fracture surface which is associated with faster crack propagation in brittle materials. Note the fluted edges of the Celion 3000 fibers which increase the surface area of the fiber-matrix interface.

In the notched material, grip-related damage was minimal. Only one notched specimen failed due to gripping, a $(0,45,0,-45,0,0,-45,0,45,0)_2$ specimen which was removed from the

(a)

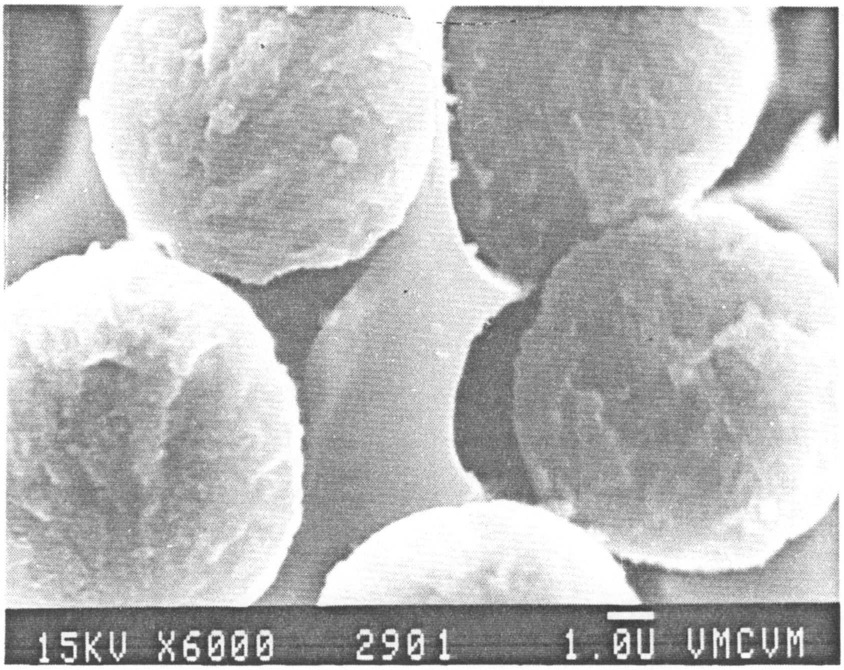

(b)

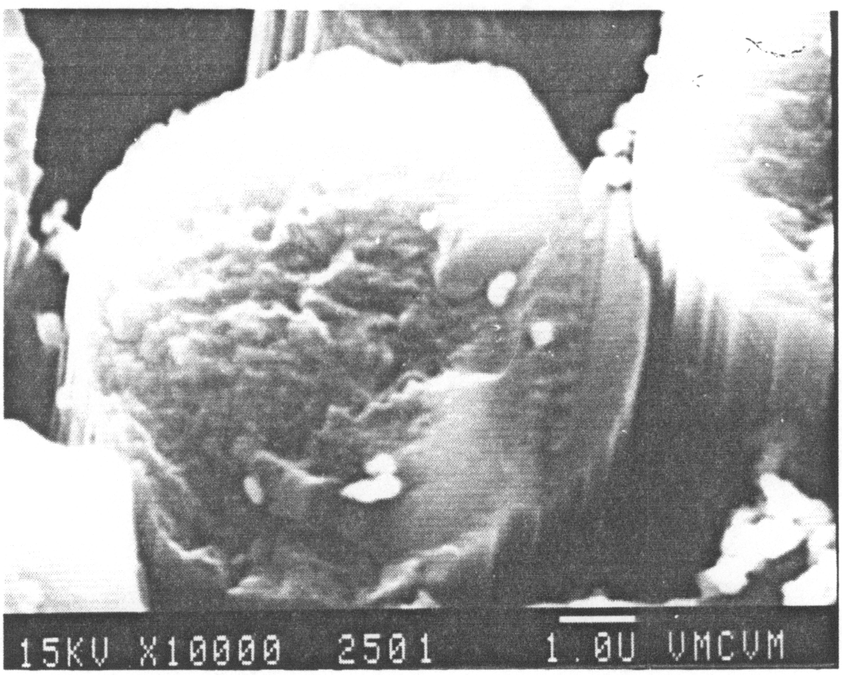

Figure 27. SEM micrographs of broken 0 deg. fibers from unnotched 20-ply 0/45 deg. specimens failing after (a) 940k and (b) 410 cycles

machine and regripped several times for X-ray radiography. All others failed through the center hole.

Damage development in a $(0)_{22}$ notched fatigue specimen has been documented in a series of X-ray radiographs taken after 10, 1k, 50k, and 205k cycles at 90% of the virgin notched tensile strength. Front views and edge views are presented in Figure 28 and Figure 29, respectively. This specimen was tested for residual tensile strength after 205,000 fatigue cycles.

After 10 cycles, relatively long 0 deg. matrix cracks have formed tangent to the hole as shown in Figure 28a. Matrix cracks in the 90 deg. direction exist between the free edges and the 0 deg. cracks, but do not extend above or below the hole. Very small delaminations do exist above and below the hole, but these were detected in radiographs prior to mechanical loading. It was assumed that these delaminations are a result of too much pressure having been applied to the core drill during machining. Less than 1 out of every 10 specimens showed such damage. From Figure 29a, it appears that the damage is spread out equally through the thickness of the coupon.

Figure 28b and Figure 29b show the state of damage after 1,000 cycles. Longitudinal cracks tangent to the hole have extended as far as the extensometer tabs and have become more dense. It appears that small delaminations parallel to these matrix cracks have initiated. The damage from machining has not significantly changed. From the edge view, it appears that damage in the surface plies is more concentrated than in the middle of the specimen.

In Figure 28c, at 50,000 cycles, the bands of 0 deg. splits at either side of the hole have increased in thickness and in length. Matrix cracks in the 90 deg. direction outside of the 0 deg. cracks are very saturated. Several 0 deg. cracks outside the area tangent to the notch have formed. In Figure 29c, it appears that the 90 deg. cracks have grown from ply to ply, as

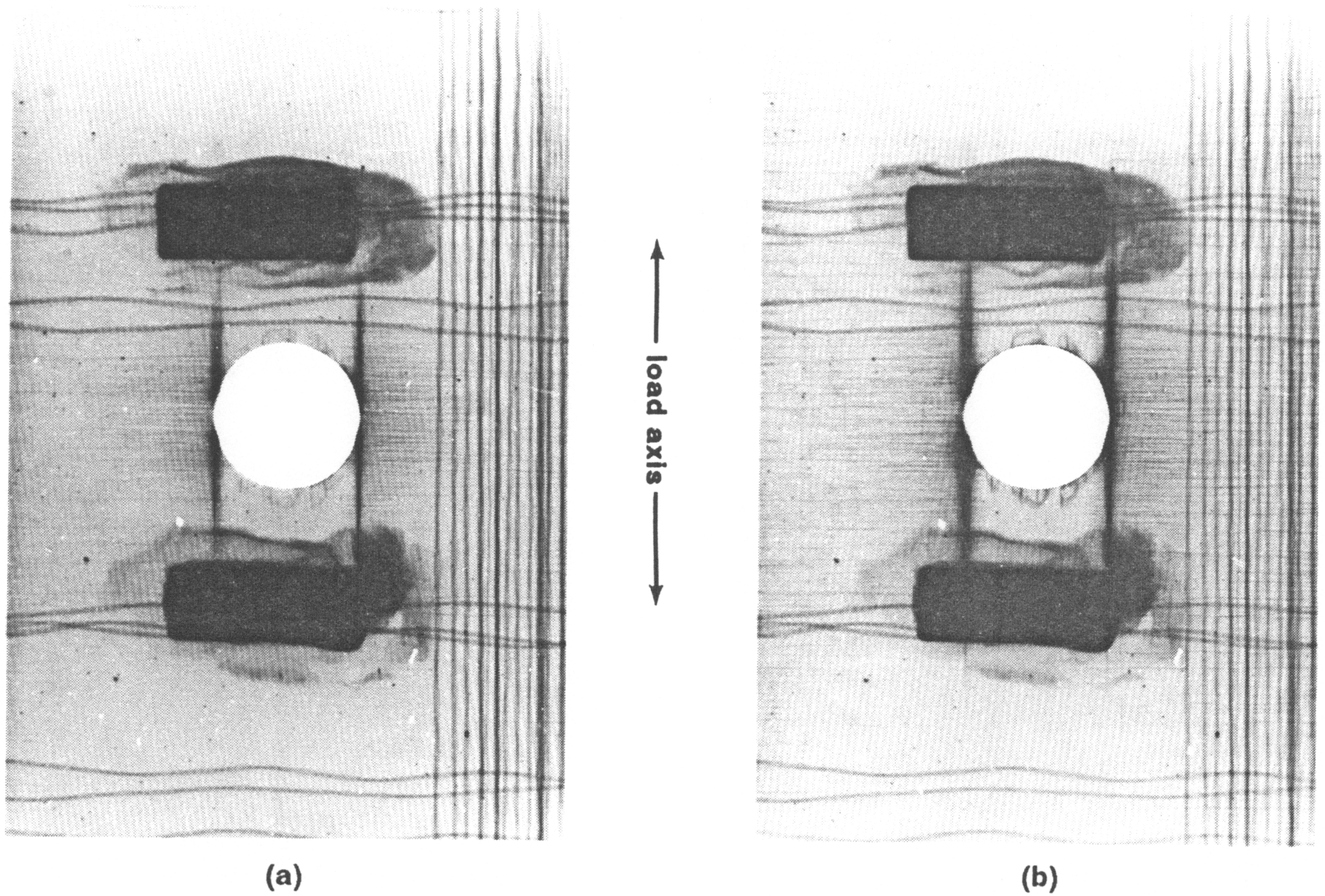

Figure 28. Radiographs showing front views of 22-ply 0 deg. specimen after (a) 10, (b) 2k, (c) 50k, and (d) 80k cycles. (continued on following page)

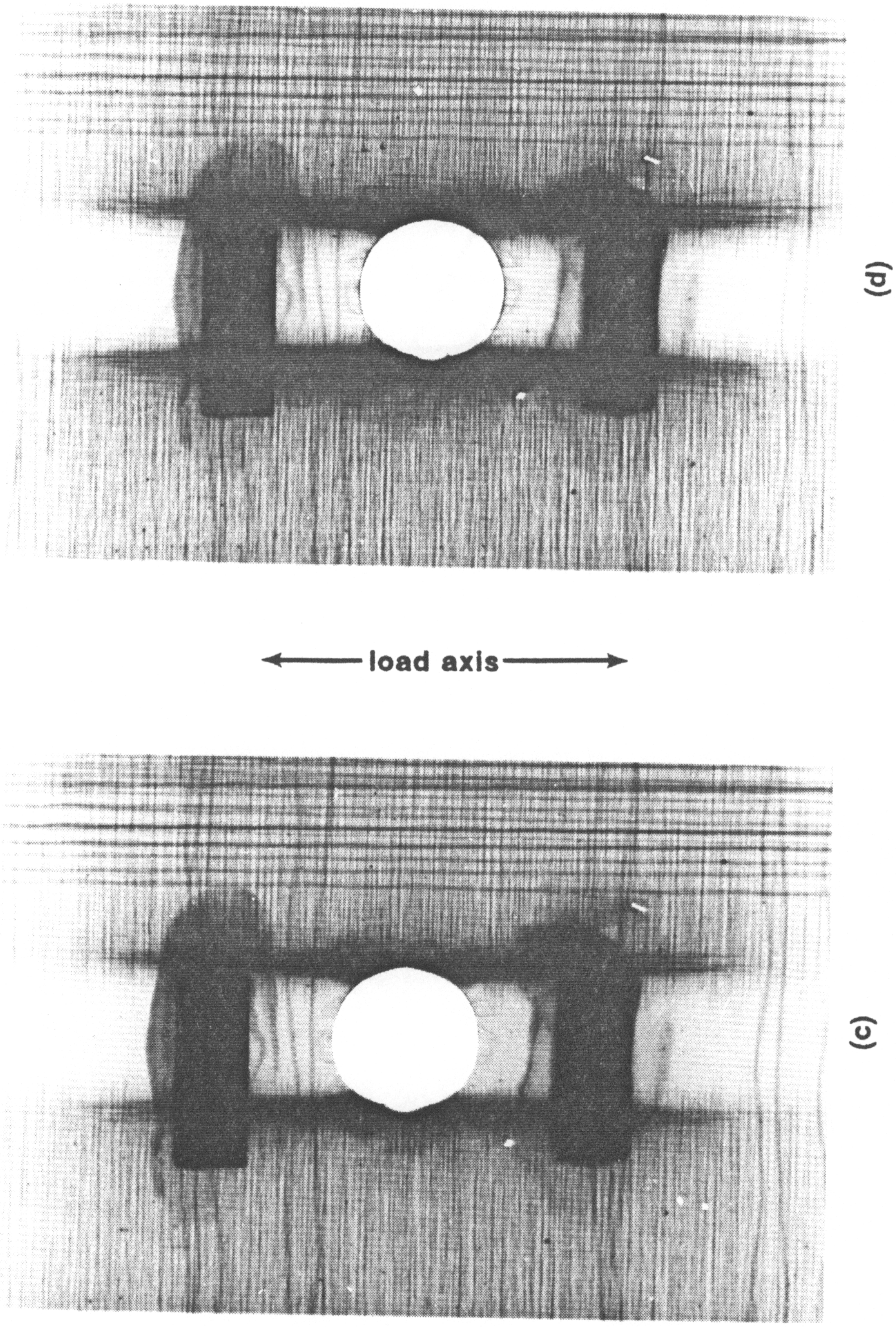

Figure 28. (continued from previous page)

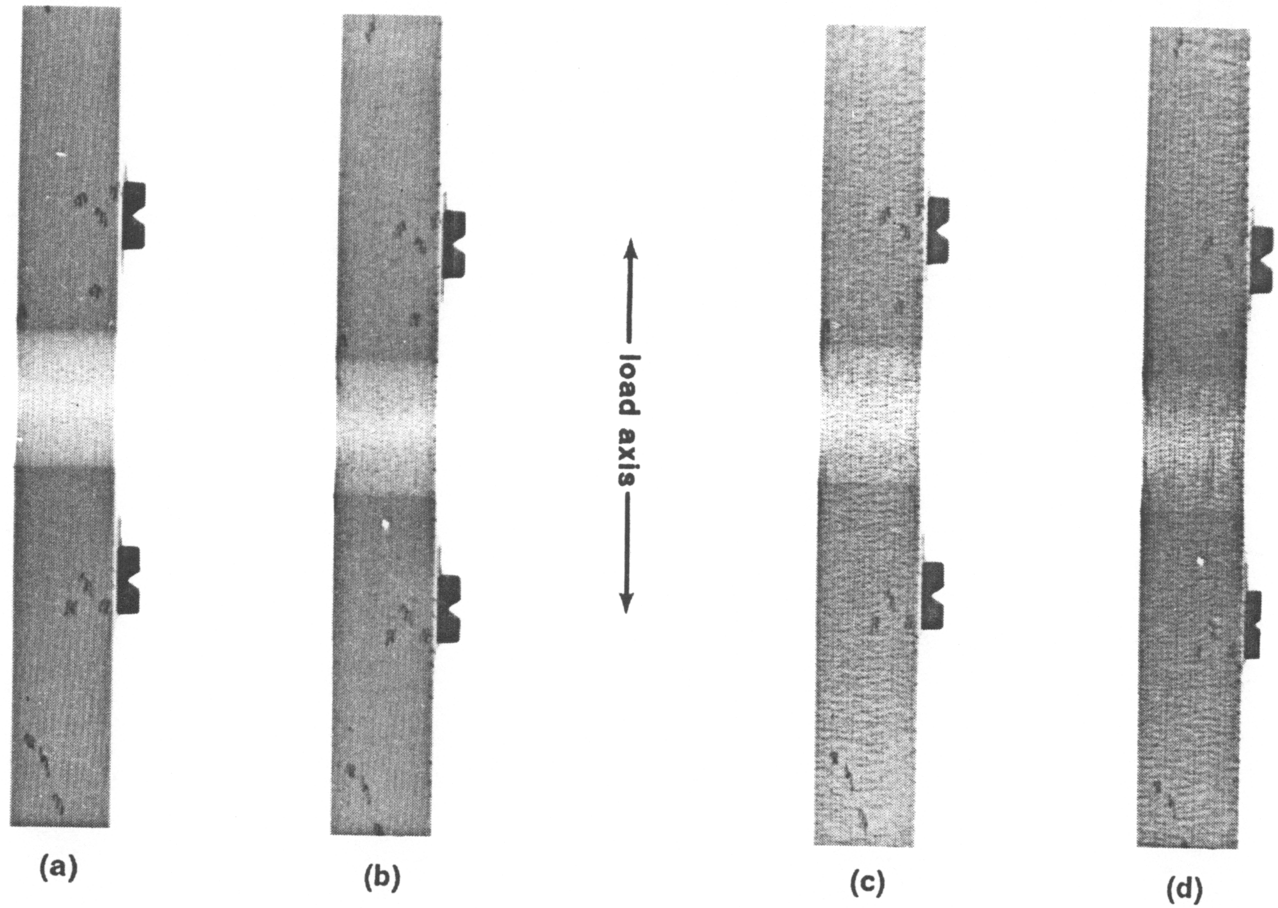

Figure 29. Radiographs showing edge views of 22-ply 0 deg. specimen after (a) 10, (b) 1k, (c) 50k, and (d) 205k cycles.

rows of cracks can be traced through the thickness. Damage in the surface plies again seems to be more dense than in the middle plies.

From the radiographs taken after 205,000 cycles, shown in Figure 28d and Figure 29d, growth of 0 deg. tangential cracks in the longitudinal direction appears to have slowed down, while growth in the transverse direction has continued. More and more 0 deg. matrix cracks have formed away from the notch area in the final stage of damage development. The machining damage is essentially the same as it was prior to fatigue cycling. No other damage is present above or below the hole. This fatigue test was stopped at this point, and the coupon was loaded monotonically to failure in tension. The residual strength was about 113% of the monotonic tensile strength of virgin specimens.

It should be noted that the small dark areas seen in the $(0,45,0,-45,0,0,-45,0,45,0)_2$ specimens did not form in this specimen. However, they were observed in several notched $(0)_{22}$ specimens that were loaded a few degrees off axis from the laminate axis. One such specimen, pictured in Figure 30 after 66,000 fatigue cycles at 90% of the ultimate strength, had a residual strength of 112%, approximately the same as that of the specimen shown in Figure 28 and Figure 29. The states of damage of the two coupons were quite different, however. The 0 deg. splits in the specimen in Figure 30 were not equal in length on both sides of the hole, suggesting that a shear load was present. Also, the splits were not nearly as dense as those observed in Figure 28d. The spots may be a result of shear stresses which are always present in the $(0,45,0,-45,0,0,-45,0,45,0)_2$ coupons. Although it may not be visible in Figure 30, close to these dark spots, very short, localized areas of 0 deg. matrix cracking are also present.

The progression of damage during tension-tension fatigue was also documented in a series of radiographs of a $(0,45,0,-45,0,0,-45,0,45,0)_2$ notched specimen. It should be kept in mind that matrix cracks originating at the free edges may be much longer than they appear

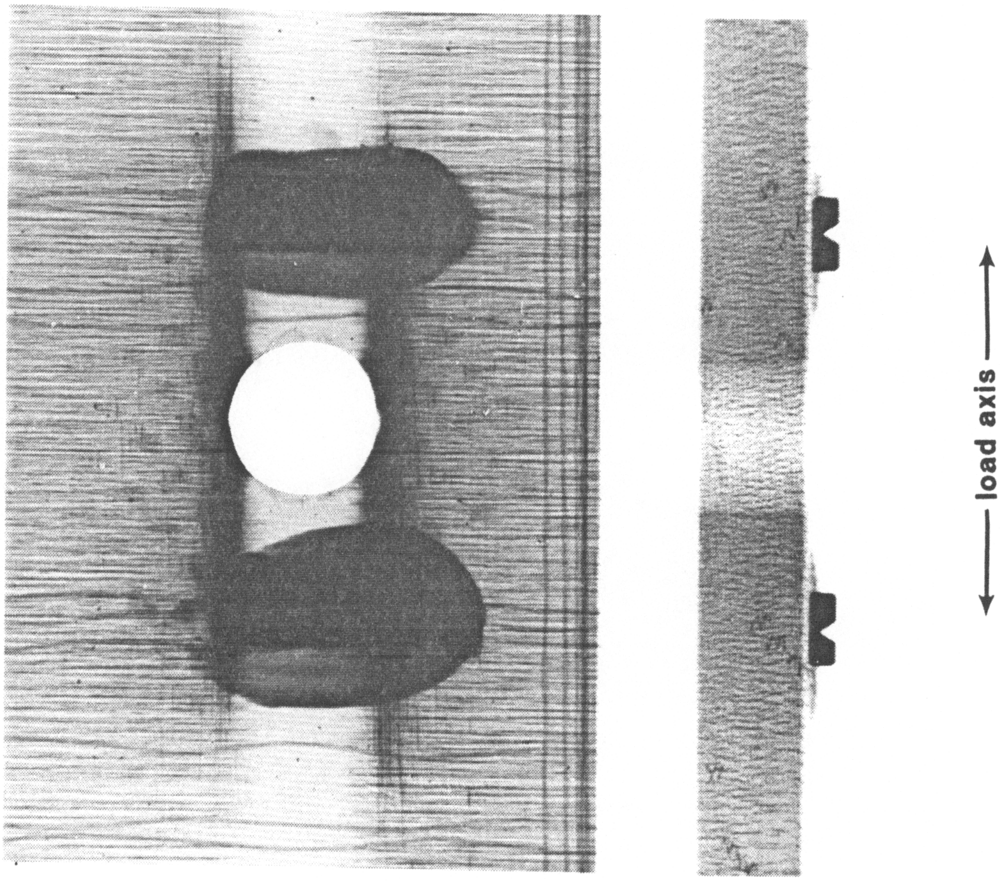

Figure 30. Radiographs showing local damage areas in a 22-ply 0 deg. notched specimen after 66k cycles at 90% of the ultimate strength.

in the radiographs due to the time-dependence of zinc iodide penetration discussed earlier in the Experimental Procedures chapter.

Figure 31 and Figure 32 illustrate damage development in a $(0,45,0,-45,0,0,-45,0,45,0)_2$ notched specimen, showing front and edge radiographic views, respectively, after 10, 2k, 50k, and 80k fatigue cycles. This coupon, cycled at 91% of the virgin tensile strength, eventually failed at 115k cycles after the top 0 deg. ply failed at the grip edge. All other plies broke through the hole.

As shown in Figure 31a, after 10 cycles, a number of 90 deg. matrix cracks are present both at the free edges and at the hole. In quasi-isotropic composited made from unidirectional plies, the damage does not have this symmetry about the notch; more cracks will develop in either the +45 or -45 deg. plies, whichever are closer to the 90 deg. plies [59]. Cracks parallel to the loading direction have formed tangent to the hole. From Figure 32a, this damage is evenly spread out through the thickness. The damage after 10 fatigue cycles at 91% of the tensile strength is very similar to that observed in the monotonic specimen in Figure 19 at 94% of the tensile strength. The only difference is that in the fatigue specimen, damage appears to be growing slightly more in the loading, rather than in the transverse, direction compared to the monotonic tensile specimen.

The density of matrix cracks around the hole increased as cycling was continued. More 0 deg. cracks formed near the hole and +45 and -45 deg. cracks initiated at the free edges after 2,000 cycles, as shown in Figure 31b. Damage in the surface plies was slightly more concentrated than in the inner plies as is evident from Figure 32b.

After 50,000 cycles, very dense matrix cracking, and possibly delamination, were present around the hole as shown in Figure 31c. The small dark spots believed to be localized damage at fiber bundle crossovers, previously observed in unnotched specimens in Figure 18b and c, began to appear on the radiographs at either side of the hole. The edge view in

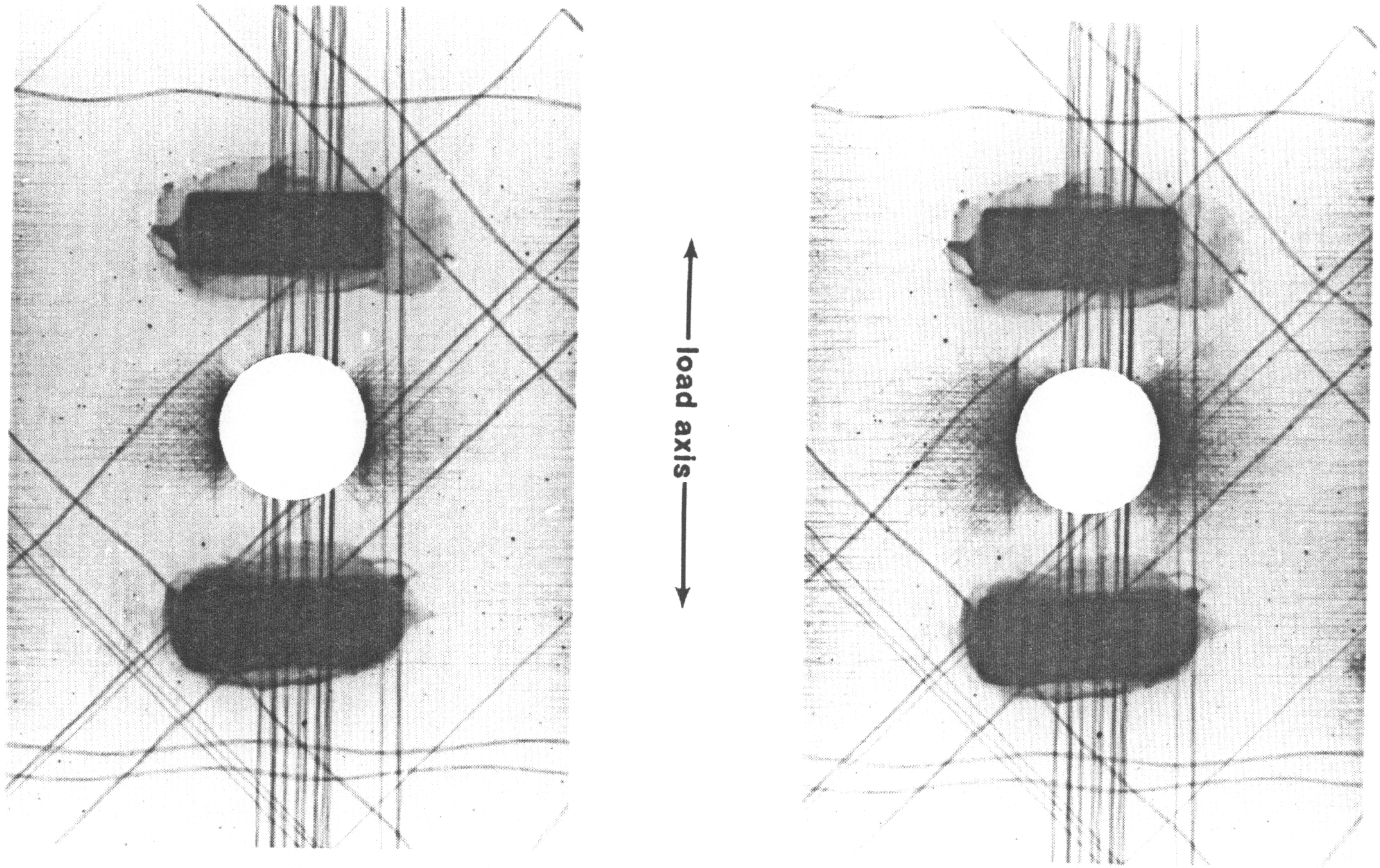

(a) (b)

Figure 31. Radiographs showing front views of 20-ply 0/45 deg. specimen after (a) 10, (b) 2k, (c) 50k, and (d) 80k cycles. (continued on following page)

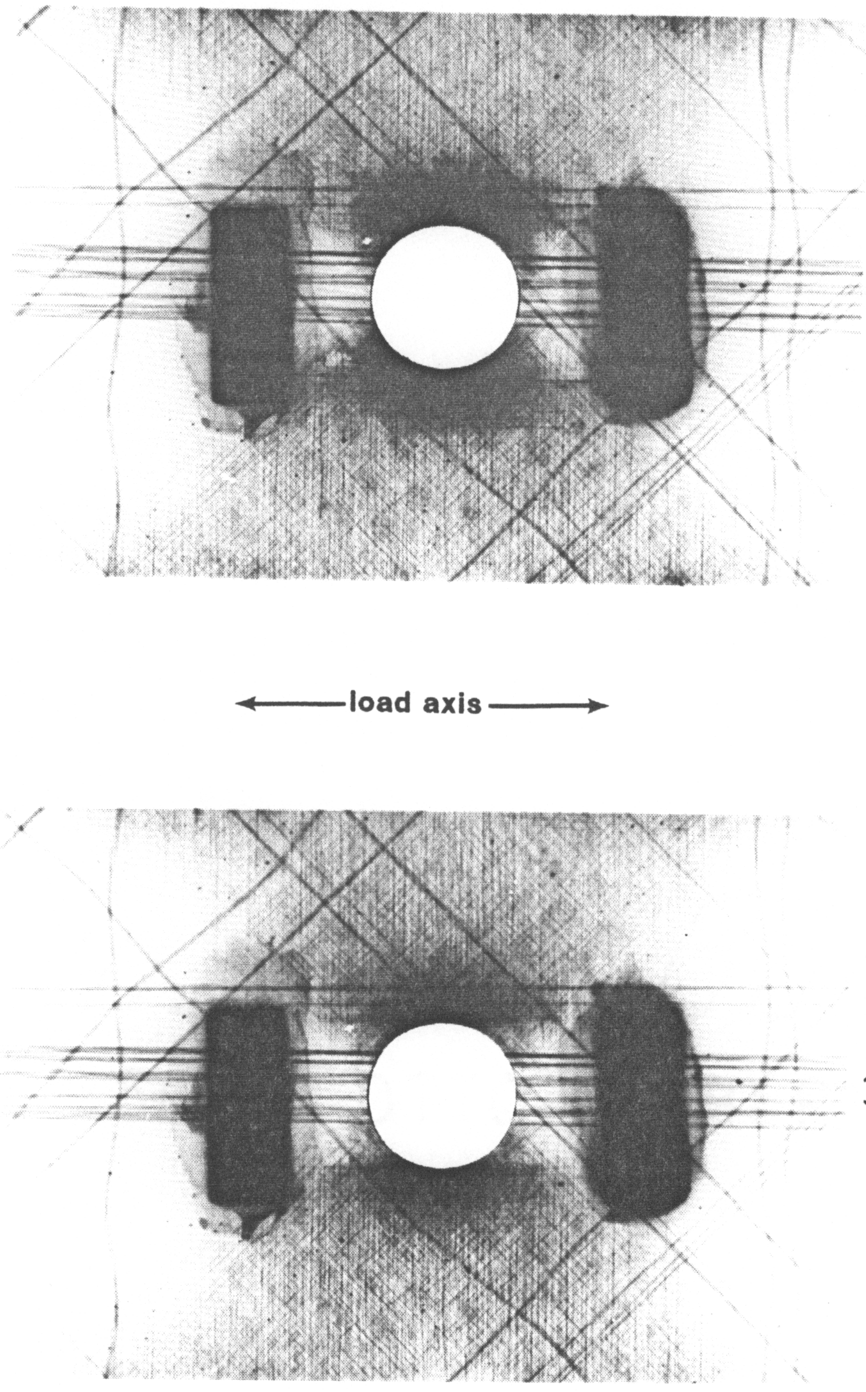

(d)

(c)

Figure 31, (continued from previous page)

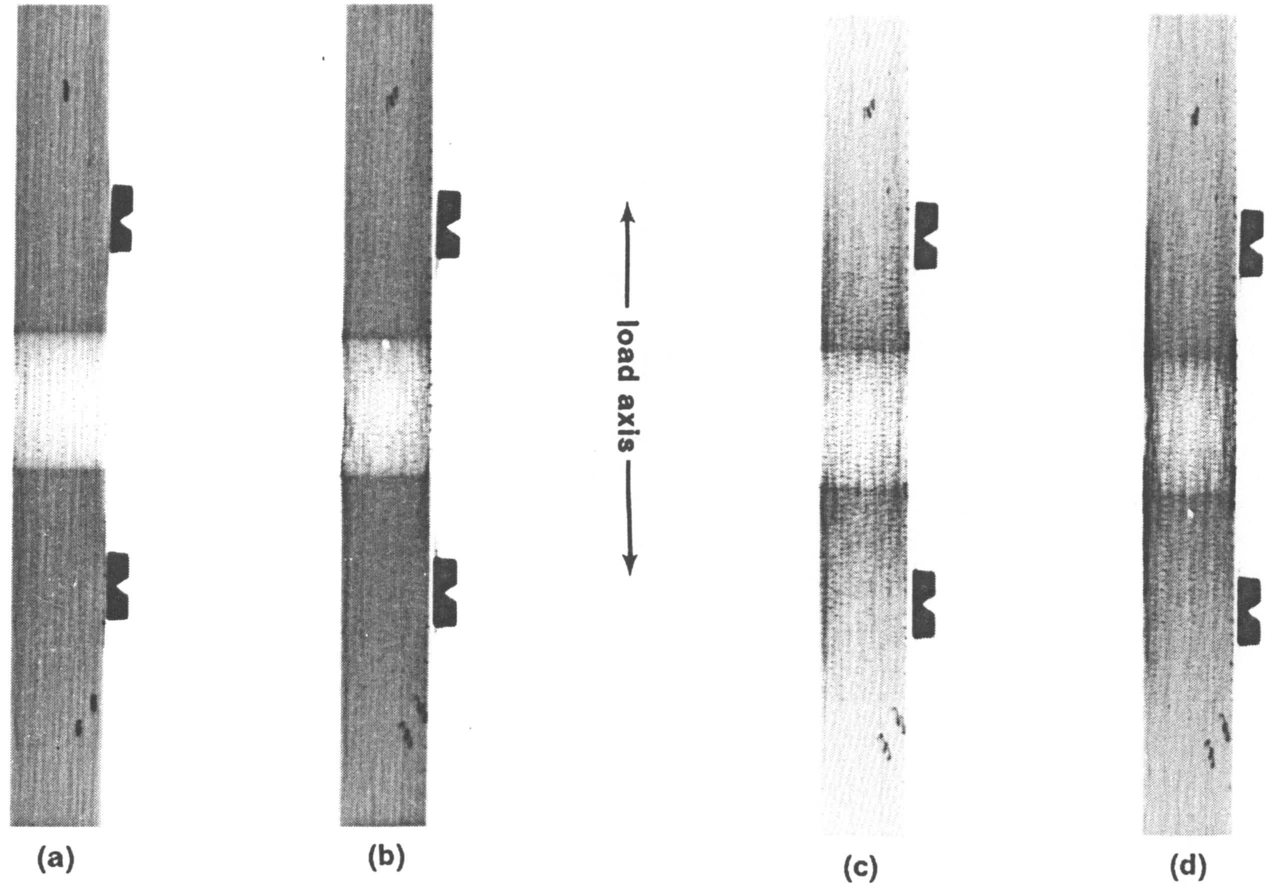

Figure 32. Radiographs showing edge views of 22-ply balanced specimen after (a) 10, (b) 2k, (c) 50k, and (d) 80k cycles.

Figure 32c shows that damage is particularly dense in the outermost plies. The damage state at 50,000 cycles is extremely more developed than that of the monotonic tensile specimen at failure as seen in Figure 19.

At 80,000 cycles, the dark spots are more pronounced as illustrated in Figure 31d. With the exception of damage spreading around the hole edges, no damage appears to be present in the regions directly above and below the notch. This specimen failed 35,000 cycles later after the surface ply (opposite the extensometer tabs in Figure 32) delaminated and broke at the grip. All other plies failed through the hole.

Thermographic examination was performed on notched $(0,45,0,-45,0,0,-45,0,45,0)_2$ coupons to determine the thermal patterns on the front and back plies, one having predominantly 0 deg. fibers on the surface, the other, 90 deg. fibers on the surface. Difficulty was encountered in performing the scans, as large loads were required to cause detectable heat generation. Thermal signals were weak and contained considerable amounts of noise, however, hot and cold patches following the weave pattern were observed in undamaged specimens. The weave pattern was not as distinct in specimens cycled to mid life. It is interesting to note that thermal patterns, which are dependent on damage and stress states, were not identical on the two sides of the specimens.

Fiber fracture studies were done on $(0)_{22}$ and $(0,45,0,-45,0,0,-45,0,45,0)_2$ notched coupons to determine the extent of fiber damage during tension-tension fatigue. Specimens were cycled at various load levels and deplied for scanning electron microscopic examination. It was found that very few fibers were broken late in life in either laminate, although the damage in the matrix system was extensive. Scattered broken 0 deg. fiber fractures were seen throughout the laminate, but 90 deg. fiber fractures were less common. In the $(0,45,0,-45,0,0,-45,0,45,0)_2$ notched material, essentially no broken +45 and -45 deg. fibers were observed. It is believed that the majority of fiber fractures occur over a very small percentage of life, in this woven graphite-polyimide material system, in possibly no more than

1,000 cycles in long term (over 1 million cycles) tests. In non-woven graphite-epoxy, fiber fractures have been observed to occur both early and late in life prior to the final catastrophic failure of notched specimens [70].

Figure 33 shows a 0 deg. ply from a $(0,45,0,-45,0,0,-45,0,45,0)_2$ notched coupon fatigued to late in life. This SEM micrograph was taken in the area tangent to the hole within the region of intense matrix damage observed in radiographs. It cam be seen that some 0 deg. and no significant 90 deg. fracture is present, implying that the internal ply constraint of the weave has not been lost. Although 0 deg. matrix cracking is present, these cracks are held together by the transverse 90 deg. fibers. In non-woven graphite-epoxy cross-ply laminates (0,90 deg. plies), 0 deg. matrix splitting is not constrained by the 90 deg. fibers in the adjacent plies [32].

Residual Strength Tests

Prior to residual strength testing, all specimens were X-rayed to help assess the state of damage of the material. In general, the greater the extent of matrix damage observed at the notch, the higher the residual tensile strength was. Very late in life, when damage to the load-bearing fibers becomes intense, the residual strength decreases until the strength of the specimen matches the applied cyclic stress and fatigue failure occurs.

Figure 34 and Figure 35 show two notched $(0)_{22}$ coupons with very different states of damage. Figure 34 is a radiograph of a specimen cycled for 3.4 million cycles at a maximum stress of 70% of the ultimate tensile strength of similar specimens. This loading is referred to as "very low" load, as fatigue failure is not expected to occur at such a load level. From the radiograph, 90 deg. matrix cracking is rather heavy, and some 0 deg. cracks have formed tangent to the hole. This specimen, considered to be at an early stage of life, had a residual

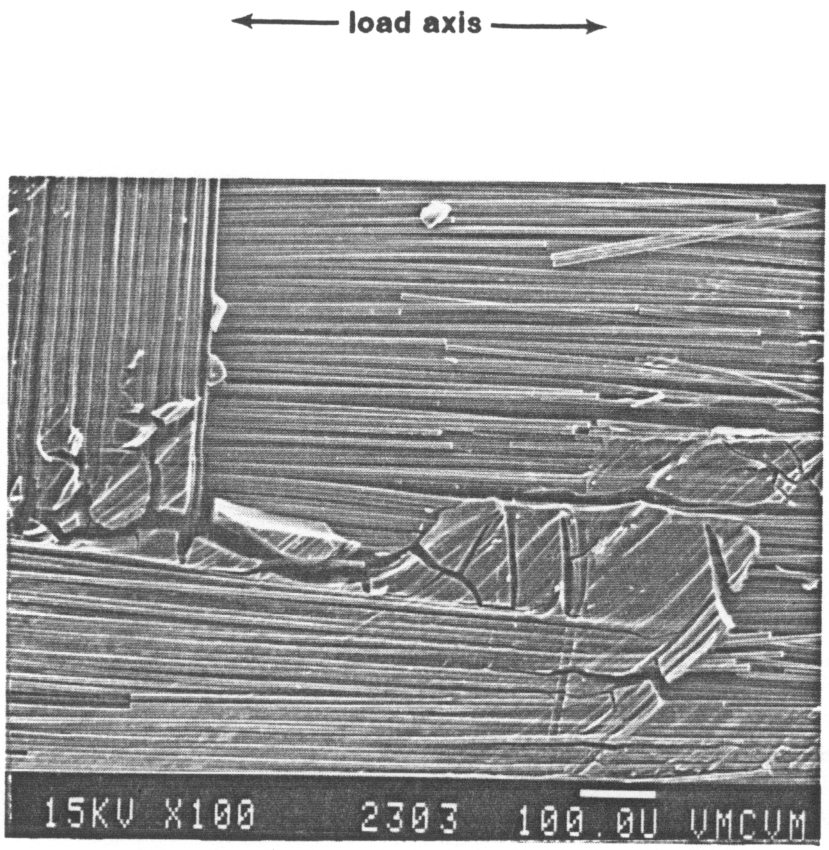

Figure 33. SEM micrograph of a 0 deg. ply from a 20-ply 0/45 deg. laminate showing fractured 0 deg. fibers.

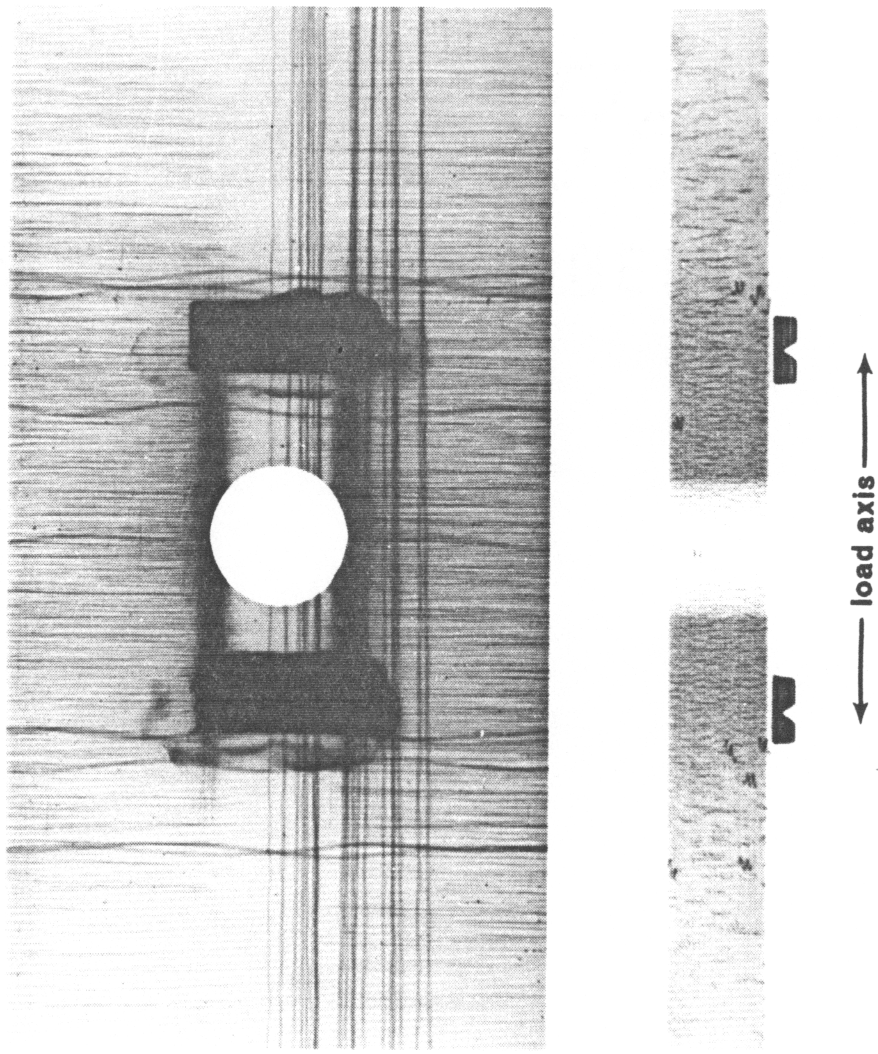

Figure 34. Notched 22-ply 0 deg. specimen fatigued for 3.4 M cycles at 70% of the tensile strength.

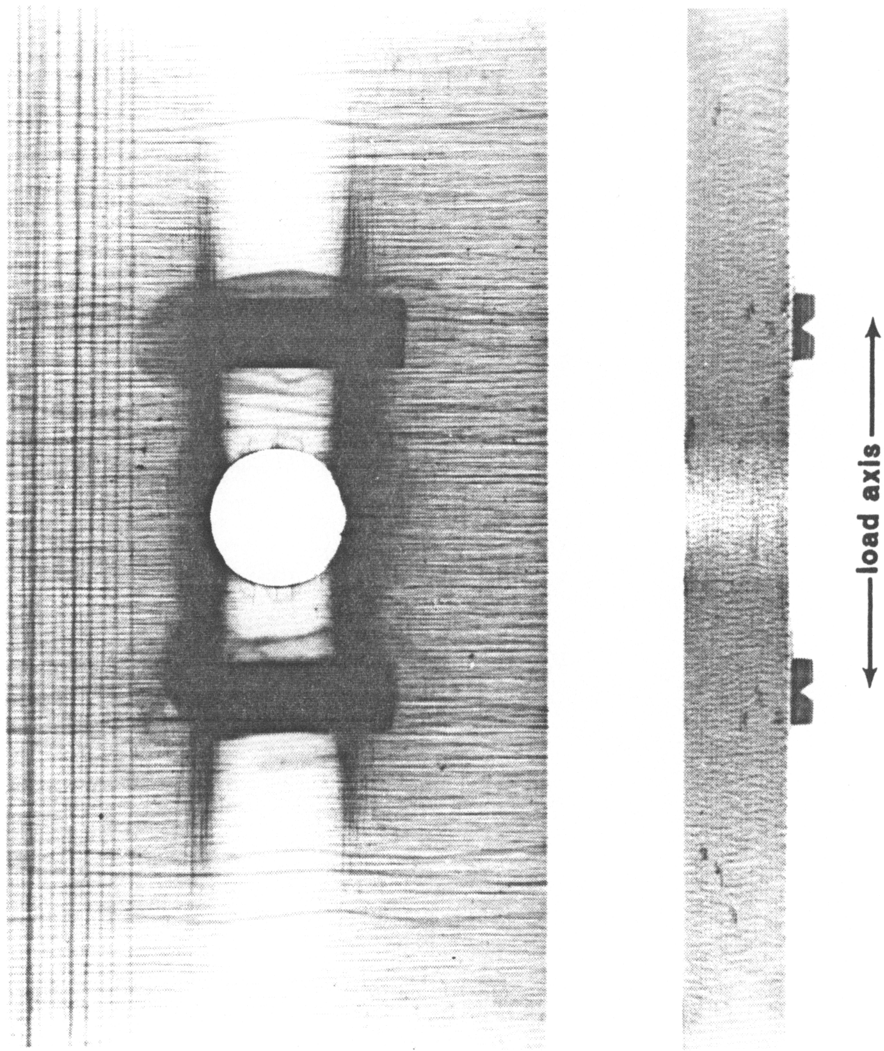

Figure 35. Notched 22-ply 0 deg. specimen fatigued for 205 k cycles at 96% of the tensile strength.

tensile strength of 107%, as compared to 113% for the specimen pictured in Figure 35 (previously shown in Figure 28 and Figure 29).

The "high" load, late life coupon in Figure 35 was cycled at 96% of the tensile strength for 205,000 cycles. It was expected to fail in an additional 50,000 to 100,000 load cycles. The damage in this coupon was much more extensive than that in the very low load coupon in Figure 34. Matrix cracking in the 90 deg. direction was slightly more concentrated. Cracks tangent to the hole in the 0 deg. direction were much longer and denser.

The net effect of the highly developed damaged state in the late life specimen was to decrease the stress concentration at the hole and increase the tensile strength more than the less developed damage state did in the early life specimen. Based on other residual strength tests run on $(0)_{22}$ notched material, the residual strength for a given state of damage is independent of the of stress level or number fatigue cycles needed to create that state of damage. That is, if a very low load specimen was cycled so that the state of damage matched that of a high load specimen, the residual strengths of the two would be identical.

Similar trends were observed in the notched $(0,45,0,-45,0,0,-45,0,45,0)_2$ coupons. Figure 36 and Figure 37 show radiographs of a high load, middle life, and a low load, late life specimen, respectively. The high load specimen, fatigued for 5,500 cycles at a maximum stress of 94% of the notched tensile strength, is saturated with 90, +45, and -45 deg. matrix cracks. Delamination around the hole is very limited if at all present. Small localized damage regions have begun to form a pattern of small dark spots away from the hole. Note that matrix cracks have extended above and below the hole at a distance approximately one hole diameter away from the edge of the notch. This was not observed in the $(0)_{22}$ material. This specimen had a residual tensile strength of 104% of the tensile strength of similar specimens, showing that the net effect of the damage on strength was very minimal.

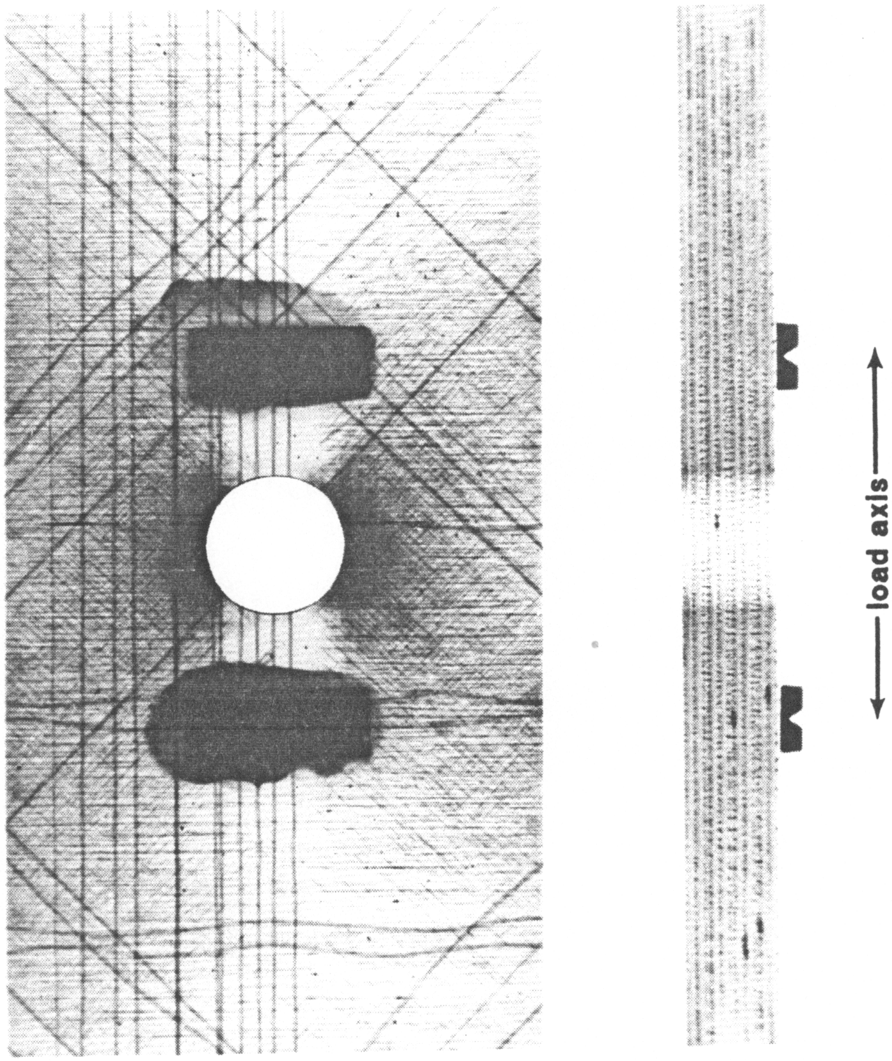

Figure 36. Notched 20-ply 0/45 deg. specimen fatigued for 5.5 k cycles at 94% of the tensile strength.

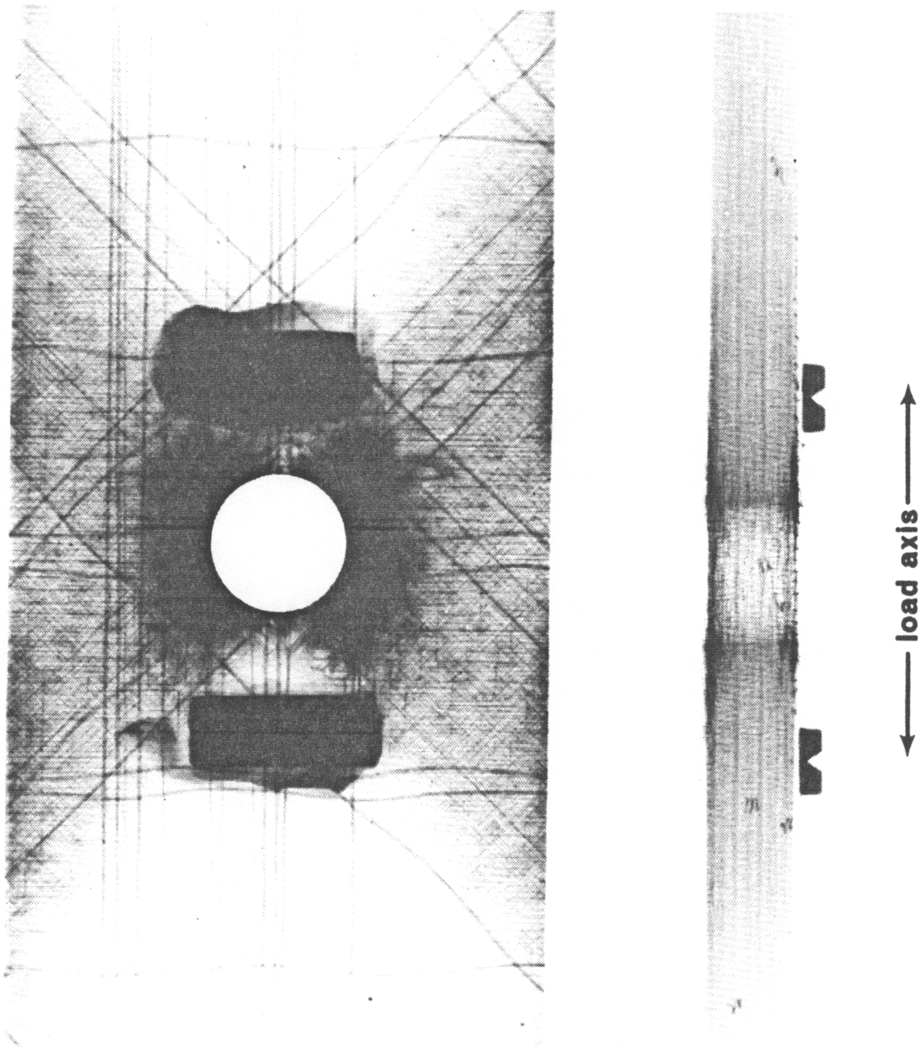

Figure 37. Notched 20-ply 0/45 deg. specimen fatigued for 1.8 M cycles at 91% of the tensile strength.

The low load coupon shown in Figure 37 was subjected to 1.8 million cycles at 91% of the notched tensile strength. Damage development has progressed much further in this late life specimen than in the middle life specimen in Figure 36. Matrix cracks in the 90, +45, and -45 deg. directions are very heavy, and most likely extend above and below the hole as in the middle life coupon. Numerous 0 deg. cracks exist away from the notch. It appears that the surface plies are delaminating near the hole. Also, the pattern of small localized damage areas is well developed. This specimen had a residual tensile strength of 109%, exhibiting a slightly higher strength than that of the middle life specimen. Note that damage in the $(0,45,0,-45,0,0,-45,0,45,0)_2$ notched material has grown more in the transverse direction and less in the loading direction than did the damage in the $(0)_{22}$ material, and as a result, had smaller increases in residual strength. It appears that damage growing in the loading direction is "good" damage as it tends to help reduce the stress concentration around the hole, while damage growing transversely is "bad" damage, as it tends to degrade residual strength. That is, under uniaxial tension-tension fatigue loading, longitudinal damage appears to increase residual tensile strength, while transverse damage appears to decrease residual tensile strength.

Figure 38 shows a radiograph of a notched, non-woven $(0,90,+/-45)_s$ graphite-epoxy specimen [59] fatigued under tension-tension loading ($R=0.1$, $f=10$ Hz) for 600,000 cycles at 80% of the virgin notched tensile strength. Matrix cracking was more dense in the graphite-polyimide specimens than in the graphite-epoxy specimen due to matrix brittleness. Delaminations grew at every ply interface both above and below the hole in the non-woven material. Matrix cracks also extended above and below the notch. This was not the case with the woven graphite-polyimide specimens. Unlike the damage in the $(0,45,0,-45,0,0,-45,0,45,0)_2$ graphite-polyimide cloth laminate, more matrix cracks appeared in the +45 deg. direction than in the -45 deg. direction in the graphite-epoxy tape laminate. Damage in the non-woven specimen grew primarily in the loading direction and not towards the free edges as in the 0/45 deg. cloth material. The residual strength of this tape laminate would be as high as 120-130% [59].

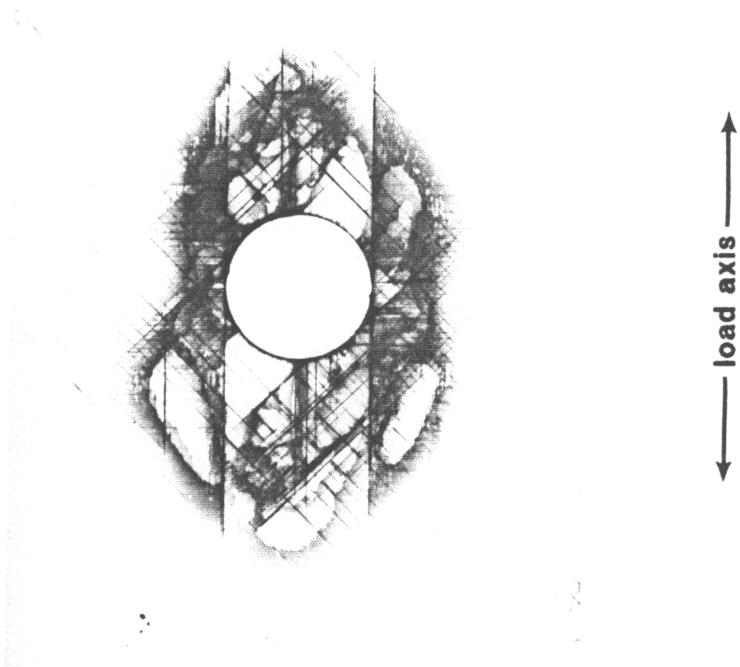

Figure 38. Radiograph of a (0,90,+/-45)s non-woven graphite-epoxy specimen fatigued at 80% of the ultimate strength for 600k cycles (mid life).

From the residual strength data on non-woven graphite-epoxy [65-67], it is evident that residual tensile strengths of the woven graphite-polyimide material are rather low. Theoretically, the highest residual strengths would occur if the stress concentration effect of the hole could be eliminated due to damage. This is only possible if the strips of material at either side of the hole became totally isolated from the interior section and these strips of material had a residual tensile strength as high as the unnotched material. In this case, the maximum residual strength for both the $(0)_{22}$ and the $(0,45,0,-45,0,0,-45,0,45,0)_2$ notched coupons would be about 125% of the virgin strength.

However, because damage consists of both "wear-in" and "wear-out" processes, such strengths most likely will not be achieved. The "wear-in" damage would tend to decrease the effect of the stress concentration at the same time the "wear-out" damage degraded the strength of the material. It is not yet known whether a lack of "wear-in" damage due to the woven architecture or excessive "wear-out" damage due to matrix brittleness is responsible for the low residual tensile strengths of the woven graphite-polyimide material. Most likely, it is some combination of the two.

IV. NOTCHED STRENGTH PREDICTIONS

In this chapter, a failure theory is presented and used to predict the notched quasi-static tensile strength of woven Celion 3000-PMR-15. Unlike the Whitney-Nuismer average and point stress failure criteria, this failure theory is applied on the ply level, rather than on the laminate level. Using experimentally determined notched strengths for two layups, a material parameter postulated to control failure is calculated by matching experimental and predicted strengths for one laminate. With this parameter, the strength of the other laminate is predicted and compared to the experimental value. Conclusions are made as to the validity of this model under quasi-static loading. Suggestions concerning the extention of this model to predict residual strength during tension-tension fatigue are also presented.

Introduction

In recent years, much research has been directed toward understanding the behavior of notched composite materials. Various fracture models, summarized in reference [70], have been developed to predict the notched strength of anisotropic materials. Because failure modes and damage mechanisms are dependent on the material system, no single failure criterion has been proven to accurately characterize all material systems. Several researchers have attempted to apply linear elastic fracture mechanics (LEFM) to composite materials. Waddoups, Eisenmann, and Kaminski [71] have created such a LEFM fracture model. They related energy release rates to stress concentration factors to explain the increase in residual strength exhibited by some composite systems.

One of the problems with applying LEFM to fiber reinforced composites is that the notched strength of a composite cannot be characterized by the stress concentration factor at a point on the notch [72]. Aware of this fact, Whitney and Nuismer [38] introduced the idea of a process zone. They claimed that the notched strength of a composite depends on the in-plane elastic stresses over a region adjacent to the circular hole boundary rather than just at the boundary itself. Two failure criteria resulting from this concept are the point stress and average stress failure models. The first predicts failure when the stress at some distance, d_0, away from the hole exceeds a critical value, while the latter predicts failure when the average stress over a distance, a_0, from the hole exceeds a different critical value. These theories may be very useful if d_0 or a_0 are proven to be material properties as postulated. If so, once a_0 or d_0 and the unnotched tensile strength have been experimentally determined, the notched strength of that material may be predicted for any given stacking sequence and geometry. Experimental results show that the average stress criterion is more accurate than the point stress criterion, however, some dependence of a_0 on stacking sequence was noted [70].

Laminate level failure theories do not account for differences in properties of individual plies; nor do they account for different damage states in individual plies. Laminate level theories predict laminate failure when global laminate stresses exceed a critical value. As a result, these theories are not always accurate when ply orientation angles are changed, or when the material around the notch has been damaged due to cyclic loads. The ply level theory used in this study accounts for differences in the properties, and hence, in the stress states of individual plies. The accuracy of predictions is not expected to be dependent on stacking sequence. The advantage of this type of a failure model is that an individual ply is predicted to fail and its moduli are discounted to simulate damage development. As a result, the stress states of the other plies are affected in a realistic and sequential manner throughout the failure process. Such a discount scheme could prove very useful in modelling the effect of fatigue "wear-in" and "wear-out" damage on residual tensile strength.

Analysis

An elliptical hole was used to model the notch because the two half lengths, a and b, could be used to model "wear-in" and "wear-out" damage, respectively. By using these two parameters rather than just the hole radius, r, to describe the notch geometry, it is possible to get increases in residual tensile strengths that have been observed during actual fatigue tests. For an analysis of monotonic tensile strength, a and b are set equal to the notch radius, r, as shown in Figure 39 Figure 40 shows the notch after a and b have been increased to simulate fatigue damage at the circular hole.

In order to model the notched strength of a material, approximate stress distributions near the notch must be known. For the case of an elliptical hole in an infinite, homogeneous plate, a closed form plane stress elasticity solution can be found by starting with the complex potentials described by Lekhnitskii [73]. The solution for a circular hole is the special case in which the axes of the ellipse are of equal dimensions. References [74] and [75] use two different approaches to derive the in-plane stresses, σ_x, σ_y, and τ_{xy}. The complete solution from [75] is presented in Appendix A.

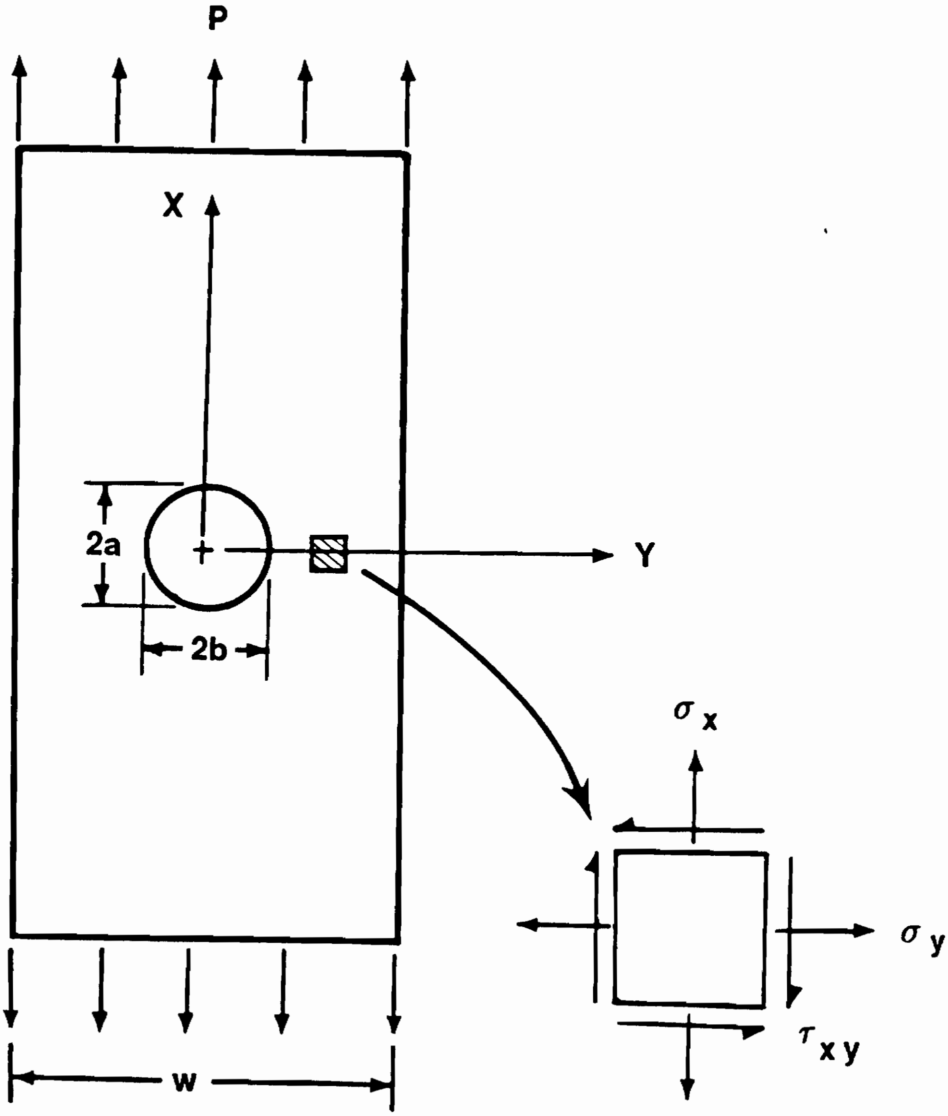

Figure 39. Specimen geometry for monotonic tensile strength analysis.

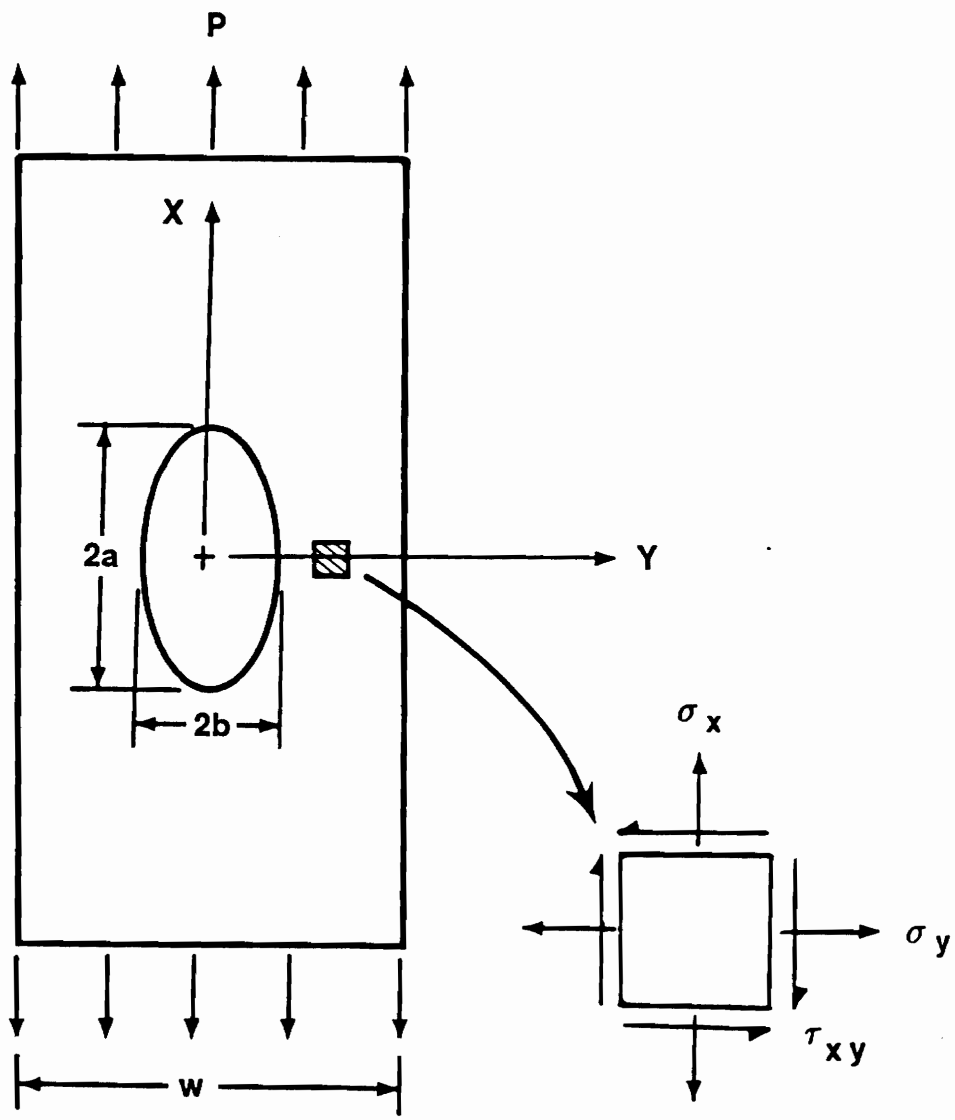

Figure 40. Specimen geometry for residual tensile strength analysis of a specimen damaged during cyclic loading.

Several assumptions are made when applying this solution to a laminate. In order to meet the requirement of homogeneity, effective laminate compliances may be used as material properties. However, this implies that stresses and strains are constant through the thickness, which is not true near a free edge such as a notch. This will affect the accuracy of results to some extent. The infinite plate assumption may not be valid for the test coupons used in experimental strength measurements. The hole diameter to thickness ratio was approximately 1.4, while the diameter to width ratio was 0.25. Whitney and Nuismer [38] used a finite width correction factor for diameter to width ratios greater than 0.04 to increase experimental strengths when the test coupons were considered finite.

If the homogeneity and infinite plate assumptions are reasonable, global laminate stresses and strains may be calculated from the elasticity solution. The resulting in-plane global stresses are constant through the thickness but vary with the in-plane coordinates, x and y. Figure 39 and Figure 40 show the coordinate system used in this chapter. After setting external force resultants equal to the global laminate stresses multiplied by the laminate thickness, classical lamination theory can be used in the determination of ply level stresses, which vary through the laminate thickness.

Borrowing concepts from the Whitney-Nuismer average stress model [38], failure criteria are calculated along the y-axis in each ply. In this case, the maximum strain failure theory was chosen. Criteria were normalized such that ply-level failure is predicted if a criterion, F_i, is greater than unity when averaged over a distance a_o in an individual ply. That is, at failure,

- $1 < \bar{F}_i = \bar{\varepsilon}_i/\varepsilon_{it}$ for $\varepsilon_i > 0$, or

- $1 < \bar{F}_i = \bar{\varepsilon}_i/\varepsilon_{ic}$ for $\varepsilon_i < 0$, where bars denote average values, and the subscripts t and c denote tension and compression.

A ply discount scheme was used to reduce ply moduli whenever failure was predicted. If a ply failed by transverse stress or by shear stress, both E_2 and G_{12}, the transverse and shear moduli, were set essentially to zero. If for some reason a ply failed due to stresses in the fiber direction before ultimate laminate failure, E_1 and G_{12} would be discounted similarly.

The notched strengths of two laminates with different stacking sequences have previously been measured. The goal of this investigation is to find a_0 by matching predicted and experimental strengths for one layup, then testing to see if the strength of the other could accurately be predicted using the same value for a_0 . Lengthy calculations were performed with the aid of a computer code which follows the algorithm outlined in Figure 41. A complete listing is included in Appendix B.

Results and Discussion

Following the procedure outlined in the previous section, numerical strength predictions were made for quasi-static tensile loading. Since all laminates to be considered are orthotropic, $S_{13} = S_{23} = 0$, in the characteristic equation (eqn. 1) given in Appendix A. Therefore, μ_k^2 can be found simply by applying the quadratic equation to the characteristic equation. The four roots are then found by taking the positive and negative square roots of the expression for μ_k^2 .

Two different laminate stacking sequences were examined, the $(0)_{22}$ and $(0,45,0,-45,0,0,-45,0,45,0)_2$ materials. Since laminate compliances are dependent only on the

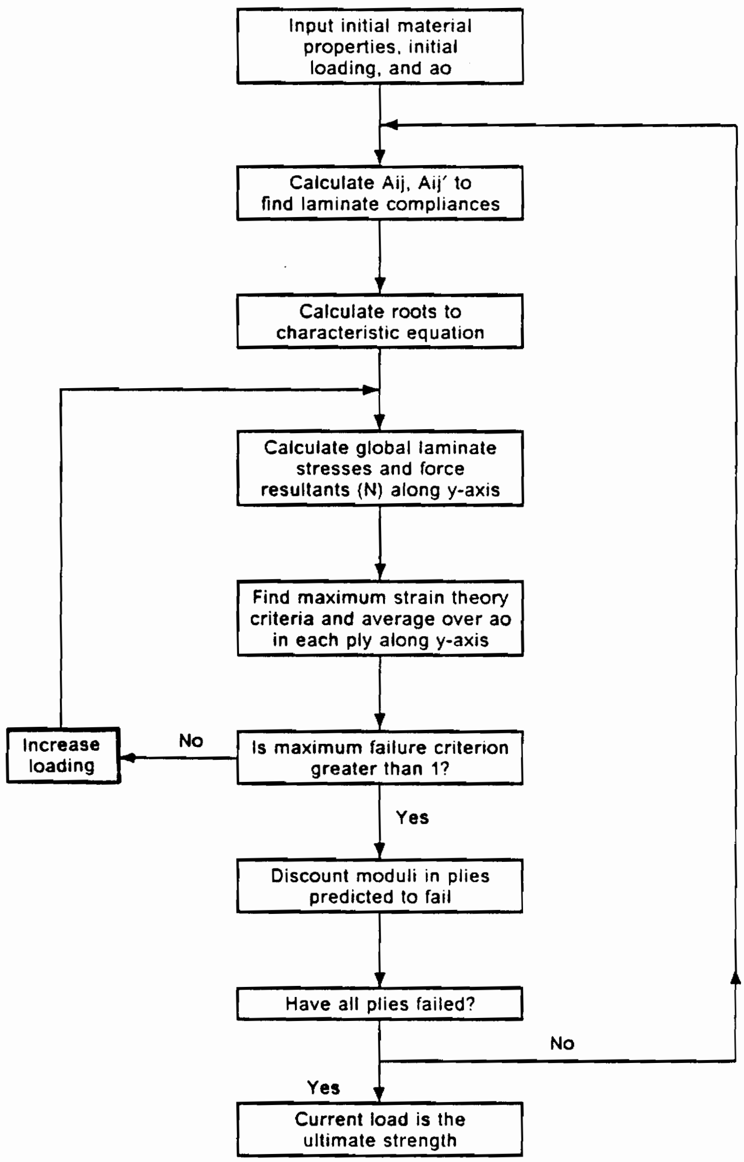

Figure 41. Computer algorithm.

ratio of ply orientation angles, for simplicity, the $(0)_{22}$ was treated as a (0) laminate and the $(0,45,0,-45,0,0,-45,0,45,0)_2$ was treated as a $(0_3, +45,-45)$ laminate. Calculations for the $(0)_{15}$ are identical to those for the $(0)_{22}$ layup. Material properties used for the analysis are listed in Table 10. These were furnished by General Electric and include strength and stiffness data.

Using the computer code listed in Appendix B, quasi-static tensile strength predictions were made for a coupon containing a 3/8" diameter hole for the both layups. Elasticity stress solutions are plotted in Figure 42 and Figure 43. In both figures, global laminate stresses are normalized to the applied axial stress. In the case of the 0 deg. laminate, global and ply level stresses are equal. Figure 42 shows the variation of axial stress, σ_x, as a function of distance from the center of the hole. The 0 deg. laminate had a maximum axial stress of about 4.9 times the applied stress at the edge of the hole. The stress quickly dropped off to the applied value at approximately 0.75 in., corresponding to the edge of the coupons tested in this study. Axial stresses in the $(0,45,0,-45,0,0,45,0,-45,0)_2$ laminate behaved similarly, except the maximum stress was about 3.2 times the applied value. For an isotropic material, the stress concentration at the hole would be 3.0.

Normalized global transverse stress, σ_y, is plotted versus distance from the center of the hole in Figure 43. For both laminates, the transverse stress at the hole edge is zero, satisfying boundary conditions. The transverse stress peaks at 22% and 35% of the applied axial stress for the 0 deg. and $(0,45,0,-45,0,0,45,0,-45,0)_2$ stacking sequences. These stresses do not reach zero at 0.75 in., the edge of the specimens used in this study. The transverse stresses are lower in the 0 deg. laminate, probably because it has a higher poissons ratio, ν_{xy}.

Figure 44 shows a plot of the predicted notched tensile strength values versus the process zone parameter, a_0. As expected, strength predictions generally increased with a_0. This occurs because stresses are highest at the hole boundary and decrease away from the

Table 10. Material Properties Used in Analysis.

- E_{1t} = 11.3 msi
- E_{1c} = 8.7 msi
- E_{2t} = 10.2 msi
- E_{2c} = 8.5 msi
- G_{12} = 0.85 msi
- ν_{12} = 0.07
- X_t = 105 ksi
- X_c = 90 ksi
- Y_t = 110 ksi
- Y_c = 82 ksi
- S = 13 ksi
- ε_{1t} = 9.3 x 10^{-3}
- ε_{1c} = 10.3 x 10^{-3}
- ε_{2t} = 10.8 x 10^{-3}
- ε_{2c} = 9.6 x 10^{-3}
- γ_{12} = 15.3 x 10^{-3}

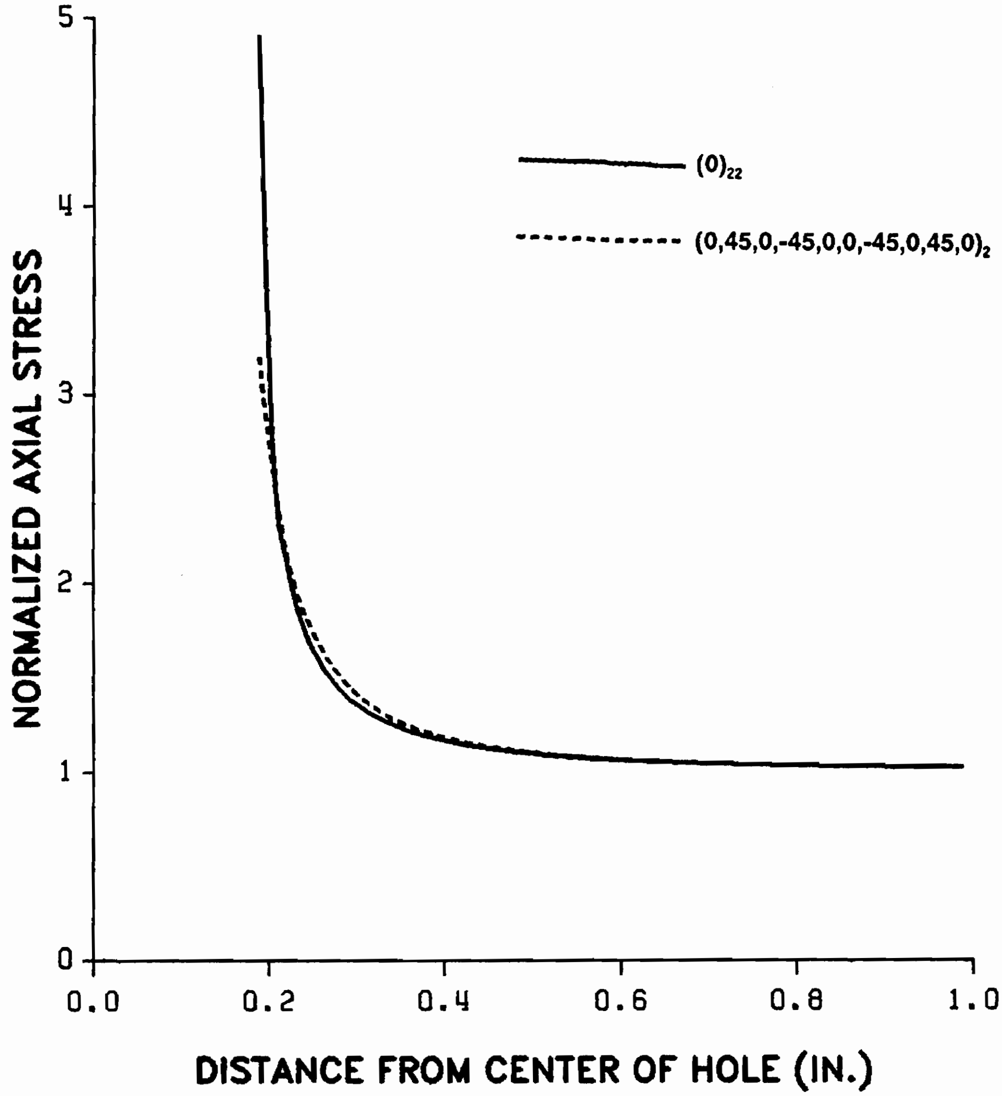

Figure 42. The variation of axial tensile stress versus distance from the center of the hole.

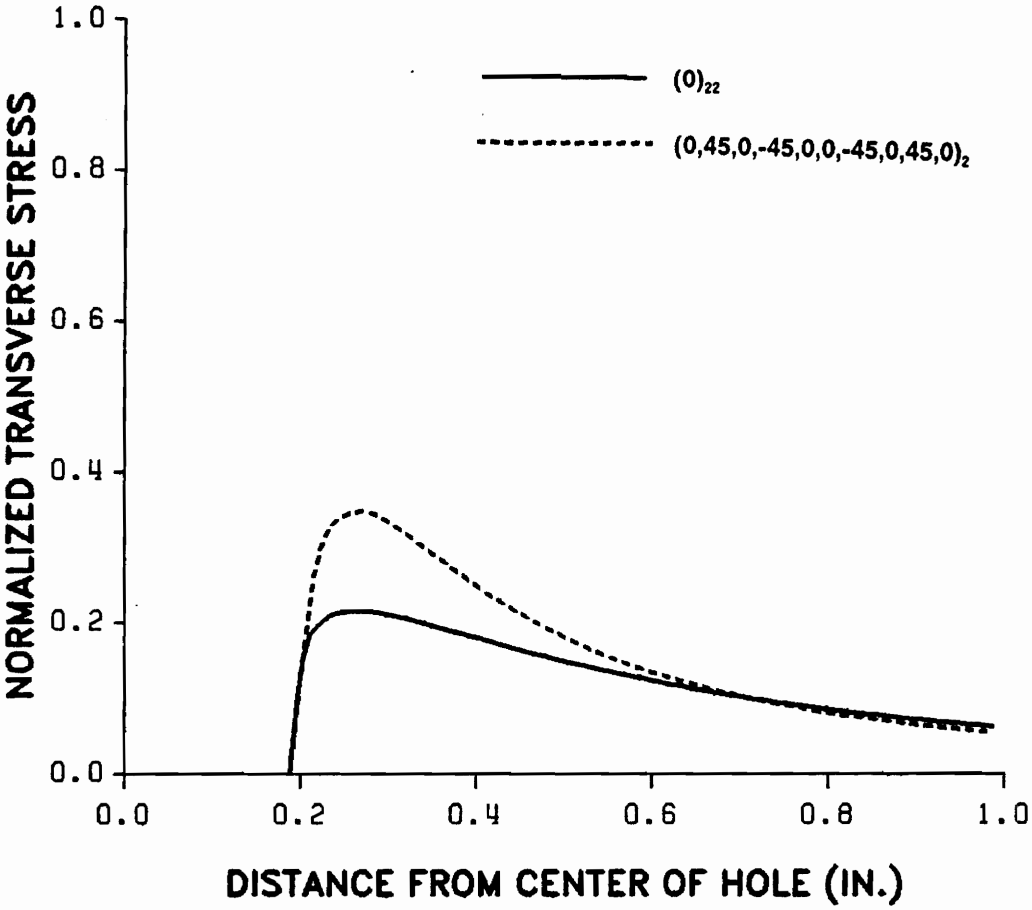

Figure 43. The variation of transverse tensile stress versus distance from the center of the hole.

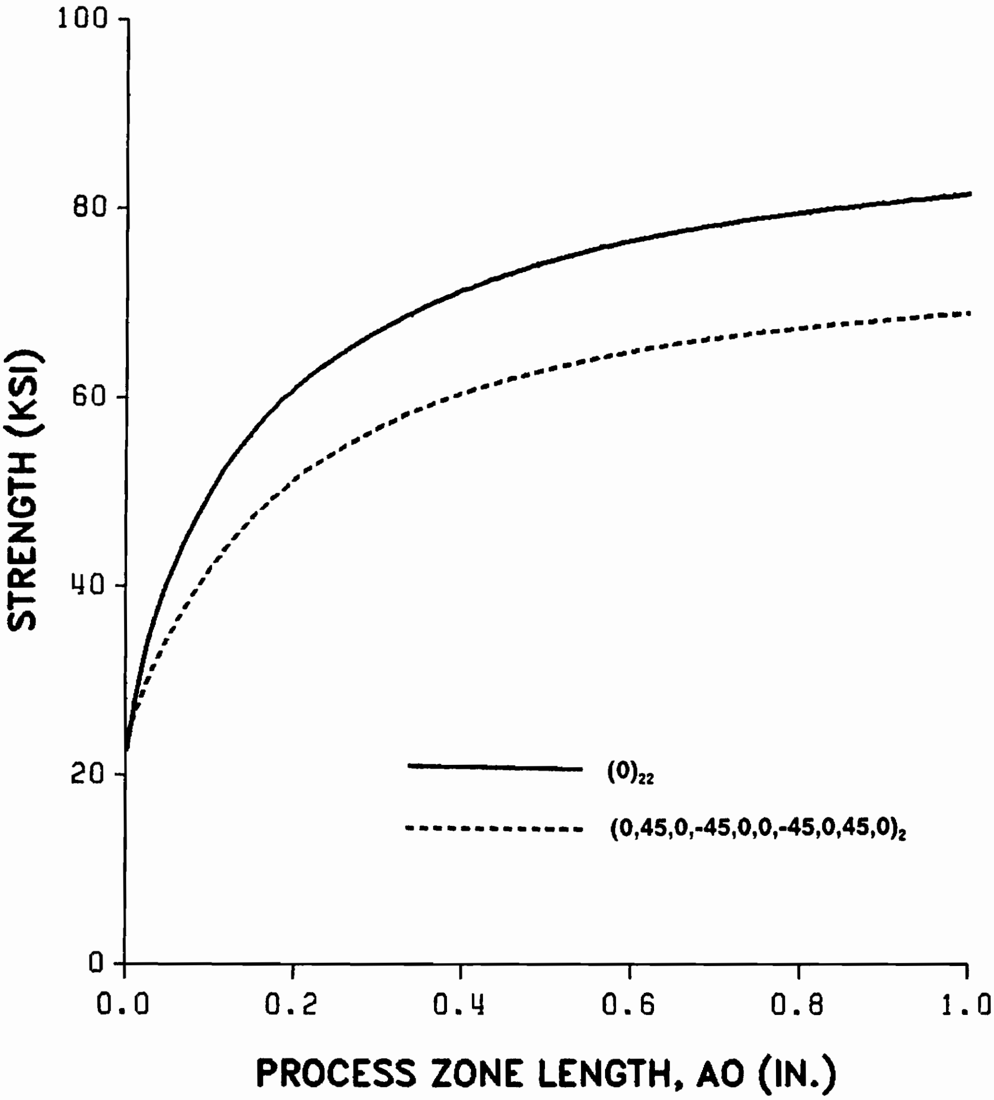

Figure 44. The variation of predicted tensile strength as a function of process zone parameter, ao.

hole. As failure criteria are averaged over larger distances, the effect of the stress concentration at the hole become less important.

For a notched strength equivalent to the experimentally measured value of 62.4 ksi, the process zone parameter, a_0, is about 0.24 in. for the 0 deg. laminate. Using this value of a_0, the predicted strength of the $(0,45,0,-45,0,0,-45,0,45,0)_2$ laminate is about 54 ksi. The experimentally measured notched tensile strength of this material is actually 51.8 ksi, less than 5% from the predicted value. Clearly, this ply level failure theory looks promising for application to this and other material systems. The Whitney-Nuismer failure theories have not been successful for many materials, because they are applied on the laminate level and do not account for the failure of individual plies, causing predictions to be sensitive to stacking sequence.

To extend this ply level notched strength model to predict residual tensile strength during tension-tension fatigue loading, fatigue damage must be accounted for in the stress state of the material. One simple way to simulate fatigue damage is to alter the half lengths of the ellipse in the elasticity solution used to calculate global laminate stresses. Originally, for the circular hole, a and b are set equal to the radius of the notch. The dimension a, measured in the loading direction, can be used to imitate "wear-in" damage. Increasing a causes a reduction in the stress concentration at the hole and an increase in residual tensile strength which is generally observed during fatigue loading of composite materials. Increases in the dimension b, which is measured transverse to the loading direction, can simulate the "wear-out" damage that reduces residual tensile strength and eventually leads to fatigue failure.

The hardest part of fatigue modeling is chosing a rational way of adjusting the ellipse dimensions to accurately describe damage development. If a and b were known as a function of life, residual strength could be predicted accurately throughout life. Because the two are independent variables, an infinite number of a and b combinations would result in the same residual strength prediction, making it difficult to work backwards from experimental data to find a and b as a function of life. Furthermore, it is unlikely that global or ply level values of a and b would be the independent on stacking sequence, since damage development in an individual ply is dependent on the nature of the neighboring plies. For example, in the $(0)_{22}$ material, long 0 deg. splits develop tangent to the hole. This does not occur in the 0 deg. plies in the $(0,45,0,-45,0,0,-45,0,45,0)_2$ material.

A very basic scheme was used to model damage in the $(0)_{22}$ material. A series of X-ray radiographs was previously taken of a notched $(0)_{22}$ coupon after various numbers of fatigue cycles. The global (and in this case local) dimensions a and b were simply taken as being the half length of the longest 0 deg. splits and the half width of the zone between the 0 deg. splits, respectively, as measured from the radiographs. These dimensions are plotted in Figure 45 as a function of normalized life. The triangular points are experimental data points. The longitudinal dimension, a, increases quickly in the first 10% of life then levels off, while the transverse length, b, increases slowly but steadily throughout the life.

Figure 46 shows the predicted residual tensile strengths calculated using the data from Figure 45. Increases in residual tensile strength are predicted to occur early in life. The maximum expected residual strength occurs at about 10% of life, having a value of 114% of the original notched tensile strength. Increases in strength between 10% and 13% are predicted during the majority of life. These predictions are very consistent with experimental data. A comparison of experimentally measured and predicted residual tensile strengths is presented in Table 11. For such a simple representation of damage,it appears that the predictions are quite accurate, certainly within experimental scatter. This method of modeling damage in the $(0)_{22}$ notched coupons appears to work very well, but no scheme has been found yet for the $(0,45,0,-45,0,0,-45,0,45,0)_2$ material. Whether a simple method of simulating damage as a function of life can be created that will work from laminate to laminate remains to be seen.

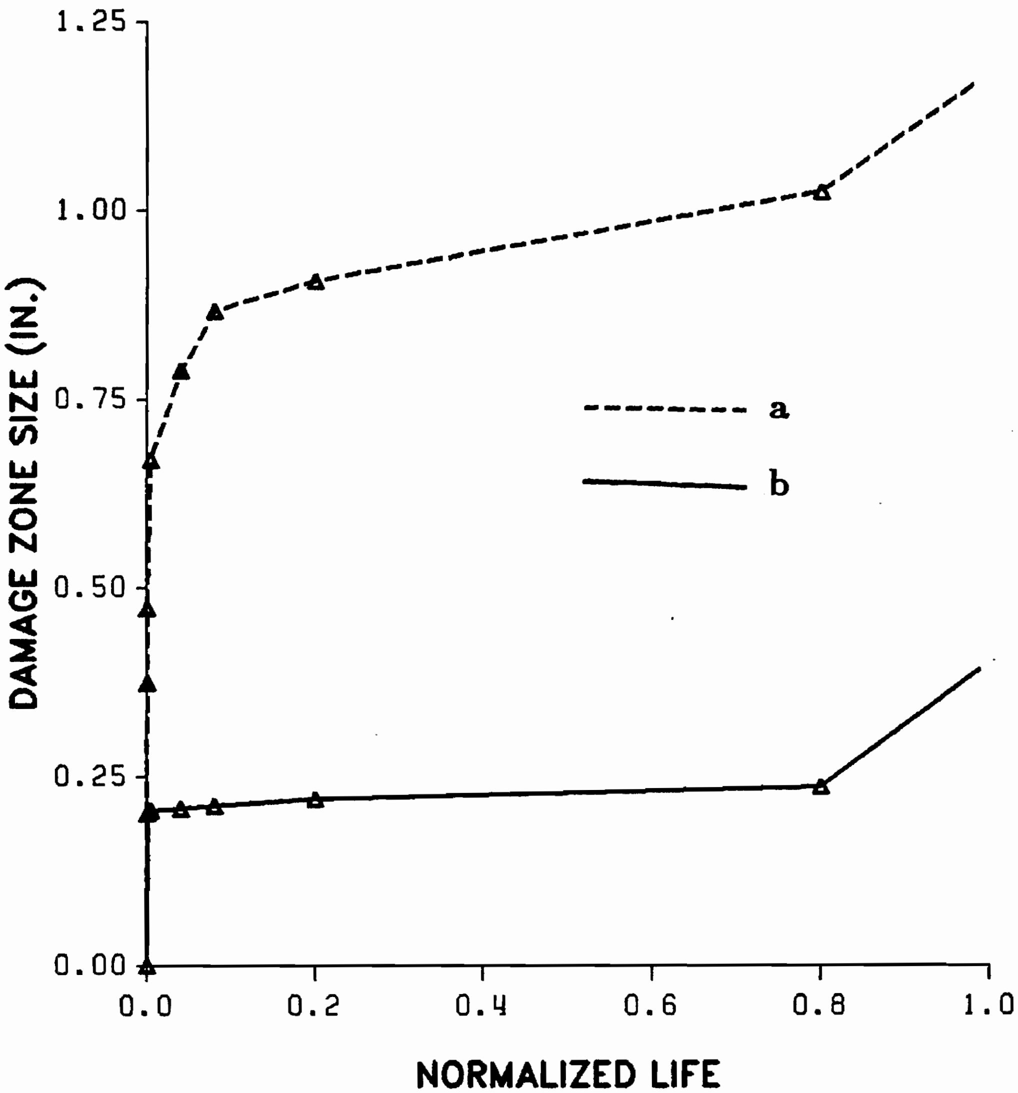

Figure 45. The variation of experimentally measured ellipse half lengths in a 22-ply 0 deg. notched coupon during its life.

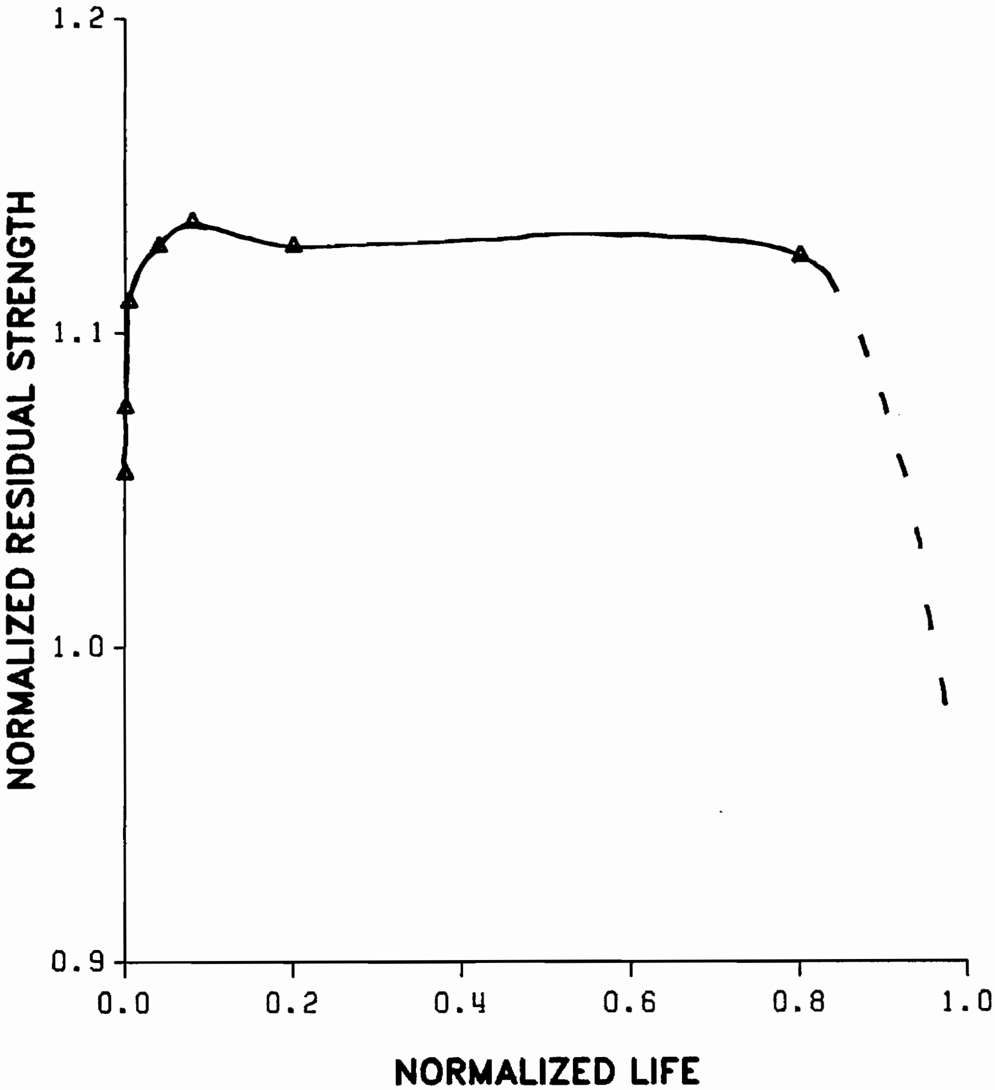

Figure 46. The variation of predicted residual tensile strengths of a 22-ply 0 deg. notched coupon during its life.

Table 11. Comparison of Experimental and Theoretical Notched Residual Strengths of a 22-ply 0 deg. Laminate

Specimen	a (in.)	b (in.)	Experimental Strength[1]	Theoretical Strength[2]
1B-4	0.886	0.221	112.	112.
1B-7	1.04	0.276	104.	107.
1B-9	0.669	0.217	107.	109.
1B-12	1.02	0.236	113.	113.

[1] Percent of notched tensile strength of similar specimens.
[2] Percent of original notched tensile strength.

V. CONCLUSIONS

Conclusions based on the work performed during this study are categorized and listed below and appear in the order in which they were discussed in this report. Because such a small number of specimens was tested and material properties of graphite-polyimide compsosites are highly dependent on the curing process, material properties listed in this report are not intended for use as design criteria.

Experimental Procedures

Mechanical Testing

- Difficulty was encountered using strain gages on the woven graphite-polyimide. Gages failed at relatively low strains, possibly due to the non-uniform strain fields associated with the weave or the extensive matrix cracking that occurred because of matrix brittleness. Extensometers were used to measure strain.

- Gripping thick, unnotched specimens (0.3 in. thick, 6.75 in. long) required grip pressures of up to 1200 psi. Best results were achieved when two layers of 80-grit sandpaper were placed between the grips and the specimen (with the grit side facing the specimen), however, all unnotched specimens failed at the grips. In future testing of thick, unnotched material, cutting coupons longer or finding a suitable tabbing arrangement could help reduce grip-induced damage.

- A newly developed test method, the Incremental Loading Test (ILT), was used to study the time-dependence of damage. Much was learned about damage development, however, improvements on data acquisition must be made for numerical results to be physically correct.

Damage Evaluation

- Ultrasonic C-scans were useful in screening panels of material for gross defects. Due to the nature of the weave, C-scans were not helpful in detecting finer defects such as matrix cracks. Penetrant-enhanced X-ray radiography provided a good alternative to assess the state of damage in test coupons.

- A zinc iodide solution was used to enhance damage such as matrix cracks and delaminations on X-ray radiographs. It was discovered that for thorough penetration, the solution should be left on specimen edges for up to 24 hours if the specimen was under no applied load.

Experimental Results

Basic Material Properties

- The $(0)_{22}$ and $(0)_{15}$ laminates had similar unnotched tensile strengths of 105.6 and 105.0 ksi, respectively. Thinner specimens, having an average modulus of 9.7 msi, broke at an average strain of 10,900 microstrain. The thicker specimens had a modulus of 10.9 msi and failure strain of 9,800 microstrain. It was determined that strains measured on either side of the laminates with an extensometer are equal.

- The unnotched $(0,45,0,-45,0,0,-45,0,45,0)_2$ coupons, having an axial modulus and strain to failure of 7.3 msi and 11,650 microstrain, respectively, failed at an average tensile stress of 84.1 ksi.

- The woven graphite-polyimide specimens from this study were not quite as strong in tension as equivalent non-woven graphite-epoxy laminates, but compared favorably with woven graphite-epoxy laminates having similar stacking sequences.

- As was the case with the unnotched coupons, the notched $(0)_{15}$ and $(0)_{22}$ coupons had similar strengths but different strains to failure. Average tensile strengths of 63.8 and 62.4 ksi and average strains to failure of 15,200 and 13,400 microstrain were measured for the $(0)_{15}$ and $(0)_{22}$ specimens, respectively.

- The $(0,45,0,-45,0,0,-45,0,45,0)_2$ laminate had an average notched tensile strength of 51.8 ksi and failed at a strain of 10,100 microstrain, a lower failure strain than either 0 deg. laminate had.

- Notched compressive strengths of about 50 and 45 ksi were measured for the $(0)_{22}$ and $(0,45,0,-45,0,0,-45,0,45,0)_2$ laminates. No significant dependence of notched compressive strength on length was found for unsupported lengths between 2.375 in. and 3.375 in..

- Under sustained incremental loading, unnotched $(0)_{22}$ coupons exhibited small decreases in stiffness and losses in strength of up to 10%. The $(0,45,0,-45,0,0,-45,0,45,0)_2$ unnotched specimens behaved differently, exhibiting larger decreases in stiffnesses and increases in tensile strength of 7-14%. For unnotched $(0)_{22}$ specimens, maximum stress levels of 70% and 75% of the tensile strength were required for tension-tension fatigue lives on the order of 10^3 and 10^6 cycles, respectively. The fatigue behavior of the $(0)_{22}$ material compared poorly to other woven materials. Grip-related fiber fracture prior to fatigue failure may account for the relatively poor performance of the materials tested in this study.

- For the unnotched $(0,45,0,-45,0,0,-45,0,45,0)_2$ coupons, fatigue lives of 10^3 and 10^6 corresponded to maximum stress levels of about 90% and 75% of the tensile strength. This laminate compared very well with other woven laminates having similar stacking sequences.

- S-N (stress-life) curves for graphite-polyimide, a thermosetting material system, appear to be rather "flat," as has been observed with thermoplastic systems. Thermoplastics perform better relative to thermosetting materials, such as graphite-epoxy systems, under low stress, long life loading conditions.

- For notched coupons, tension-tension fatigue lives of 10^3 and 10^6 were observed for maximum stress levels of about 90% and 95% of the virgin notched tensile strength for both the $(0)_{22}$ and $(0,45,0,-45,0,0,-45,0,45,0)_2$ laminates.

- Stiffness-life behavior of the unnotched coupons varied from test to test, but notched coupons tended to follow the three stages of stiffness degradation previously described for non-woven graphite-epoxy and graphite-polyimide. Fatigue failure occurred after drops in stiffness of 5-10% and 10-25% for the unnotched $(0)_{22}$ and $(0,45,0,-45,0,0,-45,0,45,0)_2$ materials, respectively, while the notched material failed at 15-25% decreases in stiffness for both layups.

- Increases in residual tensile strength for the woven graphite-polyimide were low relative to those reported for other material systems, with maximum residual strengths of 113% for the $(0)_{22}$ and 109% for the $(0,45,0,-45,0,0,-45,0,45,0)_2$ notched coupons.

Damage Mechanisms

- Specimens loaded monotonically to failure showed the least amount of matrix damage of all those tested in this study. Damage prior to failure was limited to scattered matrix cracks. Fracture surfaces were very localized. Post failure damage included delaminations, 0 deg. matrix cracks, fiber fracture, and fiber bundle pullout in a very localized region surrounding the fracture site.

- Unnotched specimens subjected to sustained incremental loading contained considerably more damage than those loaded monotonically to failure. Prior to failure, matrix cracking was very dense, except in the 0 deg. direction. In the $(0,45,0,-45,0,0,-45,0,45,0)_2$ specimens, small localized damage regions following the weave pattern appeared in the radiographs. These regions are believed to be either intralaminar matrix cracks or delaminations at the fiber bundle crossovers within a single ply. Fracture surfaces were less localized than in the incrementally loaded specimens.

- If data acquisition could be properly controlled, it is possible that repeatable "master curves" could be experimentally measured during sustained incremental loading tests that would characterize damage development in a given laminate as a function of strain. Peaks and plateaus of the change in stress versus strain curves would correspond to the development of isolated damage mechanisms in the material.

- Tension-tension fatigue specimens showed the greatest amount of damage of all unnotched specimens. Matrix cracking was more dense than in incrementally loaded specimens, especially in the +45 and -45 deg. directions in $(0,45,0,-45,0,0,-45,0,45,0)_2$ material. Fracture surfaces became more dispersed with increasing number of cycles to failure, suggesting that more damage grew in the lower load specimens prior to failure. Delamination of 0 deg. surface plies was observed during fatigue cycling prior to failure, but unlike edge delaminations resulting from interlaminar stresses, these are believed to have originated after the surface plies were broken by the grips.

- The fracture surface of individual fibers appears to be influenced by the applied stress level during tension-tension fatigue, as observed in failed unnotched $(0,45,0,-45,0,0,-45,0,45,0)_2$ specimens. In a specimen failing after nearly one million cycles, the individual 0 deg. fibers appear to have interacted with each other during failure. "Flow lines" can be seen in the fracture surfaces which travel from fiber to fiber. The fracture surfaces of 0 deg. fibers from a specimen failing after 410 cycles showed no interaction and were much rougher. Rougher surfaces are associated with faster crack propagation in brittle materials.

- In notched $(0)_{22}$ fatigue specimens, dense 0 deg. matrix cracks formed tangent to the hole but were constrained by the 90 deg. fibers in the same ply. Matrix cracking in the 90 deg. direction was heavy, but did not extend above or below the hole. The small regions of localized damage observed in unnotched $(0,45,0,-45,0,0,-45,0,45,0)_2$ coupons were only noticed when specimens were loaded slightly off-axis, suggesting that these damage regions are a result of shear stresses which are always present in the $(0,45,0,-45,0,0,-45,0,45,0)_2$ material. Fatigue failure occurred after 0 deg. cracks began to form away from the notch.

- In notched $(0,45,0,-45,0,0,-45,0,45,0)_2$ material, matrix cracking in the 90, +45, and -45 deg. directions was very dense, and unlike the damage in the $(0)_{22}$ material, it extended above and below the hole a short distance away from the hole edges. Delaminations appeared to grow in the vicinity of the hole in the surface plies. Damage grew more in the transverse and less in the loading direction than did the damage in the $(0)_{22}$ material. Fatigue failure occurred after 0 deg. matrix cracks grew away from the hole.

- In non-woven, notched $(0,90,+45,-45)_s$ graphite-epoxy, matrix cracking was not nearly as dense as in the woven graphite-polyimide. Delaminations grew at every ply interface in the graphite-epoxy near the hole. Matrix cracking in the +45 deg. direction was heavier than in the -45 deg. direction, unlike the damage in the woven $(0,45,0,-45,0,0,-45,0,45,0)_2$ specimens. Splits in the 0 deg. direction were not constrained by the 90 deg. fibers in the adjacent plies. Damage in the non-woven specimen grew primarily in the loading direction and not towards the edges as in the $(0,45,0,-45,0,0,-45,0,45,0)_2$ cloth material. Residual tensile strengths of the tape material were as high as 120-130% of the undamaged notched strength.

- There are two possible reasons that residual tensile strengths of the woven graphite-polyimide are much lower than those in the non-woven graphite epoxy. One is that "wear-in" damage, which relieves the stress concentration at the hole, is inhibited by the weave. The other is that excessive "wear-out" damage, which degrades the strength of the material, occurs due to brittleness of the polyimide matrix.

Notched Strength Predictions

- A ply level notched strength model was used to successfully predict the monotonic tensile strength of $(0,45,0,-45,0,0,-45,0,45,0)_2$ coupons based on experimental data from the $(0)_{22}$ notched coupons. Such a model can be modified to predict residual tensile strength during tension-tension fatigue loading by adjusting geometric parameters in the elasticity solution to simulate the effect of damage on the stress state of the laminate.

Closure

Woven composite materials were designed in order to improve impact tolerance, damage resistance, and ease of material handling while retaining the general properties of fiber reinforced laminates. Brittle polyimide matrices were introduced which can withstand extreme temperatures (-250°F to 600°F). The material tested in this study, an 8-harness satin woven graphite-polyimide, which combines the woven fiber architecture with the high temperature matrix, was developed to be "tough" and resist the initiation and growth of damage. Composite materials are evaluated primarily on the basis of short term, monotonic properties, but the effects of the woven fiber architecture and polyimide matrix on long term behavior cannot be comprehended on the basis these properties. The results of this investigation on notched woven composites suggest that the woven fiber architecture and polyimide matrix greatly influence fatigue damage, residual strength, and life under long term loading conditions. The long term behavior of this material system is distinctly different from that of graphite-epoxy composites fabricated from unidirectional tapes. Compared to our understanding of the behavior of non-woven material systems, relatively little is known about the behavior of woven composites. Before woven materials are certified for use in long term loading structural applications, more research must be done in order to understand what aspects of this material system limit strength and life. Additional research is also needed to optimize the material system for enhanced performance.

REFERENCES

1. Sharples, T., "Application of carbon fibre composites to military aircraft structures," **AGARD CP 288**, 1980, paper 3:1-17.

2. Leonard, R.W., Mulville, D.R., "Current and projected use of carbon composites in United States aircraft," **AGARD CP 288**, 1980, paper 1:1-19.

3. Hoff, N.J., "Composite materials in aircraft structures," **Progress in Science and Engineering of Composites**, Proc. ICCM IV, Tokyo, 1982, pp.49-62.

4. Garber, D.P., Morris, D.H., and Everett, R.A., Jr., "Elastic properties and fracture behavior of graphite/polyimide composites at extreme temperatures," **Composites for Extreme Environments, ASTM STP 768** , N.R. Adsit, Ed., ASTM, 1982, pp.73-91.

5. Illg, W., and Everett, R.A., Jr., "Fatigue and fracture," Nasa-Langley Research Center and U.S. Army Research and Technology Laboratories, in in **NASA CP-2079**, 1979, pp.259-271.

6. Poveromo, L.M., "Polyimide composites - application histories," Grumman Aerospace Corp., in in **NASA CP-2385**, 1985, pp.339-357.

7. Haskins, J.F., and Kerr, J.R., "Effects of real-time thermal aging on graphite/polyimide composites," General Dynamics Convair Division, in in **NASA CP-2385**, 1985, pp.315-327.

8. Sheppard, C.H., Hoggatt, J.T., and Symonds, W.A., "Development and demonstration of manufacturing processes for fabricating Gr/PMR-15 polyimide structural elements," Boeing Aerospace, in in **NASA CP-2079**, 1979, pp.259-271.

9. Rummler, D.R., and Clark, R.K., "Mechanical and thermophysical properties of graphite/polyimide composite materials," Nasa-Langley Research Center, in **NASA CP-2079**, 1979, pp.289-301.

10. Molyneux, M., "Prepreg tape and fabric technology for advanced composites," **Composites**, Vol.14 (1983), PP.87-91.

11. Morrison, C.E., and Bowyer, W.H., "Factors affecting the ballistic impact resistance of Kevlar laminates," **Advances in Composite Materials**, 3rd Int. Conf. on Composite Materials, Paris, 1980, pp.233-245.

12. Ko, W.L., "Fracture behavior of a nonlinear woven fabric material," **J. Composite Materials**, Vol. 9 (October 1975), pp.361-369.

13. Curtis, P.T., and Bishop, J.M., "An assessment of the potential of woven carbon fibre-reinforced plastics for high performance applications," **Composites,** Vol. 15, No.4 (October, 1984).

14. Cantwell, W.J., Curtis, P.T., and Morton, J., "Impact and subsequent fatigue damage growth in carbon fibre laminates," **Int. J. Fatigue,** Vol. 6, No.2 (April, 1984).

15. Hanagud, S., Tayebi, A., Clinton, R.G., and Nayak, B.M., "Comparative evaluation of woven graphite-epoxy composites," **A.I.A.A. Paper** No. 79-0777 (1979).

16. Shimokawa, T., and Hamaguchi, Y., "Distributions of fatigue life and fatigue strength in notched specimens of a carbon eight-harness-satin laminate," **J. Composite Materials,** Vol. 17, (January, 1983), pp.64-76.

17. Luger, M., "Fibre substrates in fabric composites - New claims for multi-axials," Proceedings of the 29th National SAMPE Symposium, April 3-5, 1984, pp.592-599.

18. Halpin, J.C., Jerine, K., and Whitney, J.M., "The laminate analogy for 2 and 3 dimensional composite materials," **J. Composite Materials** , Vol. 5 (January 1971), pp.36-49.

19. Ishikawa, T., and Chow, T.W., "Elastic behavior of woven hybrid composites," **J. Composite Materials**, Vol. 16 (1982), pp.2-19.

20. Ishikawa, T., and Chow, T.W., "In-plane thermal expansion and thermal bending coefficients of fabric composites," **J. Composite Materials**, Vol. 17 (1983), pp.92-104.

21. Ishikawa, T., and Chow, T.W., "Nonlinear behavior of woven fabric composites," **J. Composite Materials**, Vol. 17 (1983), pp.399-413.

22. Ishikawa, T., and Chow, T.W., "Stiffness and strength behavior of woven fabric composites," **J. Materials Science**, Vol. 17 (1982), pp.3211-3220.

23. Yang, J.M, Ma, C.L., and Chou, T.W., "Elastic stiffness of biaxial and triaxial woven fabric composites," Proceedings of the 29th National SAMPE Symposium, April 3-5, 1984, pp.292-303.

24. Nishimura, A., Ueda, N., and Matsuda, H.S., "New fabric structures of carbon fiber," Proceedings of the 28th National SAMPE Symposium, April 12-14, 1983, pp.71-88.

25. Abbott, N.J., and Skelton, J., "Crack propagation in woven fabrics," **J. Coated Fibrous Materials** , Vol. 1 (April 1972), pp.234-252.

26. Freeston, W.D., Jr., and Claus, W.D., Jr., "Crack propagation in woven fabric," **J. Appl. Phys.,** Vol. 44, No.7 (July, 1973), pp.3130-3138.

27. Street, S.W., "V 378A, a modified bismaleimide for advanced composites," HITCO Materials Division, in in **NASA CP-2385**, 1979, pp.359-378.

28. Dody, M., Hunsinger, J.J., Oytana, C., and Varchon, D., "Mechanical and optical assessments of damage during tensile and fatigue tests in glass taffeta fabric-epoxy laminate," **Composite Structures 3** , ed. Marshall, I.H., Third International Conference on Composite Structures, Paisley, Scotland, 1985, pp.415-426.

29. Schulte, K., Reese, E., and Chou, T.W., "Fatigue behaviour and damage development in woven fabric and hybrid fabric composites," submitted for publication in: Proceedings, ICCM-VI/ECCM-2, July 20-25, 1987, London, England.

30. Welsh, L.M., and Harding, J., "Effect of strain rate on the tensile failure of woven reinforced polyester resin composites," **Journal de Physique** , Colloque C5, supplement au n °8, Tome 46 (aout 1985), pp.C5-405 - C5-414.

31. Curtis, P.T., and Moore, B.B., "A Comparison of the fatigue response of woven and non-woven CFRP laminates," RAE Technical Report 85059, London, 1985.

32. Lagace, P.A., "Notch sensitivity of graphite/epoxy fabric laminates," **Composite Science and Technology,** Vol. 26, No. 2 (1986), pp.95-117.

33. Bailie, J.A., Duggan, M.F., Fisher, L.M., and Yee, R.C., "Effects of holes on graphite cloth epoxy laminates tension strength," **J. Aircraft,**. Vol. 19, No.7 (July 1982), pp.559-566.

34. Bailie, J.A., Duggan, M.F., Fisher, L.M., and Dickson, J.N., "The influence of holes on the compression strength of graphite epoxy cloth and tape laminate at temperatures up to 430°K," **Advances in Composites**, proc. ICCM III, Paris, France, Vol. 1, pp.198-211.

35. Mar, J.W., and Lin, K.Y., "Fracture of boron/aluminum composites with discontinuities," **J. Composite Materials**, Vol. 11 (1977), PP.405-421.

36. Mar, J.W., and Lin, K.Y., "Fracture mechanics correlation for tensile failure of filamentary composites with holes," **J. Aircraft**, Vol. 14 (1977), PP.703-714.

37. Whitney, J.M., and Nuismer, R.J., "Stress Fracture Criteria for Laminated Composites Containing Stress Concentrations," **J. Composite Materials**, Vol. 8 (1974), PP.253-265.

38. Nuismer, R.J., and Whitney, J.M., "Uniaxial failure of composite laminates containing stress concentrations," **Fracture Mechanics of Composites, ASTM STP 593,** ASTM, 1975, pp.117-142.

39. Lifshitz, J.M., "Residual tensile strength of fiberglass-cloth-reinforced plastic," Proceedings of the 29th National SAMPE Symposium, April 3-5, 1984, pp.1481-1491.

40. Hartness, J.T., and Kim, R.Y., "A comparative study on fatigue behavior of polyetheretherkeytone and epoxy with reinforced graphite cloth," Proceedings of the 28th National SAMPE Symposium, April 12-14, 1983, pp.535-544.

41. Bishop, S.M., and Morton, J., "Fatigue of notched (0,-/+45) CFRP with woven and non-woven -/+45° layers," **Advances in Fracture Research**, Vol. 4, Pergamon Press, 1984, pp.3069-3078.

42. Kellas, S., Morton, J., and Bishop, S.M., "Damage development in notched carbon fibre composites subjected to fatigue loading," **Composite Structures 3** , ed. Marshall, I.H., Third International Conference on Composite Structures, Paisley, Scotland, 1985, pp.56-68.

43. Wagnecz, L., Vittoser, J., Razvan, A., Reifsnider, K.L., and Stinchcomb, W.W., "Damage mechanisms in woven graphite-polyimide composite materials," **Preprints-23** Proc. 23rd Annual Technical Meeting, Society of Engineering Science, Buffalo, 1986, paper no. ESP23.86065.

44. Garber, D.P, "Elastic properties and fracture behavior of graphite/polyimide composites at extreme temperatures," **M.S. Thesis**, Virginia Polytechnic Institute and State University, Blacksburg, Virginia, April, 1983.

45. **Graphite/Polyimide Composites**, NASA Conference Publication 2079, ed. Dexter, H.B. and Davis, J.G., Jr., 1979.

46. **High Temperature Polymer Matrix Composites**, NASA Conference Publication 2385, ed. Sefarini, T.T., 1985.

47. Cushman, J.B., and McClesky, S.F., "Design allowables test program, C3000/PMR-15 and C6000/PMR-15, graphite/polyimide composites," Boeing Aerospace Co., NASA CR-165840 (N82-30338), 1982.

48. Awerbuch, J., and Madhukar, M.S., "Notched strength of composite laminates: predictions and experiments - a review," **J. of Reinforced Plastics and Composites**, Vol. 4 (January 1985), pp.3-159.

49. Ehret, R.M., Scanlan, P.R., and Rosen, C.D, "Development of design allowables for C6000/LARC-160, graphite/polyimide Composites," Rockwell Int., NASA Contract Report (N83-16391), 1982.

50. Maier, G., Ott, H., Protzner, A. and Protz, B., "Damage development in carbon fibre-reinforced polyimides in fatigue loading as a function of stress ratio," **Composites,** Vol. 17, No. 2, (April, 1986) pp.111-120.

51. Reifsnider, K.L., and Masters, J.E., "Investigation of characteristic damage states in composite laminates," ASME Winter Annual Meeting, San Fransisco, 1978.

52. Vittoser, J., and Reifsnider, K.L., "An incremental loading test for the investigation of composite materials," **CCMS Report Number CCMS-87-01**, Virginia Polytechnic Institute and State University, Blacksburg, Virginia, February, 1987.

53. Owens, G.R., "An experimental investigation of the material response of graphite/polyphenylene sulfide," **M.S. Thesis**, Virginia Polytechnic Institute and State University, Blacksburg, Virginia, August, 1986.

54. Bakis, C.E., "Fatigue response of notched composite laminates subjected to tension-compression loading," **M.S. Thesis**, Virginia Polytechnic Institute and State University, Blacksburg, Virginia, December, 1984.

55. Reifsnider, K.L., and Stinchcomb, W.W., "Stiffness change as a fatigue damage parameter for composite laminates," **1983 Advances in Aerospace Structures, Materials, and Dynamics - Ad-06**, U. Yuceoglu, R.L. Sierakowski, and D.A. Glasgow, Eds., the American Society of Mechanical Engineers, 1983, pp.1-6.

56. Reifsnider, K.L., Schulte, K., and Duke, J.C., "Long-term fatigue behavior of composite materials," **Long-Term Behavior of Composites, ASTM STP 813**, T.K. O'Brien, Ed., American Society for Testing and Materials, 1983, pp.136-159.

57. O'Brien, T.K., and Reifsnider, K.L., "Fatigue damage: stiffness/strength comparisons for composite materials," **Journal of Testing and Evaluation**, JTEVA, Vol. 5, No. 5, September 1977, pp.384-393.

58. Camponeschi, E.T., and Stinchcomb, W.W., "Stiffness reduction as an indicator of damage in graphite/epoxy laminates," **Composite Materials: Testing and Design, ASTM STP 787**, I.M. Daniel, Ed., American Society for Testing and Materials, pp.225-246.

59. Kress, G.R., and Stinchcomb, W.W., "Fatigue response of notched graphite-epoxy laminates," **Recent Advances in the US and Japan, ASTM STP 864**, J.R. Vinson and M. Taya, Eds., ASTM, 1985, pp.173-196.

60. Thompson, W., "On the dynamical theory of heat," **Transactions of the Royal Society of Edinburgh**,Vol. 20, 1853, pp.261-288.

61. Bakis, C.E., and Reifsnider, K.L., "Thermoelastic micromechanics of laminated fiber composites," to be published, 1987.

62. Harris, C.E., and Morris, D.H., "Fracture behavior of thick, laminated graphite/epoxy composites," NASA CR 3784, March, 1987.

63. Nuismer, R.J., and Whitney, J.M., "Uniaxial failure of composite laminates containing stress concentrations," **Fracture Mechanics of Composites, ASTM STP 593**, ASTM, 1975, pp.117-142.

64. Bakis, C.E., Simonds, R.A., and Stinchcomb, W.W., "A test method to measure the response of composite materials under reversed cyclic loads," presented at ASTM Second Symposium on Test Methods and Design Allowables for Fiber Composites, Nov. 3-4, 1986, Phoenix, AZ.

65. Simonds, R.A., Bakis, C.E., and Stinchcomb, W.W., "Effects of Matrix toughness on fatigue response of graphite fiber composite laminates," presented at Second ASTM Symposium on Composite Materials: Fatigue and Fracture, April 27-28, 1987, Cincinnati, Ohio.

66. Chang, F.H., Gordon, D.E., and Gardner, A.H., in **Fatigue of Filamentary Composite Materials**, ASTM STP 636, K.L. Reifsnider and K.N. Lauraitis, Eds., American Society for Testing and Materials, (1977), pp.57-72.

67. Roderick, G.L., and Whitcomb, J.D., in **Fatigue of Filamentary Composite Materials**, ASTM STP 636, K.L. Reifsnider and K.N. Lauraitis, Eds., American Society for Testing and Materials, (1977), pp.73-88.

68. Kress, G.R., and Stinchcomb, W.W., "Fatigue response of notched graphite/epoxy laminates," **Recent Advances in the U.S. and Japan**, ASTM STP 864, J.R. Vinson and M. Taya, Eds. American Society for Testing and Materials, (1985), pp.173-196.

69. Mirzadeh, F., and Reifsnider, K.L., Materials Response Group, Virginia Tech, unpublished research.

70. Croman, R., from seminar presented at CCMS Fall Seminar Series, Virginia Tech, 1986.

71. Reifsnider, K.L., and Stinchcomb, W.W., progress report to NADC, 1987.

72. Awerbuch, J., and Madhukar, M.S., "Notched strength of composite laminates: predictions and experiments - a review," **Journal of Reinforced Plastics and Composites**, Vol. 4 (January, 1985).

73. Waddoups, M.E., Eisenmann, J.R., and Kaminski, B.E., "Macroscopic fracture mechanics of advanced composite materials," **Journal of Composite Materials**, Vol. 5 (1971), pp.446-454.

74. Lekhnitski, S.G., **Theory of Elasticity of an Anisotropic Body,** Holden-Day, SanFran Fransisco (1963).

75. Bakis, C.E., and Reifsnider, K.L., "Application of micromechanics in the thermoelasticity of laminated fibrous composites," to be published.

76. Reifsnider, K.L., progress report to General Electric, 1986.

APPENDIX A

For plane stress, the deformation of a homogeneous, infinite orthotropic plate with an elliptical hole yields the characteristic equation,

$$S_{11}\mu^4 - 2S_{13}\mu^3 + (2S_{12} + S_{33})\mu = 0 \tag{1}$$

where S_{ij} are laminate compliances. For an orthotropic plate, two pure imaginary roots will be distinct. Denoting these roots as μ_1 and μ_2, and letting a and b represent the ellipse dimensions shown in Figure 40 (in the Notched Strength Predictions chapter), the in-plane stresses can be found along the y-axis using the following equations:

$$\sigma_x = p + 2E\left[C\left[1 - \frac{\bar{\alpha}\delta_1 y}{\delta_1^2 + \gamma_1^2}\right] - D\left[1 - \frac{\bar{\beta}\delta_2 y}{\delta_2^2 + \gamma_2^2}\right]\right] \tag{2}$$

$$\sigma_y = -2E\left[\hat{C}\left[1 - \frac{\bar{\alpha}\delta_1 y}{\delta_1^2 + \gamma_1^2}\right] - \hat{D}\left[1 - \frac{\bar{\beta}\delta_2 y}{\delta_2^2 + \gamma_2^2}\right]\right] \tag{3}$$

$$\tau_{xy} = 2E\left[\hat{C}\left[\frac{\bar{\alpha}\gamma_1 y}{\delta_1^2 + \gamma_1^2}\right] - \hat{D}\left[\frac{\bar{\beta}\gamma_2 y}{\delta_2^2 + \gamma_2^2}\right]\right] \tag{4}$$

where $\bar{\alpha}$ and $\bar{\beta}$ are the absolute values of the roots to equation (1), and

$$A_1 = \sqrt{a^2 - \bar{\alpha}^2 b}$$

$$A_2 = \sqrt{a^2 - \bar{\beta}^2 b}$$

$$C = \frac{\bar{\alpha}^2}{a - \bar{\alpha} b}$$

$$D = \frac{\bar{\beta}^2}{a - \bar{\beta} b}$$

$$\hat{C} = \frac{\bar{\alpha}^2}{a - \bar{\alpha} b}$$

$$\hat{D} = \frac{\bar{\beta}^2}{a - \bar{\beta} b}$$

$$E = \frac{pb}{2(\bar{\alpha} - \bar{\beta})},$$

and along the y-axis (x=0),

$$\delta_1 = A_1^2 + \bar{\alpha}^2 y^2$$

$$\delta_2 = A_2^2 + \bar{\beta}^2 y^2$$

$$\gamma^1 = 0$$

$$\gamma^2 = 0$$

with, p being the applied load in the x-direction.

APPENDIX B

```
C*************************************************************************************
C THIS WORK WAS SUPPORTED BY THE LBRG, A SUBSIDIARY OF THE CLBR.
C
C   C.E. BAKIS, PRESIDENT  AND A. RAZVAN, TREASURER
C*************************************************************************************
C         LAMINATE ANALYSIS INTERACTIVE PROGRAM
C
C                BY LINDA WAGNECZ
C*************************************************************************************
      DOUBLE PRECISION Q(3,3,4),QB(3,3,49),S(3,3,4),SB(3,3,49),
     $  TI(3,3,49),A(3,3),B(3,3),D(3,3),AP(3,3),BP(3,3),DP(3,3),
     $  QXY(3,49,2),Q12(3,49,2),QXYT(3,49),Q12T(3,49),T(3,3,49),
     $  THETA(49),THET(49),Z(49),E1(7),E2(7),G12(7),V12(7),
     $  ALPH(3),ALPHA(3,49),TSHILL(49,2),ALBAR(3),PLYTHI,E0T(3),
     $  S3D(6,6),SB3D(6,6,49),SLAM(3,3),EFAILT(3),EFAILC(3),SIGX(21),
     $  SIGY(21),TAUXY(21),Y(21),AA,BB,RNOTCH,APARAM
      COMPLEX UK(4)
      DIMENSION ITYPE(49),FAILCR(49,21,3),AVFAIL(49,3),IGONE(49)
      REAL*8 EXY(3,49,2),E12(3,49,2),E0(3),K0(3),ELX,ELY,NXY,
     $  NXYB(3),MXYB(3),NT(3),MT(3),NTOTAL(3),MTOTAL(3),
     $  MATRI1(3,3),MATRI2(3,3),QXYN(3,49,3),ZM(3,49),FXZ(3,49),
     $  FYZ(3,49),MAXFL,P
C*************************************************************
      LCOUNT=0
      IFAIL=0
      ISYMET=1
      IMOMEN=1
      LCASE=1
      INCR=0
      NDIV=20
      P=2000
C*** NOTE: P IS INITIAL LOADING IN X-DIRECTION (PSI), NDIV IS THE
C***  NUMBER OF POINTS IN PROCESS ZONE - TO ALTER, MUST ALSO CHANGE
C***  DIMENSIONS OF SIGX, SIGY, TAUXY, AND Y!
```

```
      WRITE(6,50)
 50   FORMAT(5X,'I HOPE YOU ARE HAVING A NICE DAY.  THIS',
     $' PROGRAM IS RATHER SIMPLE.',/5X,'JUST FOLLOW THE DIRECTIONS',
     $' AND TYPE FILE OUTPUT DATA FOR THE OUTPUT.')
C** PROBLEM SPECIFICATIONS ***
C** INPUT INFORMATION FROM TERMINAL ***
      WRITE(6,20)
 20   FORMAT(1X,'HOW MANY PLYS ARE THERE IN THIS PROBLEM?')
      READ(5,*) N
      WRITE(6,200)
      DO 30 I=1,N
 30     IGONE(I)=0
 200  FORMAT(5X,'ARE THE PLYS OF EQUAL THICKNESS? 1=YES, 2=NO',/5X,
     $ 'WHAT IS THE PLY THICKNESS?')
      READ(5,*) IPLY, PLYTHI
      IF(IPLY.EQ.2) GO TO 300
      J=N/2
      IF(J*2.NE.N) GO TO 300
      Z(1)=-J*PLYTHI
      IN=N+1
      DO 301 KKK=2,IN
 301    Z(KKK)=Z(KKK-1)+PLYTHI
      THICK=N*PLYTHI
      GO TO 302
C*** IF PLIES ARE OF DIFFERENT THICKNESSES, INPUT EACH Z-COORDINATE ***
 300  WRITE(6,21)
 21   FORMAT(1X///,5X,'STARTING IN THE NEGATIVE Z-DIRECTION, WHERE',
     $/,'ARE THE PLYS LOCATED?')
      IN=N+1
      READ(5,*) (Z(KKK), KKK=1,IN)
      THICK=Z(N+1)-Z(1)
 302  WRITE(6,22)
 22   FORMAT(1X,'WHAT ARE THE ORIENTATION ANGLES, STARTING',/,
     $'WITH THE NEGATIVE Z-DIRECTION')
      READ(5,*) (THETA(JJJ),JJJ=1,N)
      WRITE(6,23)
 23   FORMAT(5X,'HOW MANY DIFFERENT ANGLES ARE THERE?')
      READ(5,*) ITYPEN
      WRITE(6,24)
 24   FORMAT(5X,'STARTING IN NEGATIVE Z-DIR, WHAT THETA IS EACH PLY',
     $'MADE OF?',/5X,'IE, THETA1=1, THETA2=2, ETC. ...')
      READ(5,*)(ITYPE(JJJ),JJJ=1,N)
C** PRINT LAMINATE PROPERTIES TO OUTPUT ***
     DO 25 I=1,ITYPEN
      E1(I)=11.3D6
      E2(I)=10.17D6
      G12(I)=.85D6
 25   V12(I)=.07
C*** NOTE:  RNOTCH = NOTCH RADIUS; AA,BB = ELLIPSE HALF LENGTHS;
C***   APARAM = WHITNEY-NUISMER PROCESS ZONE PARAMETER;
C***   IFLAG SIGNALS FAILURE IF IFLAG NOT EQUAL TO ZERO FOR PLY&STRESS
      RNOTCH=0.1875D0
      WRITE(6,19)
 19   FORMAT(1X,'WHAT IS THE HOLE RADIUS?')
      READ(5,*) RNOTCH
      AA=RNOTCH
```

```
      BB=RNOTCH
      APARAM=0.10D0
      WRITE(6,41)
 41    FORMAT(5X,'WHAT VALUE OF AO, A, AND B WOULD YOU LIKE TO TRY?')
      READ(5,*) APARAM,AA,BB
      EFAILT(1)= 9300D-6
      EFAILT(2)=10800D-6
      EFAILT(3)= 1530D-6
      EFAILC(1)=-10300D-6
      EFAILC(2)=-9600D-6
      EFAILC(3)= -15300D-6
      NEWFAI=0
      XT=105D3
      XC=-90D3
      YT=110D3
      YC=-82D3
      SS=13D3
      DO 9 III=1,ITYPEN
      WRITE(11,10)
 10    FORMAT(/////15X,'THE LAMINAE PROPERTIES ARE:')
 9    WRITE(11,11) E1(III),E2(III),G12(III),V12(III)
 11    FORMAT(15X,'E1 =',F10.0,5X,'E2 =',F10.0,5X,'G12 =',
     $ F10.0,5X,'V12 =',F5.3)
      IN=N+1
      WRITE(11,12) (Z(I),I=1,IN)
 12    FORMAT(15X,'THE POSITIONS OF THE PLYS ARE (IN):'
     $ ,8(/5X,8(F10.3,',')))
      WRITE(11,13) (THETA(I),I=1,N)
 13    FORMAT(15X,'THE ORIENTATION ANGLES ARE (DEGREES):',
     $ 8(/5X,8(F10.3,',')))
      DO 2 I=1,N
 2     THET(I)=THETA(I)*3.141592654/180.0000000000
C** FIND TRANSFORMATION MARICES ***
      CALL TFIND(THET,N,T,TI)
C** INITIALIZE MATRICES ***
 500   CONTINUE
C** DEFINE COMPLIANCE MATRIX <S> ***
      DO 303 K=1,ITYPEN
      S(1,1,K)=1/E1(K)
      S(2,2,K)=1/E2(K)
      S(3,3,K)=1/G12(K)
      S(1,2,K)=-V12(K)/E1(K)
      S(2,1,K)=-V12(K)/E1(K)
      S(1,3,K)=0
      S(2,3,K)=0
      S(3,1,K)=0
      S(3,2,K)=0
C** CALCULATE <Q>,<SBAR> AND <QBAR> MATRICES ***
 303   CALL QFIND (K,Q,S)
      DO 3 K=1,N
      CALL QBAR(K,Q,QB,THET,ITYPE)
C      CALL SBAR(K,S,SB ,THET,ITYPE)
 3    CONTINUE
C** CALCULATE <A>;<B>, AND <D> MATRICES ***
      DO 4 I=1,3
      DO 4 J=1,3
```

```
      K=0
       CALL AFIND(I,J,K,N,QB,Z,A)
       CALL BFIND(I,J,K,N,QB,Z,B)
       CALL DFIND(I,J,K,N,QB,Z,D)
 4    CONTINUE
      WRITE(6,26)
 26    FORMAT(5X,'DO YOU WANT THE A,B,D,Q,&S MATRICES INCLUDED IN ',
    $'THE OUTPUT?',/5X,'  1=NO, 2=YES')
      READ(5,*)IPRINT
      IF(IPRINT.NE.2) GO TO 27
C*** PRINT A,B,D,Q,S,QBAR,AND SBAR TO OUTPUT ***
       WRITE(11,201)
 201    FORMAT(/////15X,'THE [A] MATRIX IS: (LB/IN)')
       CALL PRINT(A)
       WRITE(11,202)
 202    FORMAT(/////15X,'THE [B] MATRIX IS: (LB)')
       CALL PRINT(B)
       WRITE(11,203)
 203    FORMAT(/////15X,'THE [D] MATRIX IS: (LB-IN)')
       CALL PRINT(D)
       DO 310 KKK=1,ITYPEN
        DO 311 II=1,3
        DO 311 JJ=1,3
         MATRI1(II,JJ)=Q(II,JJ,KKK)
 311      MATRI2(II,JJ)=S(II,JJ,KKK)
       WRITE(11,204) KKK
 204    FORMAT(/////15X,'THE [Q] MATRIX IS: (PSI)  FOR MATERIAL ',I2)
       CALL PRINT(MATRI1)
       WRITE(11,205) KKK
 205    FORMAT(/////15X,'THE [S] MATRIX IS: (PSI-1)  FOR MATERIAL '
   $    ,I2)
 310    CALL PRINT(MATRI2)
 27     WRITE(6,206)
 206    FORMAT(5X,'DO YOU WANT THE QBAR AND SBAR MATRICES INCLUDED',
   $    'IN THE OUTPUT? 1=YES, 2=NO')
       READ(5,*) IPRINT
       IF(IPRINT.EQ.2) GO TO 304
       J=N/2
       DO 305 KKK=1,J
        DO 306 II=1,3
        DO 306 JJ=1,3
         MATRI1(II,JJ)=QB(II,JJ,KKK)
 306      MATRI2(II,JJ)=SB(II,JJ,KKK)
        WRITE(11,207) THETA(KKK)
 207     FORMAT(/////15X,'FOR THETA=',F5.1,//25X,'THE [QBAR] MATRIX
   $     IS:  (PSI)')
        CALL PRINT(MATRI1)
        WRITE(11,208)
 208     FORMAT(//25X,'THE [SBAR] MATRIX IS:  (PSI-1)')
        CALL PRINT(MATRI2)
 305     CONTINUE
 304     CONTINUE
C** CALCULATE <APRIME> AND <DPRIME> MATRICES ***
     CALL INVERT(A,AP)
     CALL INVERT(D,DP)
C*** FIND LAMINATE PROPERTIES AND LAMINATE COMPLIANCE MATRIX (SLAM) ***
```

```
      CALL LAPROP(ELX,ELY,GLXY,VLXY,AP,THICK,ALBAR,SLAM)
C*** FIND ROOTS TO ELASTICITY EQUATION FOR ELLIPTICAL HOLE IN
C***      ORTHOTROPIC PLATE
      CALL ROOTS(SLAM,UK)
C*** FIND LAMINATE FIELD STRESSES IN PROCESS ZONE
  550  JJ=NDIV+1
      CALL FIELDS(UK,P,AA,BB,APARAM,SIGX,SIGY,TAUXY,RNOTCH,Y,NDIV,JJ)
      WRITE(33,58)(Y(II),SIGX(II),SIGY(II),TAUXY(II),II=1,JJ)
  58   FORMAT(1X,4E15.5)
C*** POINT BY POINT, FIND LOADING (N'S), STRAINS, THEN FAILURE CRITERIA
     DO 575 IPOINT=1,JJ
C*** FIND LAMINATE LOADING IN PROCESS ZONES (INTEGRATE STRESSES OVER Z)
      NXYB(1)=SIGX(IPOINT)*THICK
      NXYB(2)=SIGY(IPOINT)*THICK
      NXYB(3)=TAUXY(IPOINT)*THICK
      DO 552 I=1,3
  552    MXYB(I)=0
C***  FIND MIDPLANE STRAINS, CURVATURES IF NOT SPECIFIED ***
      CALL MIDPLA(E0,K0,AP,BP,DP,ISYMET,IMOMEN,NXYB,MXYB)
C***  FIND STRAINS IN EACH PLY GIVEN MIDPLANE STRAINS, CURVATURE ***
  344  CALL ZSTRAI(Z,EXY,E0,K0,N,IMOMEN,E12,T)
      CALL CRITER(E12,EFAILT,EFAILC,N,FAILCR,IPOINT)
  575  CONTINUE
      CALL AVERG(AVFAIL,FAILCR,N,NDIV)
      CALL MAXFAI(AVFAIL,MAXFL,ITFAIL,ITYPE,IFLAG,N,INFAIL,IGONE)
     CALL DISCNT(AVFAIL,MAXFL,ITFAIL,ITYPE,IFLAG,N,P,E1,E2,G12,IGONE,
    $LFLAG,LFLAG)
      IF(LFLAG.EQ.1) GO TO 800
      IF(IFLAG.EQ.0) GO TO 550
      IFAIL=IFAIL+1
      IF(IFAIL.GE.ITYPEN)GO TO 800
      IF(IFLAG.EQ.1) GO TO 500
  800  WRITE(22,801)P,THETA(INFAIL),MAXFL,IFAIL,ITYPEN
  801  FORMAT(5X,'THE LAMINATE HAS FAILED AT A LOAD OF:',E12.5,/5X,
    $'THE FINAL PLIES TO FAIL WERE THOSE WITH THETA =',F10.1,//5X,
    $'MAXFL,IFAIL, AND ITYPEN ARE:',E12.4,2I3)
      WRITE(6,*) P
C***  FINDS STRESS GIVEN QB, STRAINS, ALPHA, AND TEMPERATURE CHANGE ***
C      CALL ZSTRES(N,EXY,QXY,Q12,T,QB,IMOMEN,ALPHA,DT,E0T)
C 312   CALL PRINT2(N,NXYB,MXYB,NT,MT,NTOTAL,MTOTAL,Q12,QXY,E12,EXY,
C    $THETA,QB,ALPH,TC,TR, ILOAD,LCASE,E0T,E0,K0)
C      CALL PRINT3(E12,EXY,Q12,QXY,N,LCASE,QXYN)
C      CALL FAILUR(Q12,N,TSHILL,XT,XC,YT,YC,SS,LCASE)
  332  WRITE(6,55)
  55   FORMAT(5X,'YOU ARE A WONDERFUL PERSON!! JUST TYPE FILE
    $ OUTPUT DATA FOR THE OUTPUT.  HAVE FUN!!')
      STOP
      END
C*******************************************************
C*********************************************************************
      SUBROUTINE QFIND (K,Q,S)
C_____________________________________________________________________
C:::  THIS SUBROUTINE CALCULATES THE REDUCED STIFFNESS OF A MATERIAL :::
C:::       IN THE LOCAL 1-2 COORDINATES                           :::
C-------------------------------------------------------------
      DOUBLE PRECISION Q,S,DD
```

```
      DIMENSION Q(3,3,4),S(3,3,4)
      DD=S(1,1,K)*S(2,2,K)-S(1,2,K)**2
      Q(1,3,K)=0
      Q(3,1,K)=0
      Q(2,3,K)=0
      Q(3,2,K)=0
      Q(1,1,K)=S(2,2,K)/DD
      Q(1,2,K)=-S(1,2,K)/DD
      Q(2,2,K)=S(1,1,K)/DD
      Q(2,1,K)=Q(1,2,K)
      Q(3,3,K)=1/S(3,3,K)
      RETURN
      END
C*********************************************************************
      SUBROUTINE QBAR (K,Q,QB,THET,ITYPE)
C_____________________________________________________________________
C:::  THIS SUBROUTINE CALCULATES THE TRANSFORMED, REDUCED STIFFNESS :::
C:::    FOR EACH PLY IN THE GLOBAL X-Y COORDINATE SYSTEM            :::
C---------------------------------------------------------
      DOUBLE PRECISION Q(3,3,4),QB(3,3,49),THET(49),X,Y,X2,Y2,X4,Y4
      DOUBLE PRECISION X3,Y3
      DIMENSION ITYPE(49)
      Y=DSIN(THET(K))
      X=DCOS(THET(K))
      Y2=Y**2
      X2=X**2
      Y4=Y**4
      X4=X**4
      X3=X**3
      Y3=Y**3
      J=K
      K=ITYPE(K)
      QB(1,1,J)=Q(1,1,K)*X4 + 2*(Q(1,2,K)+2*Q(3,3,K))*Y2*X2
     $     + Q(2,2,K)*Y4
      QB(1,2,J)= (Q(1,1,K)+Q(2,2,K)-4*Q(3,3,K))*Y2*X2
     $     + Q(1,2,K)*(Y4+X4)
      QB(2,2,J)= Q(1,1,K)*Y4 + 2*(Q(1,2,K)+2*Q(3,3,K))*Y2*X2
     $     +Q(2,2,K)*X4
      QB(1,3,J)=(Q(1,1,K)-Q(1,2,K)-2*Q(3,3,K))*Y*X3
     $     + (Q(1,2,K)-Q(2,2,K)+2*Q(3,3,K))*X*Y3
      QB(2,3,J)=(Q(1,1,K)-Q(1,2,K)-2*Q(3,3,K))*X*Y3
     $     + (Q(1,2,K)-Q(2,2,K)+2*Q(3,3,K))*Y*X3
      QB(3,3,J)=(Q(1,1,K)+Q(2,2,K)-2*Q(1,2,K)-2*Q(3,3,K))*Y2*X2
     $     + Q(3,3,K)*(Y4+X4)
      QB(3,2,J)=QB(2,3,J)
      QB(3,1,J)=QB(1,3,J)
      QB(2,1,J)=QB(1,2,J)
      K=J
      RETURN
      END
C*********************************************************************
      SUBROUTINE SBAR(K,S,SB,THET,ITYPE)
C_____________________________________________________________________
C:::  THIS SUBROUTINE CALCULATES THE TRANSFORMED, REDUCED          :::
C:::    COMPLIANCE MATRIX FOR EACH PLY IN THE GLOBAL X-Y           :::
```

```
C:::     COORDINATE SYSTEM                                   :::
C-----------------------------------------------------------
      DOUBLE PRECISION S(3,3,4),SB(3,3,49),THET(49),X,Y,X2,Y2,S11,S12
      DOUBLE PRECISION S13,S23,S22,S33,X4,Y4,X3,Y3
      DIMENSION ITYPE(49)
      X=DCOS(THET(K))
      Y=DSIN(THET(K))
      X2=X**2
      Y2=Y**2
      X4=X**4
      Y4=Y**4
      X3=X**3
      Y3=Y**3
      J=ITYPE(K)
      S11=S(1,1,J)
      S12=S(1,2,J)
      S13=S(1,3,J)
      S23=S(2,3,J)
      S22=S(2,2,J)
      S33=S(3,3,J)
      SB(1,1,K)=S11*X4+(2*S12+S33)*X2*Y2+S22*Y4
      SB(1,2,K)=S12*(Y4+X4)+(S11+S22-S33)*X2*Y2
      SB(2,2,K)=S11*Y4+(2*S12+S33)*X2*Y2+S22*X4
      SB(1,3,K)=(2*S11-2*S12-S33)*Y*X3-(2*S22-2*S12-S33)*X*Y3
      SB(2,3,K)=(2*S11-2*S12-S33)*X*Y3-(2*S22-2*S12-S33)*Y*X3
      SB(3,3,K)=2*(2*S11+2*S22-4*S12-S33)*Y2*X2+S33*(X4+Y4)
      SB(2,1,K)=SB(1,2,K)
      SB(3,1,K)=SB(1,3,K)
      SB(3,2,K)=SB(2,3,K)
      RETURN
      END
C*********************************************************************
      SUBROUTINE AFIND (I,J,K,N,QB,Z,A)
C____________________________________________________________________
C:::  THIS SUBROUTINE CALCULATES THE EXTENSIONAL STIFFNESS MATRIX,  :::
C:::   A, OF THE LAMINATE IN THE X-Y GLOBAL COORDINATE SYSTEM       :::
C-----------------------------------------------------------
      DOUBLE PRECISION QB(3,3,49),Z(49),A(3,3)
      A(I,J)=0
      IN=N+1
      DO 1 KK=2,IN
 1     A(I,J)=A(I,J)+QB(I,J,KK-1)*(Z(KK)-Z(KK-1))
      RETURN
      END
C*********************************************************************
      SUBROUTINE BFIND(I,J,K,N,QB,Z,B)
C____________________________________________________________________
C:::  THIS SUBROUTINE CALCULATES THE COUPLING STIFFNESS MATRIX, B,  :::
C:::   OF THE LAMINATE IN THE GLOBAL X-Y COORDINATE SYSTEM          :::
C-----------------------------------------------------------
      DOUBLE PRECISION QB(3,3,49),Z(49),B(3,3)
      B(I,J)=0
      IN=N+1
      DO 1 KK=2,IN
 1       B(I,J)=B(I,J)+.5*QB(I,J,KK-1)*(Z(KK)**2-Z(KK-1)**2)
      RETURN
```

```
      END
C*********************************************************************
      SUBROUTINE DFIND(I,J,K,N,QB,Z,D)
C____________________________________________________________________
C:::   THIS SUBROUTINE CALCULATES THE BENDING STIFFNESS MATRIX, D   :::
C:::     OF THE LAMINATE IN THE GLOBAL X-Y COORDINATE SYSTEM        :::
C------------------------------------------------------------
      DOUBLE PRECISION QB(3,3,49),Z(49),D(3,3)
      D(I,J)=0
      IN=N+1
      DO 1 KK=2,IN
 1      D(I,J)=D(I,J)+0.33333*QB(I,J,KK-1)*(Z(KK)**3
   $     -Z(KK-1)**3)
      RETURN
      END
C*********************************************************************
      SUBROUTINE TFIND(THET,N,T,TI)
C____________________________________________________________________
C:::   THIS SUBROUTINE CALCULATES THE TRANSFORMATION MATRICES FOR   :::
C:::         EACH PLY                                   :::
C------------------------------------------------------------
      DOUBLE PRECISION THET(49),T(3,3,49),TI(3,3,49),C,CC,S,SS
      DO 1 I=1,N
      C=DCOS(THET(I))
      CC=C**2
      S=DSIN(THET(I))
      SS=S**2
      T(1,1,I)=CC
      T(1,2,I)=SS
      T(1,3,I)=2*S*C
      T(2,1,I)=SS
      T(2,2,I)=CC
      T(2,3,I)=-2*S*C
      T(3,1,I)=-S*C
      T(3,2,I)=S*C
      T(3,3,I)=CC-SS
      TI(1,1,I)=CC
      TI(1,2,I)=SS
      TI(1,3,I)=-2*S*C
      TI(2,1,I)=SS
      TI(2,2,I)=CC
      TI(2,3,I)=2*S*C
      TI(3,1,I)=S*C
      TI(3,2,I)=-S*C
 1    TI(3,3,I)=CC-SS
      RETURN
      END
C*********************************************************************
      SUBROUTINE PRINT(MATRIX)
C____________________________________________________________________
C:::  THIS SUBROUTINE PRINTS A 3X3 MATRIX                   :::
C------------------------------------------------------------
      DOUBLE PRECISION MATRIX(3,3)
      DO 1 I=1,3
 1     WRITE(11,11) (MATRIX(I,J),J=1,3)
 11   FORMAT(/1X,3E20.5)
```

```
      RETURN
      END
C*****************************************************************
      SUBROUTINE INVERT(X,XP)
C_____________________________________________________________________
C:::  THIS SUBROUTINE INVERTS A 3X3 MATRIX                      :::
C-----------------------------------------------------------
      DOUBLE PRECISION X(3,3),XP(3,3),DET,THIS(3,3)
      DET=X(1,1)*X(2,2)*X(3,3)-X(1,1)*X(2,3)*X(3,2)
    $ + X(1,2)*X(2,3)*X(3,1) - X(1,2)*X(2,1)*X(3,3)
    $ + X(1,3)*X(2,1)*X(3,2)-X(1,3)*X(2,2)*X(3,1)
      XP(1,1)=(X(2,2)*X(3,3)-X(2,3)*X(3,2))/DET
      XP(1,2)=-(X(1,2)*X(3,3)-X(1,3)*X(3,2))/DET
      XP(1,3)=(X(1,2)*X(2,3)-X(1,3)*X(2,2))/DET
      XP(2,1)=-(X(2,1)*X(3,3)-X(2,3)*X(3,1))/DET
      XP(2,2)=(X(1,1)*X(3,3)-X(1,3)*X(3,1))/DET
      XP(2,3)=-(X(1,1)*X(2,3)-X(1,3)*X(2,1))/DET
      XP(3,1)=(X(2,1)*X(3,2)-X(2,2)*X(3,1))/DET
      XP(3,2)=-(X(1,1)*X(3,2)-X(1,2)*X(3,1))/DET
      XP(3,3)=(X(1,1)*X(2,2)-X(1,2)*X(2,1))/DET
      RETURN
      END
C*****************************************************************
      SUBROUTINE MIDPLA(E0,K,AP,BP,DP,ISYMET,IMOMEN,
    $ N,M)
C_____________________________________________________________________
C:::   THIS SUBROUTINE CALCULATES MIDPLANE STRAINS AND CURVATURES  :::
C:::     BASED ON THE A,B,&D INVERSE MATRICES AND THE FORCE AND   :::
C:::     MOMENT RESULTANTS N AND M                              :::
C-----------------------------------------------------------
      REAL*8 E0(3),K(3),N(3),M(3)
      DOUBLE PRECISION AP(3,3),BP(3,3),DP(3,3)
      DO 1 I=1,3
      E0(I)=0
      K(I)=0
      DO 1 J=1,3
  1     E0(I)=E0(I)+AP(I,J)*N(J)
      IF(ISYMET.EQ.1.OR.IMOMEN.EQ.1) GO TO 4
      DO 2 I=1,3
      DO 2 J=1,3
  2     E0(I)=E0(I)+BP(I,J)*M(+J)
  4    IF(ISYMET.EQ.1) GO TO 5
      DO 3 I=1,3
      DO 3 J=1,3
  3    K(I)=K(I)+BP(I,J)*N(J)
  5    IF(IMOMEN.EQ.1) GO TO 7
      DO 6 I=1,3
      DO 6 J=1,3
  6     K(I)=K(I)+DP(I,J)*M(J)
  7    CONTINUE
C     WRITE(6,*)(E0(I),I=1,3),(K(J),J=1,3)
      RETURN
      END
C*****************************************************************
      SUBROUTINE ZSTRAI(Z,EXY,E0,K0,N,IMOMEN,E12,T)
C_____________________________________________________________________
```

```
C:::  CALCULATES THE STRAINS IN EACH LAYER GIVEN THE MIDPLANE       :::
C:::     STRAINS AND CURVATURES IN BOTH THE LOCAL 1-2 AND THE      :::
C:::     GLOBAL X-Y COORDINATE SYSTEMS                          :::
C-----------------------------------------------------------
      DIMENSION Z(49),T(3,3,49),XEXY(3,49,2),XE12(3,49,2)
      REAL*8 E0(3),K0(3),EXY(3,49,2),E12(3,49,2)
      DOUBLE PRECISION Z,T,XEXY,XE12
      DO 3 I=1,N
       EXY(1,I,1)=Z(I)*K0(1) + E0(1)
       EXY(2,I,1)=Z(I)*K0(2) + E0(2)
 3     EXY(3,I,1)=Z(I)*K0(3) + E0(3)
      DO 4 I=2,N
      DO 4 K=1,3
 4     EXY(K,I-1,2)=EXY(K,I,1)
      DO 5 I=1,3
 5     EXY(I,N,2)=E0(I) + K0(I)*Z(N+1)
      DO 6 I=1,N
      DO 6 K=1,2
       XEXY(1,I,K)=EXY(1,I,K)
       XEXY(2,I,K)=EXY(2,I,K)
 6     XEXY(3,I,K)=EXY(3,I,K)/2
      DO 9 I=1,N
      DO 9 J=1,3
      DO 9 L=1,2
 9     XE12(J,I,L)=0
      DO 7 I=1,N
      DO 7 J=1,3
      DO 7 K=1,3
      DO 7 L=1,2
 7     XE12(J,I,L)=XE12(J,I,L)+XEXY(K,I,L)*T(J,K,I)
      DO 8 I=1,N
      DO 8 K=1,2
       E12(1,I,K)=XE12(1,I,K)
       E12(2,I,K)=XE12(2,I,K)
 8     E12(3,I,K)=2*XE12(3,I,K)
      RETURN
      END
C*********************************************************************
      SUBROUTINE ZSTRES(N,EXY,QXY,Q12,T,QB,IMOMEN,ALPHA,DT,E0T)
C______________________________________________________________________
C:::  THIS SUBROUTINE CALCULATES STRESSES IN EACH LAYER GIVEN BOTH  :::
C:::    MECHANICAL AND THERMAL LOADING INFORMATION IN BOTH THE      :::
C:::    LOCAL 1-2 AND GLOBAL X-Y COORDINATE SYSTEMS               :::
C-----------------------------------------------------------
      REAL*8 EXY(3,49,2)
      DOUBLE PRECISION QXY(3,49,2),Q12(3,49,2),T(3,3,49),QB(3,3,49)
      DOUBLE PRECISION ALPHA(3,49),E0T(3),ACHECK(49)
      DO 3 I=1,N
      DO 3 J=1,3
      DO 3 K=1,2
       QXY(J,I,K)=0
 3     Q12(J,I,K)=0
      DO 1 L=1,2
      DO 1 J=1,N
      DO 1 I=1,3
      DO 1 K=1,3
```

```
      QXY(I,J,L)=QB(I,K,J)*(EXY(K,J,L)) + QXY(I,J,L)
      ACHECK(J)=ALPHA(K,J)*DT
 1     QXY(I,J,L)=QXY(I,J,L)-ACHECK(J)*QB(I,K,J)
      WRITE(6,*)(ACHECK(LLL),LLL=1,N)
      DO 2 J=1,N
      DO 2 I=1,3
      DO 2 K=1,3
      DO 2 L=1,2
 2    Q12(I,J,L)=QXY(K,J,L)*T(I,K,J) + Q12(I,J,L)
      RETURN
      END
C**********************************************************************
      SUBROUTINE ALPBAR(N,ALPH,QB,TI,TR,TC,NT,MT,Z,ALPHA,DT,INCR,AP,
     $ALBAR,E0T)
C_________________________________________________________________________
C:::   THIS SUBROUTINE CALCULATES THE COEFFICIENTS OF THERMAL      :::
C:::     EXPANSION IN THE GLOBAL X-Y COORDINATE SYSTEM           :::
C-----------------------------------------------------------------
      REAL*8 QB(3,3,49),ALPH(3),ALPHA(3,49),TI(3,3,49),Z(49),AP(3,3),
     $ALBAR(3),NT(3),MT(3),E0T(3)
      WRITE(6,1)
 1     FORMAT(10X,'TO CALCULATE ALPHABAR FOR THE LAMINATE CORRECTLY,
     $INPUT ROOM TEMP=     1000, STRESS FREE TEMP=0 WHEN ASKED')
      CALL THERMO(N,ALPH,QB,TI,TR,TC,NT,MT,Z,ALPHA,DT,INCR,E0T,AP)
      ALBAR(1)=0
      ALBAR(2)=0
      ALBAR(3)=0
      DO 10 I=1,3
       DO 10 J=1,3
 10    ALBAR(I)=ALBAR(I) + AP(I,J)*NT(J)
      DO 20 I=1,3
 20     ALBAR(I)=ALBAR(I)/1000
      RETURN
      END
C**********************************************************************
      SUBROUTINE LAPROP(ELX,ELY,GLXY,VLXY,AP,THICK,ALBAR,SLAM)
C_________________________________________________________________________
C:::   THIS SUBROUTINE CALCULATES VARIOUS LAMINATE PROPERTIES-     :::
C:::     MODULI, POISSONS RATIO (NUXY), AND COEFFICIENTS OF MUTUAL :::
C:::     INFLUENCE AND PRINTS TO OUTPUT                          :::
C-----------------------------------------------------------------
      DOUBLE PRECISION AP(3,3),ALBAR(3),SLAM(3,3)
      REAL*8 ELX,ELY,NXYCY,NXYCX,NXCXY,NYCXY
      ELX=1/(AP(1,1)*THICK)
      ELY=1/(AP(2,2)*THICK)
      VLXY=-AP(1,2)/AP(1,1)
      GLXY=1/(AP(3,3)*THICK)
      NXYCX=AP(1,3)/AP(1,1)
      NXYCY=AP(2,3)/AP(2,2)
      NXCXY=AP(1,3)/AP(3,3)
      NYCXY=AP(2,3)/AP(3,3)
      SLAM(1,1)=1/ELX
      SLAM(2,2)=1/ELY
      SLAM(3,3)=1/GLXY
      SLAM(1,2)=-VLXY/ELX
      SLAM(2,1)=SLAM(1,2)
```

```
      SLAM(1,3)=0
      SLAM(2,3)=0
      SLAM(3,2)=0
      SLAM(3,1)=0
      WRITE(11,1) ELX,ELY,GLXY,VLXY,NXYCX,NXYCY,NXCXY,NYCXY,
     $ ALBAR(1),ALBAR(2),ALBAR(3)
  1   FORMAT(////15X,'THE LAMINATE PROPERTIES ARE:',///15X,
     $ 'EX =',E12.4,7X,'EY =',E12.4,/15X,'GXY =',E12.4,6X,'VXY = ',
     $ F5.3,/15X,'NXY,X=',E12.4,5X,'NXY,Y=',E12.4,/15X,'NX,XY=',E12.4,5X
     $ 'NY,XY=',E12.4,/15X,'ALPHAX=',E12.4,4X,'ALPHAY=',E12.4,5X,
     $ 'ALPHAXY=',E12.4)
      RETURN
      END
C*********************************************************************
      SUBROUTINE PRINT2(N,NXYB,MXYB,NT,MT,NTOTAL,MTOTAL,Q12,QXY,E12
     $,EXY,THETA,QB,ALPH,TC,TR,ILOAD,LCASE,E0T,E0,K0)
C______________________________________________________________________
C:::   PRINTS LOADING CONDITIONS                              :::
C----------------------------------------------------------------
      REAL*8 NXYB(3),MXYB(3),THETA(49),Q12(3,49,2),E0(3),K0(3)
      DOUBLE PRECISION ALPHN(3),QXY(3,49,2)
      DOUBLE PRECISION QB(3,3,49),ALPH(3)
      REAL*8 NT(3),MT(3),NTOTAL(3),MTOTAL(3)
      REAL*8  E12(3,49,2),EXY(3,49,2),E0T(3)
      WRITE(11,1) LCASE
  1   FORMAT('1',15X,'LOADING INFORMATION - LOADCASE #',I2)
      WRITE(11,20)
      IF(ILOAD.EQ.2) GO TO 30
  20   FORMAT(//15X,'MECHANICAL LOADING')
      WRITE(11,2)(NXYB(I),I=1,3)
      WRITE(11,3)(MXYB(I),I=1,3)
  2   FORMAT(///15X,'NX =',F12.4,5X,'NY =',F12.4,5X,'NXY =',F12.4)
  30   WRITE(11,21)
  21   FORMAT(///15X,'THERMAL FORCE RESULTANTS')
      DO 55 INX=1,3
  55   ALPHN(INX)=ALPH(INX)*10**6
      WRITE(11,6)(ALPHN(I), I=1,3)
  6   FORMAT(/15X,'ALPHA1 =',F5.2,5X,'ALPHA2 =',F5.2,5X,
     $'ALPHA12 =',F5.2,5X,'(10**(-6) in/in/degree F)')
      WRITE(11,7) TR,TC,(E0T(I),I=1,3)
  7   FORMAT(/15X,'ROOM TEMPERATURE =',F6.1,5X,'STRESS FREE ',
     $'TEMPERATURE =',F6.1,//15X,'MIDPLANE STRAINS DUE TO THERMAL'
     $,' LOADING',/20X,3F15.6)
      IF(ILOAD.EQ.2) GO TO 44
      WRITE(11,2)(NT(I),I=1,3)
      WRITE(11,3)(MT(I),I=1,3)
      IF(ILOAD.EQ.2) GO TO 44
      WRITE(11,22)
  22   FORMAT(///15X,'TOTAL LOADING')
      WRITE(11,2)(NTOTAL(I),I=1,3)
      WRITE(11,3)(MTOTAL(I),I=1,3)
  3   FORMAT(/15X,'MX =',F12.4,5X,'MY =',F12.4,5X,'MXY =',F12.4)
  44   IF(ILOAD.EQ.2) WRITE(11,40)(E0(I),I=1,3),(K0(I),I=1,3)
  40   FORMAT(///15X,'THE LOADING WAS SPECIFIED IN TERMS OF MIDPLANE',
     $ ' STRAINS AND CURVATURES.'//15X, 'MIDPLANE STRAINS:',/20X,3F15.6,
     $/15X,'CURVATURES:',/20X,3F15.6)
```

```
      RETURN
      END
C*********************************************************************
      SUBROUTINE THERMO(N,ALPH,QB,TI,TR,TC,NT,MT,Z,ALPHA,DT,INCR,E0T,
     $  AP)
C______________________________________________________________________
C:::   CALCULATES THERMAL FORCE AND MOMENT RESULTANTS AND MIDPLANE :::
C:::     THERMAL STRAINS (ALSO INPUTS THERMAL PROPERTIES)          :::
C----------------------------------------------------------------
      DOUBLE PRECISION QB(3,3,49),E0T(3),AP(3,3)
      DOUBLE PRECISION ALPH(3),ALPHA(3,49),TI(3,3,49),Z(49)
      REAL*8 NT(3),MT(3)
      IF(INCR.EQ.1) GO TO 4
      WRITE(6,1)
 1    FORMAT(///5X,'WHAT ARE THE COEFFICIENTS OF THERMAL EXPANSION?
     $(ALPHA1,ALPH2,ALPHA12)')
      READ(5,*) (ALPH(I),I=1,3)
 4    WRITE(6,2)
 2    FORMAT(///5X,'WHAT ARE THE ROOM AND STRESS FREE TEMPERATURES?')
      READ(5,*) TR,TC
      DT=TR-TC
      DO 3 I=1,3
      DO 3 J=1,N
 3    ALPHA(I,J)=0
      ALPH(3)=ALPH(3)/2
      DO 10 I=1,N
      DO 10 J=1,3
      DO 10 K=1,3
 10    ALPHA(J,I)=ALPH(K)*TI(J,K,I) + ALPHA(J,I)
      ALPH(3)=ALPH(3)*2
      DO 12 I=1,N
 12    ALPHA(3,I)=ALPHA(3,I)*2
      DO 44 I=1,3
      MT(I)=0
 44    NT(I)=0
      DO 20 I=1,3
      DO 20 J=1,3
      DO 20 K=1,N
       NT(I)=DT*QB(I,J,K)*ALPHA(J,K)*(Z(K+1)-Z(K))
     $ +NT(I)
 20     MT(I)=DT*QB(I,J,K)*ALPHA(J,K)*(Z(K+1)**2-Z(K)**2)
     $ +MT(I)
      DO 25 I=1,3
 25    E0T(I)=0
      DO 30 I=1,3
      DO 30 J=1,3
 30    E0T(I)=E0T(I)+AP(I,J)*NT(J)
      RETURN
      END
C*********************************************************************
      SUBROUTINE FAILUR(Q12,N,TSHILL,XT,XC,YT,YC,S,LCASE)
C______________________________________________________________________
C:::   THIS SUBROUTINE PERFORMS TSAI-HILL AND TSAI-WU (TENSOR      :::
C:::     POLYNOMIAL) FAILURE ANALYSIS AND PRINTS RESULTS          :::
C----------------------------------------------------------------
      DOUBLE PRECISION Q12(3,49,2),TSHILL(49,2),TSWU(49,2)
```

```
      DO 1 I=1,15
      DO 1 L=1,2
  1    TSHILL(I,L)=0
      DO 2 I=1,N
      DO 2 L=1,2
       X=XT
      IF(Q12(1,I,L).LT.0.) X=XC
       Y=YT
      IF(Q12(2,I,L).LT.0.) Y=YC
  2     TSHILL(I,L)=(Q12(1,I,L)/X)**2 + (Q12(2,I,L)/Y)**2 -
    $     Q12(1,I,L)*Q12(2,I,L)/X**2 + (Q12(3,I,L)/S)**2
      WRITE(11,3)LCASE,XT,XC,YT,YC,S
  3   FORMAT(1H1,//15X,'FAILURE ANALYSIS OF PLYS - LOADCASE #',I2,//15X
    $'XT =',F10.0,5X,'XC =',F10.0,//15X,'YT =',F10.0,5X,
    $'YC =',F10.0,//15X,'S =',F10.0)
      WRITE(11,4)
   4   FORMAT(/////15X,'THE TSAI-HILL FAILURE CRITERIA ARE:
    $',//20X,'FAILURE IF GREATER THAN 1.0')
      DO 6 I=1,N
  6    WRITE(11,5) I,(TSHILL(I,L),L=1,2)
  5    FORMAT(//15X,'PLY #',I3,/15X,'AT TOP =',F12.3,5X,
    $'AT BOTTOM =',F12.3)
C       WRITE(6,4)
C       DO 8 I=1,N
C       WRITE(6,5) I,(TSHILL(I,J),J=1,2)
  7    FORMAT(5X,I3,5X,2F10.2)
C*** FIND TENSOR POLYNOMIAL (TSAI-WU) FAILURE CRITERIA ***
      F11=-1/(XT*XC)
      F22=-1/(YT*YC)
      F1=(1/XT)+(1/XC)
      F2=(1/YT)+(1/YC)
      F66=1/(S**2)
      DO 20 I=1,N
      DO 20 L=1,2
  20    TSWU(I,L)=Q12(1,I,L)*F1+Q12(2,I,L)*F2+(Q12(1,I,L)**2)*F11
    $ +(Q12(2,I,L)**2)*F22+ (Q12(3,I,L)**2)*F66
     WRITE(11,3) LCASE,XT,XC,YT,YC,S
     WRITE(11,11)
     DO 12 I=1,N
  12    WRITE(11,5) I,(TSWU(I,L),L=1,2)
  11    FORMAT(/////15X,'THE TENSOR POLYNOMIAL FAILURE CRITERIA ARE:',
    $ //20X,'FAILURE IF GREATER THAN 1.0',//20X,'NOTE: THIS MODEL',
    $' NEGLECTS INTERACTION TERMS AND INTERLAMINAR STRESSES')
      RETURN
      END
C**********************************************************************
      SUBROUTINE PRINT3(E12,EXY,Q12,QXY,N,LCASE,QXYN)
C______________________________________________________________________
C:::   THIS SUBROUTINE PRINTS STRESSES AND STRAINS IN BOTH THE     :::
C:::     LOCAL 1-2 AND GLOBAL X-Y COORDINATE SYSTEMS              :::
C----------------------------------------------------------------
      DOUBLE PRECISION E12(3,49,2),EXY(3,49,2),Q12(3,49,2),QXY(3,49,2)
      DOUBLE PRECISION QXYN(3,49,3),Q12N(3,49,3),EXYN(3,49,3)
      REAL*8 E12N(3,49,3)
      DO 55 I=1,N
       DO 55 J=1,3
```

```
      QXYN(J,I,1)=QXY(J,I,1)/1000.
      Q12N(J,I,1)=Q12(J,I,1)/1000.
      EXYN(J,I,1)=EXY(J,I,1)*100.
      E12N(J,I,1)=E12(J,I,1)*100.
      QXYN(J,I,3)=QXY(J,I,2)/1000.
      Q12N(J,I,3)=Q12(J,I,2)/1000.
      EXYN(J,I,3)=EXY(J,I,2)*100.
      E12N(J,I,3)=E12(J,I,2)*100.
      E12N(J,I,2)=(E12N(J,I,1)+E12N(J,I,3))/2
      QXYN(J,I,2)=(QXYN(J,I,1)+QXYN(J,I,3))/2
      Q12N(J,I,2)=(Q12N(J,I,1)+Q12N(J,I,3))/2
 55   EXYN(J,I,2)=(EXYN(J,I,1)+EXYN(J,I,3))/2
      WRITE(11,1) LCASE
 1    FORMAT(1H1,//25X,'STRESSES (KSI) - LOADCASE#',I2,/////15X,'PLY',
     $19X,'SIGX',23X,'SIGY',25X,'TAUXY')
      DO 2 I=1,N
 2    WRITE(11,3) I,((QXYN(J,I,L),J=1,3),L=1,3)
 3    FORMAT(//14X,I2,2X,'TOP',10X,F13.6,15X,F13.6,15X,F13.6,/18X,
     $'MID',10X,F13.6,15X,F13.6,15X,F13.6,/18X,
     $'BOT',10X,F13.6,15X,F13.6,15X,F13.6,/)
      WRITE(11,4) LCASE
 4    FORMAT(1H1,//25X,'STRESSES (KSI) - LOADCASE#',I2,/////15X,'PLY',
     $19X,'SIG1',23X,'SIG2',25X,'TAU12',//)
      DO 5 I=1,N
 5    WRITE(11,3)I,((Q12N(J,I,L),J=1,3),L=1,3)
      WRITE(11,6) LCASE
 6    FORMAT('1',/////25X,'STRAINS (%) - LOADCASE #',I2,//15X,'PLY',21X
     $'EPSX',23X,'EPSY',21X,'GAMXY')
      DO 7 I=1,N
 7    WRITE(11,3)I,((EXYN(J,I,L),J=1,3),L=1,3)
      WRITE(11,8) LCASE
 8    FORMAT(1H1,///25X,'STRAINS (%) - LOADCASE #',I2,//////15X,'PLY',
     $21X,'EPS1',23X,'EPS2',21X,'GAM12')
      DO 9 I=1,N
 9    WRITE(11,3) I,((E12N(J,I,L),J=1,3),L=1,3)
      RETURN
      END
C*********************************************************************
C******************************************************************
      SUBROUTINE ROOTS(SLAM,UK)
      REAL*8 SLAM(3,3)
      COMPLEX UK(4),D
C***  RESULTS VALID FOR ORTHOTROPIC MATERIALS ONLY!!!  ***
      A=SLAM(1,1)
      B=2*SLAM(1,2)+SLAM(3,3)
      C=SLAM(2,2)
      E=(B*B-4*A*C)
      D=CSQRT(CMPLX(E,0.0))
      UK(1)=(-B-D)/(2*A)
      UK(3)=(-B+D)/(2*A)
      UK(1)=CSQRT(UK(1))
      UK(3)=CSQRT(UK(3))
      UK(2)=UK(1)
      UK(4)=UK(3)
      WRITE(6,*)UK(1),UK(2),UK(3),UK(4)
      RETURN
```

```
      END
C***********************************************************************
      SUBROUTINE FIELDS(UK,P,A,B,AO,SIGX,SIGY,TAUXY,RNOTCH,YY,NDIV,IN)
      REAL*8 SIGX(IN),SIGY(IN),TAUXY(IN),YY(IN),A,B,AO,RNOTCH,P
      COMPLEX UK(4)
      BETAB=ABS(AIMAG(UK(1)))
      ALPHAB=ABS(AIMAG(UK(3)))
C      IF(ABS(ALPHAB-BETAB).LT.0.001) ALPHAB=BETAB+.001
      A1=A*A-((ALPHAB*B)**2)
      A2=A*A-((BETAB*B)**2)
     WRITE(6,14)A1,A2
 14   FORMAT(5X,'WELL, IT LIKES A1,A2',2E10.3)
      C=(ALPHAB**2)/(A-ALPHAB*B)
      D=(BETAB**2)/(A-BETAB*B)
     WRITE(6,15)C,D,ALPHAB,BETAB
 15   FORMAT(5X,'WELL, IT LIKES C,D,ALPHAB,BETAB',5E10.3)
      E=.5*P*B/(ALPHAB-BETAB)
     WRITE(6,16)E,P,A,B,RNOTCH
 16   FORMAT(5X,'WELL, IT LIKES E,P,A,B,R',E10.3,4E10.3)
      CB=1/(A-ALPHAB*B)
      DB=1/(A-BETAB*B)
     WRITE(6,10)
 10   FORMAT(5X,'WELL, ITS FOUND A1,A2,C,D,E,CB,AND DB',5E10.3)
      X=0
      IN=NDIV+1
C*** DEFINE Y'S IN PROCESS ZONE, CALCULATE AND STORE FIELD STRESSES
     DO 1 I=1,IN
      YY(I)=RNOTCH+ AO*(I-1)/NDIV
      Y=YY(I)
      R1=A1+(ALPHAB*Y)**2
      R2=A2+(BETAB*Y)**2
      S1=-2*ALPHAB*X*Y
      S2=-2*BETAB*X*Y
      RR1=R1+S1
      RR2=R2+S2
C      THETA1=ATAN(S1/R1)
C      THETA2=ATAN(S2/R2)
     THETA1=0
     THETA2=0
      TT1=THETA1/2
      TT2=THETA2/2
      IF(RR1.LT.0.000)RR1=-RR1
      IF(RR2.LT.0.000)RR2=-RR2
      DELTA1=SQRT(RR1)*COS(TT1)
      DELTA2=SQRT(RR2)*COS(TT2)
      GAMMA1=SQRT(RR1)*SIN(TT1)
      GAMMA2=SQRT(RR2)*SIN(TT2)
      D1=DELTA1**2+GAMMA1*2
      D2=DELTA2**2+GAMMA2*2
    SIGX(I)=P+2*E*(C*(1-(ALPHAB*DELTA1*Y/D1))
   $  -D*(1-(BETAB*DELTA2*Y/D2)))
    SIGY(I)=-2*E*(CB*(1-(ALPHAB*DELTA1*Y/D1))
   $  -DB*(1-(BETAB*DELTA2*Y/D2)))
 1  TAUXY(I)=2*E*((CB*ALPHAB*GAMMA1*Y/D1)-(DB*BETAB*GAMMA2*Y/D2))
      RETURN
```

```
      END
C**********************************************************************
      SUBROUTINE AVERAG(SIGX,SIGY,TAUXY,Y,NDIV,AVSIGX,AVSIGY,AVTAU,IN)
      REAL*8 SIGX(NDIV),SIGY(NDIV),TAUXY(NDIV),Y(IN)
C*** PERFORM AVERAGING OF STRESSES OVER PROCESS ZONE, LENGTH AO
      AVSIGX=0
      AVSIGY=0
      AVTAU=0
      IN=NDIV+1
      DO 1 I=1,IN
       AVSIGX=AVSIGX+SIGX(I)
       AVSIGY=AVSIGY+SIGY(I)
 1     AVTAU=AVTAU+TAUXY(I)
      DIST=Y(IN)-Y(1)
      AVSIGX=AVSIGX/DIST
      AVSIGY=AVSIGY/DIST
      AVTAU=AVTAU/DIST
      RETURN
      END
C**********************************************************************
     SUBROUTINE DISCNT(AVFAIL,MAXFL,ITFAIL,ITYPE,IFLAG,N,P,E1,E2,G12,
    $IGONE,LFLAG)
      REAL*8 MAXFL,P,E1(7),E2(7),G12(7)
      DIMENSION AVFAIL(49,3),ITYPE(49),IGONE(49)
      LFLAG=0
      LKOUNT=0
      DO 1 I=1,N
       K=ITYPE(I)
       IF(IGONE(I).EQ.1) GO TO 1
C*** IF A PLY HAS FAILED, REDUCE APPROPRIATE MODULI ***
        IF(AVFAIL(I,1).LT.1.00000000) GO TO 2
      IGONE(I)=1
        L=1
        E1(K)=1.
        G12(K)=1.
       WRITE(22,10)I,L
 10     FORMAT(5X,'PLY NUMBER',I3,' HAS FAILED DUE TO STRESS',
    $' COMPONENT',I2)
 2      IF(AVFAIL(I,2).LT.1.00000000) GO TO 3
       IGONE(I)=1
        L=2
        E2(K)=1.
        G12(K)=1.
       WRITE(22,10)I,L
 3      IF(AVFAIL(I,3).LT.1.0000000) GO TO 1
       IGONE(I)=1
        L=3
        E2(K)=1.
        G12(K)=1.
       WRITE(22,10)I,L
 1      CONTINUE
C      GO TO 200
 100   CONTINUE
C*** IF NO PLIES HAVE FAILED, INCREASE LOAD ***
      IF(IFLAG.EQ.1) GO TO 200
      IF(MAXFL.LT.0.100) P=P*2.50
```

```
      IF(MAXFL.LT.0.100) GO TO 190
      P=P/MAXFL + 20
 190  WRITE(22,11) P,MAXFL
    WRITE(6,99)(AVFAIL(I,1),AVFAIL(I,2),IGONE(I),I=1,N)
 99 FORMAT(5X,'AVERAGE FAILURE CRITERIA FOR 1,2 AND IGONE ARE:',
   $ 2E10.4,I3)
 11   FORMAT(5X,'THE LOAD HAS BEEN INCREASED TO',E10.5,'SINCE NO',
   $' FURTHER PLIES HAVE FAILED',/5X,'THE MAXIMUM FAILURE CRITERIA',
   $' WAS',F10.5)
200   CONTINUE
      DO 300 I=1,N
300    IF(IGONE(I).EQ.1) LKOUNT=LKOUNT+1
      IF(LKOUNT.EQ.N) LFLAG=1
      RETURN
      END
C*******************************************************************
      SUBROUTINE CRITER(E12,EFAILT,EFAILC,N,FAILCR,IPOINT)
      REAL*8 E12(3,49,2),EFAILT(3),EFAILC(3)
      DIMENSION FAILCR(49,21,3)
C*** AT GIVEN A POINT, CALCULATE FAILURE CRITERIA IN EACH PLY AND STORE
      DO 1 IPLY=1,N
       DO 1 ISTR=1,3
        EFAIL=EFAILT(ISTR)
        IF(E12(ISTR,IPLY,1).LT.0) EFAIL=EFAILC(ISTR)
 1       FAILCR(IPLY,IPOINT,ISTR)=E12(ISTR,IPLY,1)/EFAIL
      RETURN
      END
C*******************************************************************
      SUBROUTINE AVERG(AVFAIL,FAILCR,N,NDIV)
      DIMENSION AVFAIL(49,3),FAILCR(49,21,3)
C*** FIND AVERAGE FAILURE CRITERIA OVER PROCESS ZONE IN EACH PLY ***
      INDIV=NDIV+1
      DO 1 IPLY=1,N
      DO 1 ISTR=1,3
 1       AVFAIL(IPLY,ISTR)=0
      DO 2 IPOINT=1,INDIV
       DO 2 IPLY=1,N
        DO 2 ISTR=1,3
 2     AVFAIL(IPLY,ISTR)=AVFAIL(IPLY,ISTR)+FAILCR(IPLY,IPOINT,ISTR)
      DO 3 IPLY=1,N
      DO 3 ISTR=1,3
 3     AVFAIL(IPLY,ISTR)=AVFAIL(IPLY,ISTR)/INDIV
      RETURN
      END
C*******************************************************************
      SUBROUTINE MAXFAI(AVFAIL,MAXFL,ITFAIL,ITYPE,IFLAG,N,INFAIL,
   $IGONE)
      DIMENSION AVFAIL(49,3),ITYPE(49),IGONE(49)
      REAL*8 MAXFL
C*** FIND PLY MOST LIKELY TO FAIL AND MAXIMUM FAILURE CRITERIA
C***  IF FAILURE PREDICTED, IFLAG=1
      IFLAG=0
      MAXFL=0
      ITFAIL=0
      DO 1 IPLY=1,N
       DO 1 ISTR=1,3
```

```
        IF(IGONE(IPLY).EQ.1) GO TO 1
        IF(AVFAIL(IPLY,ISTR).GT.MAXFL) MAXFL=AVFAIL(IPLY,ISTR)
        IF(AVFAIL(IPLY,ISTR).GT.MAXFL) INFAIL=IPLY
        IF(AVFAIL(IPLY,ISTR).GT.MAXFL) ITFAIL=ITYPE(IPLY)
 1      CONTINUE
       IF(MAXFL.GT.1.00) IFLAG=1
       RETURN
       END
C**********************************************************************
```

VITA

Linda Wagnecz was born on August 22, 1963 to Sylvia and Alexander Wagnecz. She grew up in Mine Hill, New Jersey, and graduated as valedictorian from Dover High School in 1981. While studying mechanical engineering at Virginia Tech, she spent her summers working with a materials research group at Picatinny Arsenal in Dover, New Jersey. Miss Wagnecz graduated magna cum laude in June, 1985, recieving a Bachelor of Science degree in Mechanical Engineering. Enrolling in the Engineering Science and Mechanics Department to study composite materials, she was awarded a Pratt Fellowship and Graduate Research Assistantship. Miss Wagnecz will marry Brian Vick in August, 1987, and start work at Polyscientific in Blacksburg, Virginia.

Linda Wagnecz